# THE ROLE OF SUBDUCTION IN THE FORMATION AND EVOLUTION OF CONTINENTAL FRAGMENTS AND MICROCONTINENTS

by

**Joost Martijn van den Broek**

***THESIS***

*for the degree of*

***Philosophiae Doctor***


***Faculty of Mathematics and Natural Sciences***
*University of Oslo*

*July 2020*

*Series of dissertations submitted to the*
*Faculty of Mathematics and Natural Sciences, University of Oslo*
*No. 2324*

ISSN 1501-7710



Cover: Hanne Baadsgaard Utigard.
Print production: Reprosentralen, University of Oslo.

# Acknowledgements

Although there is only a single name on the cover, the completion of this PhD was not a singular effort. I am thus deeply indebted and very grateful to all the people who helped and supported me throughout this endeavor.

First and foremost, I would like to thank Carmen. You gave me the opportunity to do this PhD and all your help, guidance and wisdom was invaluable along the way. From your help interpreting geophysical data to the more philosophical discussions about science, you were there to help me with all of it. I am also deeply indebted to Valentina. You introduced and to the world of numerical modelling and where always there to help, give me your opinion and provide me with feedback and advice. Thank you very much! Susanne, despite the infrequent interactions, your sharp mind was always a big inspiration and I never left any meeting with you without a new insight or idea. Torgeir, thank you for all the help with Lundin and your insights into Corsica.

Roy, this whole thing would not have happened without you. Although the project took another direction, I would never have started it if you would not have pointed me to this opportunity. Thank you very much for introducing me to the University of Oslo, the (geology of the) Oslo region and Norwegian culture in general. I sincerely hope you may run and ski for a long time!

Agi, without your help and guidance the analogue modelling in Rome and analyzing the data would not have been possible. Thank you for the time and patience needed to teach me new analogue modelling skills and how to deal with those insanely stick hands. This leads me to the three lovely months I spent in Rome. I would like to sincerely thank Francesca, Claudio and all the other people at University of Roma Tre for their hospitality. I always felt very welcome and Rome was a wonderful place to spend the autumn of 2017.

Moving to Norway was one of the best things I ever did. Although physically, Oslo is a wonderful place to live, the best part about living there has to be the people. CEED is a really nice place to work and the people are the most important part of that. Everyone was always very open and welcoming, so a big thank you to all the lovely people at CEED. I want to especially thank Eivind and Sruthi for being such lovely office mates and teaching me about Kubb (Eivind) and planetary science (Sruthi). Thanks also to Björn for his patience when helping me with some strange script and Johannes for his seemingly infinite knowledge on all aspects of geology. Hans-Jørgen, thank you for all your advice, your patience (with the Norwegian language and skiing) and your overal friendship. I fondly remember our countless runs, bike rides and ski-trips.

This project was part of the European SUBITOP ITN. Being a part of SUBITOP and sharing the experience with 13 other PhD's was a wonderful experience. The various courses, fieldtrips and conference experiences where lovely and I learnt a lot. So, thank you Nico, Manar, Malwina, Arthur, Eshan, Carlos, KB, Ajay, Antoine, Kristof, Sam,

Jessica, Richard and Boris for your friendship and for teaching me all kinds of things about subduction, tectonics and science in general. I also have to thank Niels and Micha. SUBITIP would not have been possible without your hard work and super smooth organization.

During the final (corona-isolating) stages of my PhD I learnt a lot from the DEEP virtual writing retreat. So I have to thank Matthew, Nanna, Annette and Hanne-Kristin for teaching and helping me write the thesis and starting my (isolated) work days!

There is more to life than just work. In that regard I have to thank all the wonderful people from OSI Friidrett. From running endless loops through the Bislett tunnel in winter or post-run swims in the summer, it was always a lot of fun! Thanks all my 'Oslo' friends for the ski-trips, BBQ's and countless dinners. Thank you to all my Dutch friends who not only made time for during my infrequent visits but remain friends to this day.

Finally, Lisa, thank you so much. You are always there for me and I could not have done this without you.

Joost van den Broek
*July 2020*

# Summary

Microcontinents are pieces of continental lithosphere that detached from their parent continent and are surrounded by oceanic lithosphere. Continental fragments are similarly defined with the exception that they are still attached to their parent continent via highly extended continental crust. Whilst usually associated large-scale continental rifting processes. However, several in-situ microcontinents and continental fragments formed in contemporary subduction systems. However, recognition and understanding of the formation of these features in subduction systems is limited. Therefore, this thesis investigates the processes and parameters that control the formation of such microcontinents and continental fragments in subduction systems. First, I characterize microcontinents and continental fragments in subduction settings by analyzing geological and geophysical data. I then use analogue and numerical modelling to better understand the dynamics of their formation.

The analysis of geological and geophysical data shows that microcontinents and continental fragments tend to form in the back-arc region of long-lived subduction zones that have a complex tectonic setting. The long tectonic histories of the case studies chosen here are reflected in the presence of inherited structures that can, later on, become regions of weakness that preferentially localize deformation. Moreover, I find that that kinematics of back-arc basin opening –and thus microcontinent/continental fragment formation– are oblique or rotational. All studied microcontinents and continental fragments formed quickly (<50 Myr) and in Cenozoic times, suggesting that subduction associated microcontinents are generally short lived.

Because the presence of inherited structures was proven to be a common feature, I conducted analogue modelling to investigate the relationship between the driving forces of overriding plate extension and the location of inherited weak zones. Results indicate that extension driven by shallow lithospheric forces (e.g. generated by a moving wall in our experiments) localizes extension close to the trench/wall. In this scenario, extension is thus controlled by the lithosphere. On the other hand, extension driven by a subducting slab is dominated by the mantle and results in more distal localization of extension. The subduction results are in accordance with previous work and matches observed back-arc basin locations.

The other important common denominator is the oblique and/or rotational kinematics during microcontinents formation in subduction zones. To investigate the role of inherited weak zones together with the effect of rotational kinematics on continental fragment formation I conducted numerical experiments. Arrival of a buoyant continental block at the subduction interface exerts a torque on the trench that results in trench rotation and retreat. Results indicate that both the presence of an inherited structure and rotational trench kinematics are required for back-arc extension to localize. Furthermore, I find that the required inherited structure must be weaker than

the surrounding lithosphere by at least one order of magnitude for sufficient strain to localize.

My results indicate that the presence of inherited structures as well as rotational or oblique extensional kinematics are important ingredients for microcontinent or continental fragment formation in subduction systems. Such complex requirements suggests multiple mechanisms can explain microcontinent and continental fragment formation in subduction systems. On a more fundamental level, it appears that rapid changes in subduction dynamics can act as a trigger for microcontinent or continental fragment formation in subduction systems.

This new knowledge about formation of microcontinent and continental fragments increases our understanding about the relationship between subduction dynamics and surface tectonics, allows us to identify new in-situ or accreted microcontinents, and understand Earth's continental crust evolution through time.

# Samenvatting

Microcontinenten zijn stukken continentale lithosfeer die losgeraakt zijn van een groter (hoofd)continent en omringd zijn door oceanisch materiaal. Een continentaal fragment is een vergelijkbaar fenomeen, het enige verschil is dat het nog vast zit aan het oorspronkelijke continent via sterk uitgerekte continentale korst. Formatie van deze continentale fragmenten en microcontinenten is typisch geassocieerd met grootschalige continentale rift systemen. Echter, verscheidene hedendaagse subductie systemen bevatten ook microcontinent en continentale fragmenten. Het herkennen en begrip van deze fenomenen in een subductie situatie is beperkt. Deze scriptie onderzoekt dan ook hoe microcontinenten en continentale fragmenten vormen in subductie systemen. Ik start met het analyseren van geologische en geofysische data. Deze analyses stellen mij in staat om microcontinenten en continentale fragmenten in subductie systemen beter te identificeren en te begrijpen. Vervolgens gebruik in analoge en numerieke modeleer technieken om meer te weten te komen over de formatie dynamiek.

Geologische en geofysische observaties laten zien dat de onderzochte microcontinenten en continentale fragmenten vaak vormen in achterboog bekkens (back-arc basins). De desbetreffende subductie zones hebben vaak een lange tektonische geschiedenis en een tektonisch complexe omgeving. De lange tektonische geschiedenis suggereert dat de bovenliggende plaat geërfde structuren bevat. Deze structuren zijn het resultaat van eerdere deformatie en zijn zwakker dan het omliggende gesteente. Bij een nieuwe deformatie fase zal deze structuur dus eerder (re)activeren. De gerelateerde sedimentaire bekkens openen zich vrijwel altijd op een schuine of draaiend manier. Het feit dat alle bestudeerde voorbeelden zijn gevormd in het Cenozoïcum en dat formatie relatief kort duurt (¡50 Myr) suggereert dat microcontinenten en continentale fragmenten in subductie systemen een kort leven beschoren is.

De aanwezigheid van geërfde structuren was een gemeenschappelijke observatie in de bestudeerde voorbeelden. Om de relatie tussen extensie van de bovenliggende plaat, geërfde structuren en de krachten die extensie aandrijven beter te begrijpen gebruik ik analoge modellen. Resultaten laten zien dat wanneer extensie ondiep wordt aangedreven (door een bewegende muur), de extensie zich voornamelijk dichtbij het aangrijppunt (de bewegende muur) lokaliseert. Extensie als gevolg van subductie is wijder verspreid en lokaliseert zich verder van de trog. De subductie resultaten zijn overeenkomstig met eerder onderzoek alsmede met observaties van natuurlijke achterboogbekken.

Naast dat alle bestudeerde voorbeelden geërfde structuren bevatten maken alle bestudeerde voorbeelden zich los van het oorspronkelijke continent via een draaiende of schuine beweging. Om de relatie tussen geërfde structuren en draaiende bekken opening te bestuderen gebruik ik driedimensionale numerieke modellen. Door botsing van een continentaal blok op de neergaande plaat met de trog veroorzaak ik rotatie in de

bovenliggende plaat. Deze rotatie zorgt voor een verandering in de stresssituatie hetgeen resulteert in extensie in de bovenliggende plaat. De resultaten laten overduidelijk zien dat zowel zwakkere geërfde structuren alsmede draaiende extensie vereisten zijn voor het lokaliseren van deformatie en het vormen van een continentaal fragment. Verder komt uit de resultaten naar voren dat voor voldoende deformatie te lokaliseren, de geërfde structuren minstens een orde van grote zwakker moeten zijn dan het omliggende materiaal.

Mijn resultaten impliceren dat geërfde structuren en een schuine of draaiende extensie kinematica belangrijke ingrediënten zijn voor de formatie van microcontinenten of continentale fragmenten in een subductie omgeving. Deze complexe vereisten suggereren dat de formatie van microcontinenten en continentale fragmenten in subductie systemen door meerdere mechanismen te verklaren is. Op een meer fundamenteel niveau suggereren mijn resultaten dat rappe veranderingen in subductie dynamiek een onderliggende oorzaak kan zijn.

De resultaten van deze scriptie zorgen ervoor dat nieuwe microcontinenten of continentale fragmenten eenvoudiger en beter kunnen worden geïdentificeerd. Het beter begrijpen van de formatie van microcontinenten en continentale fragmenten in subductie systemen resulteert ook in een beter begrip van de relatie tussen subductie dynamiek en tektonische processen aan de oppervlakte. Dit kan dan gebruikt worden voor het verbeteren van tektonische reconstructies. Tot slot kunnen mijn resultaten gebruikt worden om de evolutie van de continentale korst op Aarde beter te begrijpen.

# Sammendrag

Mikrokontinenter er små biter av kontinental litosfære som er separert fra en større kontinental, tektonisk plate og er omringet av oseanisk litosfære. Kontinentale fragmenter har en lignende definisjon, men fragmentene henger fortsatt sammen med en større kontinental tektonisk plate via en sone med fortynnet kontinental skorpe. Mikrokontinenter og kontinentale fragmenter er vanligvis assosiert med dannelsen av riftede marginer som separerer store kontinentale landmasser. Men flere mikrokontinenter og kontinentale fragmenter er også funnet i moderne subduksjonssystemer verden rundt. Anerkjennelse og forståelse av disse funksjonene is subduksjonssystemer er begrenst. Derfor, denne oppgaven undersøker prosesser og parametere som kontrollerer dannelsen av mikrokontinenter og fragmentering av kontinental skorpe i subduksjonssystemer

Ved å bruke geologiske og geofysiske data har jeg identifisert og karakterisert flere mikrokontinenter og kontinentale fragmenter i subduksjonssettinger. De har en tendens til å dannes i øybuesettinger hvor det har foregått subdusksjon i lang tid og hvor subduksjonsonene har komplekse geometrier. Den lange tektoniske historien til systemene som er undersøkt indikerer at pre-eksisterende svakhetssoner fra tidligere geologiske hendelser er tilstede. Kinematikken til dannelsen av mikrokontinenter og kontinentale fragmenter og den assosierte bassengåpningen har ofte en komponent av skrå- eller roterende deformasjon. Alle eksemplene studert her har blitt dannet raskt (¡50 Myr) og i Kenozoikum, hvilket indikerer at subduksjonsrelaterte mikrokontinenter har en relativ kort levetid.

I denne oppgaven har jeg utført analoge eksperimenter som ser på relasjonen mellom ekstensjons drivkreftene i den øvre platen i subduksjonssystemet, den kinematiske utviklingen til denne platen og plassering av pre-eksisterende svakhetssoner. Resultatene indikerer at ekstensjon drevet av grunne litosfæriske krefter (f.eks. en vegg som blir flyttet) lokaliserer ekstensjon nær subduksjonsgrøften/veggen. Ekstensjon som blir drevet av en subduserende plate resulterer i mer distal lokalisering av ekstensjonen. Resultater fra subduksjon eksperimenter er også i overenstemmelse med tidligere forskning og observasjoner av hvor øybuesystemer dannes.

Alle eksempler på mikrokontinenter og kontinentale fragmenter i subduksjonssettinger skra eller roterende kinematikk under dannelse. Å etterforske rollen till pre-eksisterende svakhetssoner og roterende subduksjonskinematikk på mikrokontinent/kontinental fragment dannelse bruker jeg numeriske eksperimenter. Resultatene indikerer at både tilstedeværelsen av pre-eksisterende strukturer og rotasjoner av subduksjonsgrøften er nødvendige for at ekstensjon i øybuen skal lokaliseres. Rotering av subduksjonsgrøften kan oppnås ved at en lett kontinentalblokk når subduksjonssonen. Denne blokken induserer så et moment på subduksjonsgrøften som resulterer i at subduksjonsgrøften roterer og trekker seg tilbake. Videre, må den pre-eksisterende strukturen være svakere enn den rundt liggende litosfæren med minst en størrelsesorden for at tilstrekkelig deformasjon skal lokaliseres.

Mine resultater viser derimot at tilstedeværelsen av pre-eksisterende svakhetssoner så vel som rotasjon- og skrå ekstensjons kinematikk er viktig. Silke komplekse kravene for å danne mikrokontinenter og kontinentale fragmenter i subduksjonssystemer viser at flere dannelsesmekanisme kan forklare dannelsen. De fundamentale implikasjonene er at raske forandringer i subduksjonsdynamikken kan være potensielle utløsere for dannelsen av mikrokontienter/kontinent fragmenter i subduksjonssystemer.

Resultater fra oppgaven min tillater bedre identifikasjon av mikrokontinenter og kontinental fragmenter i subduksjonssystemer. Det også øke vår forståelse av forhold mellom subduksjonsdynamikk og flatetektonikk. Sistntnevnte kan også brukes till forbedre av platetektoniske gjenoppbyging. Endelig, resultater min kan også bidra til bedre forstå av Jordens kontinental skorpe evolusjon.

# Contents

# Part I: Kappa

# 1

# Aim of the thesis

A microcontinent is a small piece of continental lithosphere that detached from its parent continent and is surrounded by oceanic crust (Scrutton, 1976) (Figure 1.1). Continental fragments are similar features, except that highly extended continental crust connects them to their parent continent (Lister et al., 1986) (Figure 1.1). Only a handfull of microcontinents where initially identified (Scrutton, 1976). This is pherhaps unsurprising, as microcontinents are often submerged and/or found in remote locations. Since then, improvements in the resolution and precision of geophysical data resulted in a significant increase in the number of identified microcontinents and continental fragments (e.g. Gaina and Whittaker, 2020; Tetreault and Buiter, 2014).

Understanding the evolution of microcontinents and continental fragments is important as they play an important role in the evolution and global distribution of continental crust. The majority (86%) of continental crust on Earth is non-cratonic in nature (Paper 1 – this thesis). This non-cratonic continental crust is distributed over the

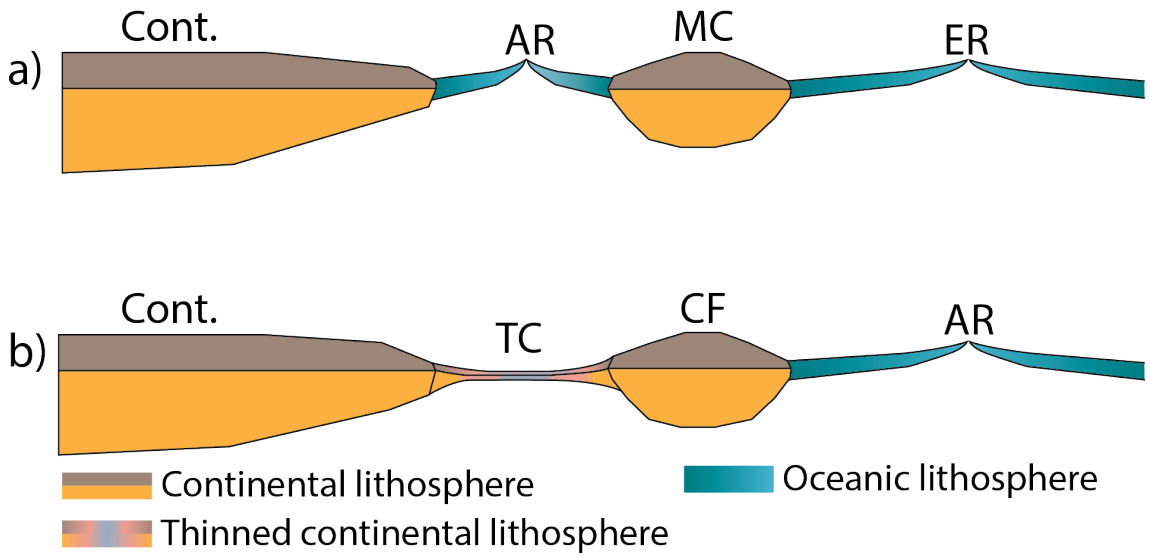


**Figure 1.1:** Schematic cartoon visually depicting the definition of (a) microcontinents and (b) continental fragments. The active and extinct ridges bordering the microcontinent (a) imply that the ages of these oceanic basins are ages. Note that in nature, the active ridge can be extinct and vice versa. Cont.: (Parent) continent; MC: Microcontinent; CF; Continental fragment; TC: Thinned continental lithosphere; AR: Active spreading ridge; ER: Extinct spreading ridge.

Earth in a very heterogeneous manner (Bouysse, 2014), suggesting that amalgamation of continental terranes is an important part of continental growth. The deformation associated with this amalgamation often results in the formation of inherited structures, suggesting that continental crust is also rheologically heterogeneous. As such, the redistribution of continental crust due to microcontinent formation likely plays an important role in the evolution of continental crust.

As the number of identified microcontinents and continental fragments increased in the last decades, so did the interest of the scientific community in their formation and evolution. The definition of microcontinents and continental fragments places constraints on any proposed formation mechanism. First, their formation requires extension between the parent continent and the future microcontinent/continental fragment. This extension then has to relocate on the other side of the microcontinent, abandoning the initial plate boundary and isolating a piece of continental lithosphere (Figure 1.1).

As most known microcontinents are identified in full-fledged oceanic basins such as the Atlantic Ocean, their formation is classically associated with the diverging stages of the Wilson cycle (Box 1) (e.g. formation of 'Atlantic type' rifted margins). However, several present-day subduction systems contain microcontinents and continental fragments (Manuscript 1 – this thesis). And whilst the diverging phases of the Wilson Cycle create oceanic basins, plate convergence and the associated subduction results in the destruction of such basins (Box 1). Formation of microcontinents or continental fragments in such a convergent setting still requires continental rifting. However, the tectonic setting in which they form is fundamentally different.

Because microcontinents and continental fragments consist of continental lithosphere, they can potentially exert significant influence on the subsequent regional tectonic evolution. However, at present, microcontinents or continental fragments in subduction settings are often overlooked and our understanding of their formation is limited. To address these issues, this thesis investigates the processes and parameters controlling the formation of microcontinents/continental fragments in subduction settings.

By identifying present-day microcontinents and continental fragments in subduction zone settings and studying their geological history I identify controlling parameters that may have resulted in their formation. Secondly, using analogue modelling techniques, I study the relationship between forces driving overriding plate extension and the role of inherited lithospheric structures. Finally, I investigate the interaction between changes in subduction dynamics and heterogeneous overriding continental lithosphere, and their role in continental fragment formation using numerical modelling techniques.

## **Box 1:** The Wilson Cycle

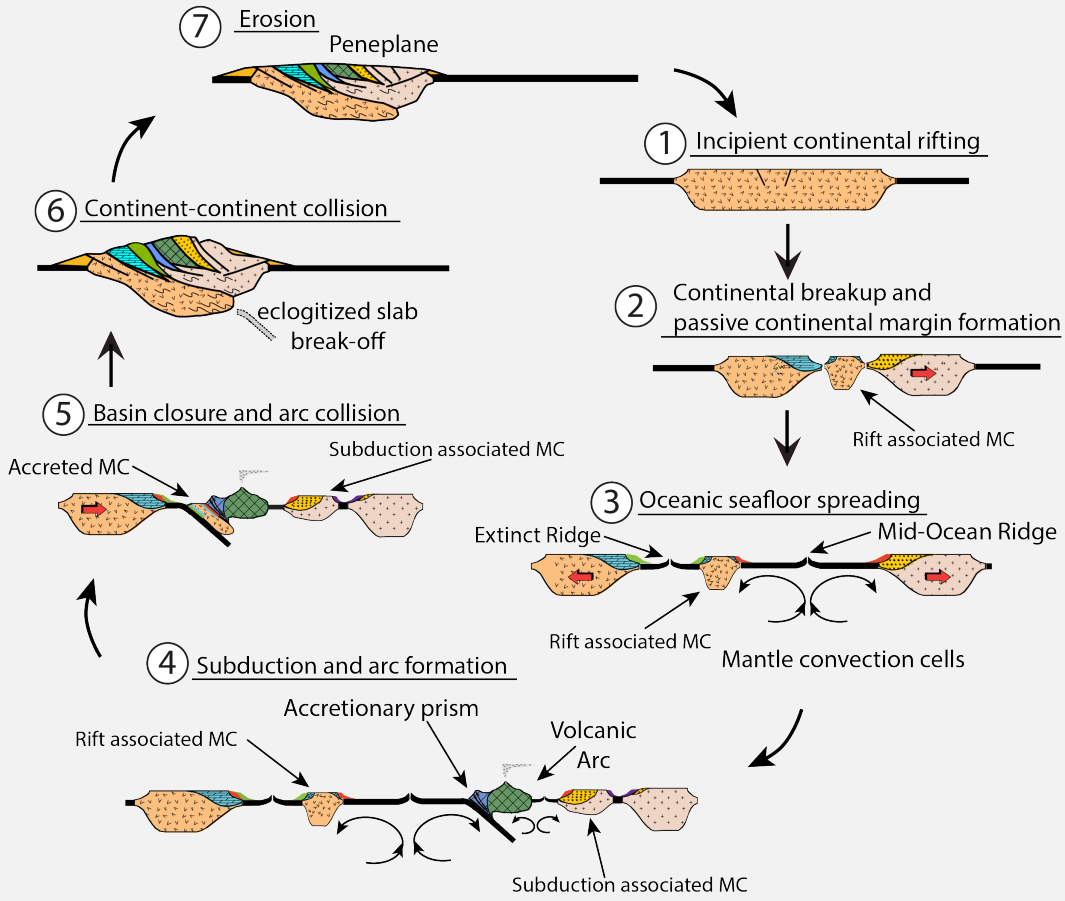


Schematic cartoon depicting the various stages of the Wilson Cycle. Figure modified from Fichter (1996) via Kjøll (2019)

The **Wilson cycle**, named after James Tuzo Wilson, describes the cyclical evolution of continental margins and oceans due to plate tectonics (Dewey and Burke, 1974; Wilson, 1966). Incipient continental rifting starts when continental lithosphere is extending (1) followed by possible rift relocation that generates continental blocks of various thickness. One of the rifting episodes will end up in continental breakup, (2) followed by oceanic seafloor spreading This process forms rifted continental margins and adjacent oceanic basins (3). Subduction of oceanic lithosphere initiates and during subduction, formation of subduction associated microcontinents occur (4). The oceanic basin is gradually destroyed until (5) continental collision occurs (6), forming a mountain belt. Subsequent erosion and gravitational collapse thins the lithosphere, eventually forming a peneplane (7).

# 2

# Tectonic settings of microcontinent formation

The Wilson Cycle plays an important role in the (re)distribution of Earth's continental crust (Box 1). Because microcontinents and continental fragments can move (relatively) independent from their parent continents, they play an important role in said (re)distribution of continental crust. As such, formation of microcontinents and continental fragments –in either continental rifted margin or subduction settings– can be considered important intermediate stages in the Wilson Cycle.

## 2.1 Microcontinent formation associated with rifted continental margins

Classical examples of microcontinents and possible mechanisms for their formation where first described for passive margin settings (Nunns, 1983; Scrutton, 1976; Vink et al., 1984). Over the last few decades, our understanding of rifted margin formation and geophysical techniques have increased significantly. The amount of identified microcontinents and continental fragments has grown in parallel with these developments. Initially only a few microcontinents where defined, with the Seychelles bank being the classic example (Scrutton, 1976). Since then, the number of identified microcontinents, mainly in extensional setting associated with passive margins, has increased significantly (Figure 2.1) (e.g. Gaina and Whittaker, 2020; Tetreault and Buiter, 2014). This increase in identified microcontinents led to a variety of proposed mechanisms to explain their creation.

This knowledge is important for understanding the overall geometry of microcontinents and continental rifting and break-up processes. This knowledge is also useful to decipher the formation of microcontinents and continental fragments in subduction systems. Therefore I present a brief overview of microcontinents and continental fragments formed in 'classic' rifted margin settings.

To explain the isolation of continental slivers from a larger continental mass, some authors propose a plate boundary relocation (or rift jump) due to impinging of a mantle plume on the continental lithosphere adjacent to an already active spreading ridge (Gaina et al., 2003; Müller et al., 2001). In this case, the continental lithosphere


**Figure 2.1:** Overview of microcontinents and continental fragments around the globe. Figure modified from Tetreault and Buiter (2014). AM: Alpha Mendelev Ridge, B: Bower's Ridge, Bo: Bounty Plateau, BL: Bill Bailey and Lousy banks, C: Campbell Plateau, CH: Challenger Plateau, Ck: Chukchi Plateau, CS Corsica-Sardinia block, Ct: Chatham Rise, EL: Elan Bank, Ex: Exmouth Plateau, ET: East Tasman Plateau, F: Faroe Bank, FC: Flemish Cap, FP: Falkland Plateau, HR: Hattor and Rockall Banks, JM: Jan Mayen, LH: Lord Howe Rise, LM: Lomonosov Ridge, , MB: Macclesfield Bank, NA: Naturaliste Plateau, N: Norfold and Fairway Ridges, NR: Northwind Ridge, P: Porcupine Bank, Q: Queensland Plateau, RB: Reed Bank S: Seychelles, SGM: South Georgia Microcontinent, SOM: South Orkney Microcontinent ST: South Tasman Plateau.

weakens due to the thermal effect of the mantle plume, which induces rifting and continental breakup (Figure 2.2a). However, more recent work indicates that whilst such excessive magmatism might play an important role, it is unlikely that such a large thermal anomaly is the only mechanism driving microcontinent formation (Gaina et al., 2009).

Molnar et al. (2018) conducted analogue experiments that indicate a pre-existing weak zone in the lithosphere as well as rotational extensional kinematics are required to form a microcontinent (Figure 2.2b). Nemcok et al. (2016) proposes four possible formation mechanisms; microcontinents can be released due to (1) isolation of a continental block due to competing horsetail faults nucleating at the propagating end of a large strike-slip fault (Figure 2.2c), (2) competing strike-slip faults (Figure 2.2d), (3) multiple tectonic events with different stress orientations and (4) competing rift zones.

The concept of competing rift zones is also invoked by various other authors. Abera et al. (2016) suggested a conceptual formation mechanism whereby an active spreading

ridge becomes magma starved and cools down, strengthening the ridge. Subsequent extension then localizes in a different position on the continent owing to the fact that continental lithosphere is weaker than oceanic lithosphere (Abera et al., 2016). Based on conjugate margins in the North Atlantic, Peron-Pinvidic and Manatschal (2010)suggest that microcontinents and continental fragments can form due to differential thinning on pre-existing or early formed structures (Figure 2.2e). Microcontinent formation is then associated with specific rifting sequences during rifted margin formation.

Whilst the concept of competing rifts is conceptually difficult to envision – an active zone of extension or spreading is already mechanically very weak – results from numerical modelling provide support for such a mechanism (Naliboff and Buiter, 2015; Tetreault and Buiter, 2018; van Wijk and Cloetingh, 2002). In these mechanisms, the rifts do not really compete as much as laterally relocate the extension (section 2.2).

The abundance of microcontinents and continental fragments in present day basins as well as the variety in their proposed formation mechanisms suggests that they can form due to numerous different processes. This is perhaps unsurprising as our understanding of continental rifting and rifted margin architecture has advanced significantly since the early conceptual models of McKenzie (1978) and Wernicke (1985).

## 2.2 Continental rifting and rifted margins

The margins of microcontinents and continental fragments can be considered as rifted margins. To understand their structure and associated dynamics, it is therefore important to understand continental rifting processes.

Continental rifting is typically studied using analogue or numerical modelling or via observations of rifted margins and their architecture. The latter is commonly done using geophysical techniques (e.g. Ding et al., 2013; Franke et al., 2011) or by making field observations on accreted examples (e.g. Andersen et al., 2012; Jakob et al., 2019).

The numerous studies on various rifted margins show that there is high variety in rifted margin architecture. For example, the South China Sea margin is very wide ( 1000 km ) and relatively symmetric (Franke et al., 2014), whereas the Angola-Brazil margins are very asymmetric (Peron-Pinvidic et al., 2013). And whilst the rifted Vøring margin was heavily modified by break-up related magmatic activity (Planke et al., 2005), other margins, like the Iberian rifted margin offshore Portugal, developed in a magma-starved regime (Peron-Pinvidic et al., 2013).

### Dynamics of continental rifting

Despite the high variability in rifted margin architecture, the first order evolution from rifting to breakup usually follows a similar (first-order) pattern. Incipient continental rifting starts by distributed extension of the lithosphere. Normal faulting accommodates extension in the brittle domain whilst at deeper levels ductile shear zones accommodate extension. Subsequent thinning of the lithosphere and the accompanying isostatic compensation result in rising of the underlying mantle. This potentially results in decompression melting. These hot and buoyant melts then migrate upwards and may intrude the overlying rocks or erupt at the surface. Continued localization of extension in the center of the rift may eventually lead to breakup of the continental lithosphere. A new mid-oceanic ridge then forms, accommodating all divergence be-

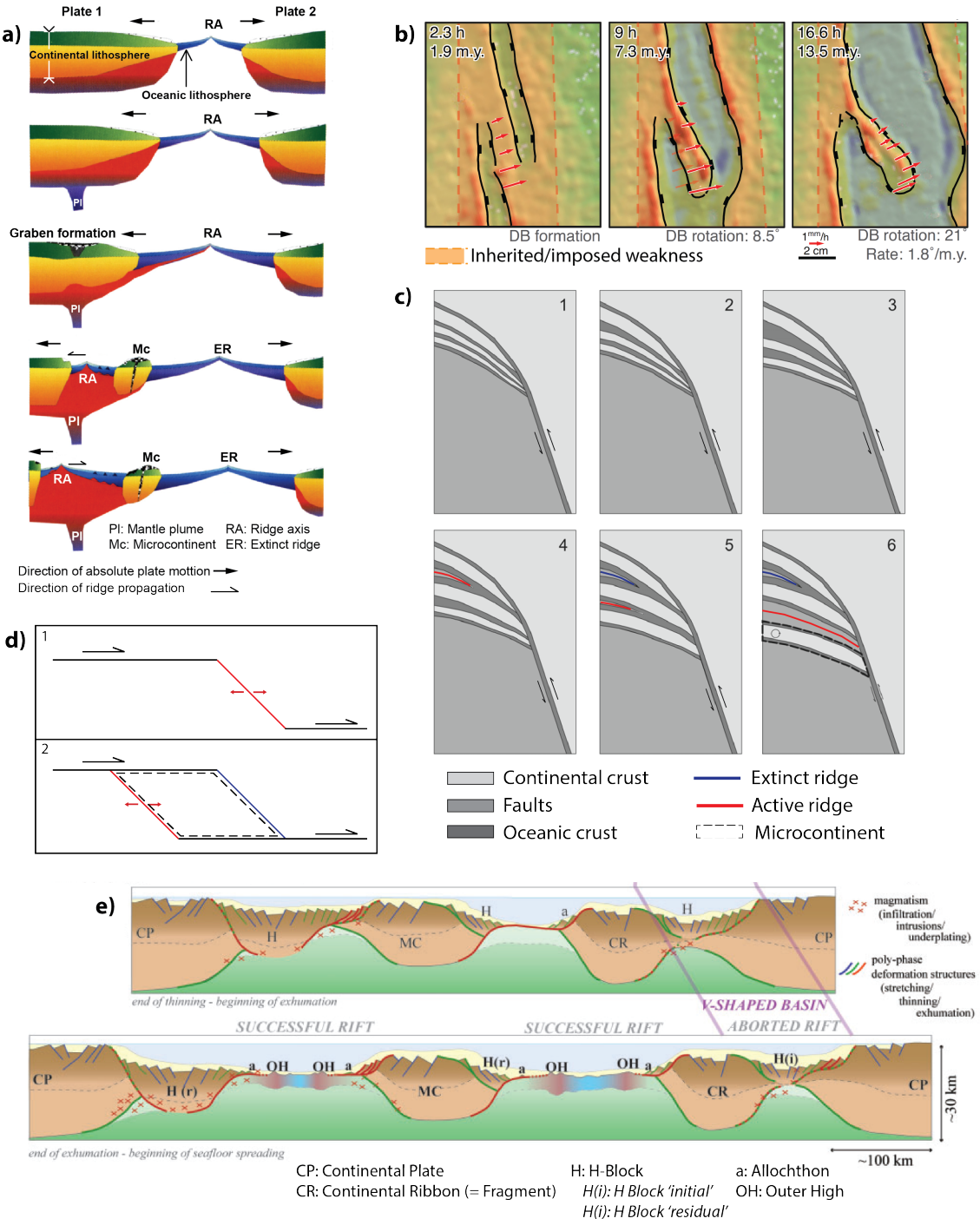


**Figure 2.2:** Overview of the generally proposed mechanisms for microcontinent formation in rifted margin settings. a) Microcontinent and continental rift formation due to competing rift zones (Peron-Pinvidic and Manatschal, 2010). b) Microcontinent formation due to mantle plume impingement (Gaina et al., 2003). c) Microcontinent formation due to competing horsetail structures (Nemcok et al., 2016). d) Microcontinent formation due to rotational rifting and inherited weakzones (Molnar et al., 2018). e) Microcontinent formation due to competing transform/wrench faults (legend as in panel c) (Nemcok et al., 2016).

tween the two newly formed continental plates. At this point all extensional structures in the continental lithosphere that accommodated extension become inactive, forming a rifted margin.

The thinning and extension of the continental lithosphere that occurs during rifting is driven by divergent tectonic forces. These forces often originate at plate boundaries or from viscous coupling between the lithosphere and the convecting mantle (e.g. Ziegler, 1992). Plate boundary forces originate from slab pull, ridge push or frictional forces on the plate interface (e.g. Forsyth and Uyeda, 1975). There are thus multiple forces that drive and/or influence continental rifting and (potential) subsequent breakup.

Although the numerous oceanic basins around the world indicate that continental breakup is common, several authors argue that the horizontal forces that drive extension are insufficient to produce crustal separation (e.g. Buck, 2004; Ziegler and Cloetingh, 2004). Indeed, initiation of continental rifting is no guarantee for achieving continental breakup and the rates and timespan of rifting vary widely (Box 2.2). Several mechanisms have been proposed to address this discrepancy.

Some authors suggest that the interaction of a mantle plume with the (extending) lithosphere aids continental rifting, yielding crustal separation (e.g. Buiter and Torsvik, 2014). Other authors propose that positive interference between mantle flow induced shear stresses and far field stresses can aid continental rifting and result in breakup (e.g. Ziegler, 1992; Ziegler and Cloetingh, 2004). Alignment of the mantle flow induced stress and far field stress vectors can then result in sufficient stress for continental breakup to occur.

## **Box 2:** Continental rifting variability

**Length and speed of continental rifting**
The length as well as the extension velocities of continental rifting can vary widely. Rifting of the western Norwegian margin initiated around Late Paleozoic/Permian times (∼300-250 Ma), but breakup occurred only in the Early Eocene (∼54 Ma) (Peron-Pinvidic et al., 2013). On the other hand, rifting in the Gulf of Aden initiated around 35 Ma and breakup occurred around 17.6 Ma (Leroy et al., 2004). Furthermore, a compilation of the tectonic histories of various rifted margins as well as analytical and numerical experiments strongly suggest that rifting starts slow but rapidly increases in the ∼10 Myr before breakup (Brune et al., 2016).

**Failure of continental rifting**
Initiation of continental rifting is no guarantee for achieving continental breakup. In the North Sea basin rifting started around Late Permian to Early Triassic times, (partly) accommodating the North-American – Eurasian divergence. The, during Cretaceous times, rifting activity in the North Sea declined as extension focused on the axis of future crustal separation (e.g. the North Atlantic spreading ridge) (e.g. Ziegler, 1992). The reasons for rift abandonment can be changes to the stress state, localization of deformation elsewhere or just insufficient stress and/or a (too) strong lithosphere

Finally, the presence of inherited weak zones is also suggested as an effective mechanism that aids continental rifting. Inherited weak zones form during previous tectonic activity where deformation of the crust or lithosphere results in permanent damage (more details in section 2.3). The resulting structure is weaker with respect to its surroundings and subsequent reactivation of this structure then occurs at a lower stress. The preferential activation of these structures then also localizes deformation, aiding continental rifting and, because these inherited structures are weaker, achieving breakup requires less stress.

## Rifted margin architecture

As highlighted at the beginning of section 2.2 , continental rifted margins display a wide variety of architectures. One of the main spectra on which rifted margins are classified is the magma-rich to magma-poor spectrum (Figure 2.3.).

In magma-poor rifted margins the tectonic processes are dominant. Whilst there still are volcanic intrusions and extrusion, the total volume of volcanics is significantly lower than that of magma-rich margins (Tugend et al., 2018; Whitmarsh et al., 2001). Due to the low magma supply, continental extension and crustal thinning accommodate most of the extension (Figure 2.3). This can result in local exhumation of sub-continental lithospheric mantle (e.g. Peron-Pinvidic and Manatschal, 2009; Peron-Pinvidic et al., 2013).

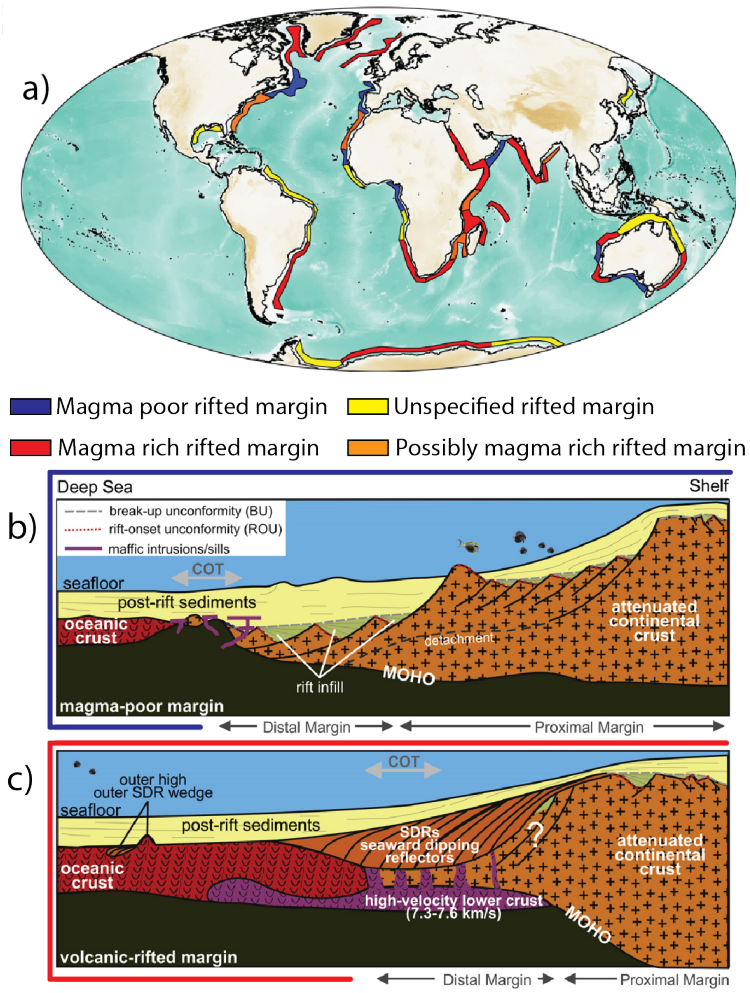


**Figure 2.3:** a) Overview of rifted margin types and their distribution around the world (figure from Berndt et al. (2019)). Schematic cartoon displaying the general architecture of b) magma poor and c) magma rich rifted margin end-members (figure from Franke (2013)).

At magma-rich rifted margins magmatic processes related to decompression melting or elevated temperatures at the lithosphere-asthenosphere boundary dominate over tectonic processes. These margins often contain high volumes of intruded and extruded volcanics such as basaltic lava flows and mafic intrusions in the lower crust (Figure 2.3) (e.g. Franke, 2013; Jakob et al., 2019).

In addition to the magmatic budget, rifted margin architecture is generally thought to be influenced by coupling between the mantle and the

lithospheric mantle as well as coupling of the brittle and ductile crust. This coupling is dependent on the initial temperature and rheology of the lithosphere, extension velocities and the occurrence of periods of tectonic quiescence (Brune et al., 2017; Naliboff and Buiter, 2015; Svartman Dias et al., 2015; Tetreault and Buiter, 2018).

Very low crust-mantle coupling occurs when the crust is very hot and/or weak or extension is ultra-slow. This situation tends to produce very wide symmetric margins (Brune et al., 2017; Tetreault and Buiter, 2018) . Very high coupling generally occurs for a cold and strong crust or very fast extension rates. This tends to produce symmetric, narrow margins (Svartman Dias et al., 2015; Tetreault and Buiter, 2018).

Asymmetric margins are produced by a variety of initial architectures and processes. Moderately weak crust or the presence of crustal ductile layers decrease coupling, resulting in asymmetric margin formation (Brune et al., 2017; Tetreault and Buiter, 2018). In very low strain rate scenarios, conductive cooling rates can be higher than deformation rates, resulting in local strengthening of the lithosphere and lateral relocation of extension (Naliboff and Buiter, 2015; Sonder and England, 1989; van Wijk and Cloetingh, 2002).

From above it is clear that final rifted margin architecture is influenced by a wide variety of processes and parameters. As a result, an exact classification of a rifted margin is often difficult as many margins fall somewhere on a spectrum. Furthermore, the factors affecting margin architecture often change during rift evolution. For example, many margins contain features of both end-members and some margins start with magma-poor rifting and change into magma-rich margins (e.g. the Mid-Norwegian margin - Lundin and Doré (2011)) or vice versa. Rheological changes due to (local) cooling or heating of the lithosphere or positive feedback loops in rheological behavior also occur, influencing rift evolution (Brune et al., 2016; Svartman Dias et al., 2015). Therefore, the dynamic nature of rifted margin formation and the high observed variability indicates that the final rifted margin architecture is non-unique with respect to the configuration of the pre-extensional lithosphere (e.g. Brune et al., 2017; Tetreault and Buiter, 2018).

### The Continent-Ocean Boundary

The Continent-Ocean Boundary (COB) defines the border between continental and oceanic lithosphere. It is of interest as it defines two fundamentally different domains; inboard of the COB lies the rifted margin, formed by tectonic extension whilst outboard of the COB the lithosphere is formed by oceanic lithosphere. However, this binary classification, whilst useful at times, comes with a high degree of uncertainty and bias (Eagles et al., 2015). In case of microcontinents or continental fragments, detailed study of the COB can provide clues to the processes and mechanisms active during breakup. Furthermore, the COB defines the (exact) extent of the feature and it is relevant for area and volume calculations.

Continental breakup and the onset of seafloor spreading is very rarely, if ever, an abrupt event. As such there is often a zone of crust that has geophysical characteristics of both continental and oceanic crust. For example, a succession of positive and negative magnetic anomalies (often referred to as "magnetic stripes") are normally associated with oceanic lithosphere. However, they can also form in transitional crust due to magmatic intrusions in extended continental crust or the presence of exhumed serpentinised mantle (Funck et al., 2003; Sibuet and Tucholke, 2013). The presence of transitional crust

along continental margins complicates a binary COB classification; this zone is often referred to as the Continent-Ocean Transition zone (COT).

The rifted margin archetype exerts a significant influence on the nature the COB/COT. In magma rich settings, high volumes of available magma often erupt on the margin, forming large sequences of Seaward Dipping Reflectors (SDR's). These SDR's often have a strong signature in geophysical data (e.g. isotropic seismic signature, strong magnetic and gravity signals). As crustal thinning occurs over relatively short distances, the COT is relatively abrupt (50-100 km) and it is usually located close to, or below the SDR sequence (Franke, 2013). However, the outboard edge of the COT can be difficult to identify due to the heavily intruded nature of the transitional crust (Minshull, 2009).

**Box 3:** 'Layer 3'

Based on seismic refraction experiments, layer 3 is defined as the lower crustal layer of oceanic lithosphere. It is generally considered to have a P wave velocity of 6.7-7.3 km $s^{-1}$ and a low velocity gradient of 0-0.2 $s^{-1}$ [Mutter and Mutter, 1993]. Layer 1 describes sediments and layer 2 is the upper oceanic crust (e.g. Mutter and Mutter, 1993).

Lacking significant volumes of magma, the COT at magma-poor rifted margins is generally considered to contain exhumed mantle rocks (Eagles et al., 2015; Reston, 2009; Whitmarsh et al., 2001). In magma-poor settings, determining the COB/COT is oftentimes difficult. In seismic reflection data the COB/COT generally lacks a clear Moho reflector (Minshull, 2009). Seismic refraction experiments, if properly spaced, can be used to identify the COT (Reston, 2009). Generally, COT have a high P wave velocity at shallow depths (5 km s-1 at the surface to 8 km s-1 at 5 km depth) and an intermediate velocity gradient (0.2 s-1) (Minshull, 2009; Reston, 2009). Based on the extensively studied Iberian rifted margin, Minshull (2009) proposed that the absence of the lower crustal layer 3 (Box **??**) is an additional indication for transitional crust.

Ideally, a wide variety of geophysical techniques is needed to allow relatively precise identification of the COB/COT (e.g. Eagles et al., 2015; Minshull, 2009). The resolution of geophysical data is generally considered to be on the order of 10-100 km (Eagles et al., 2015). However, global compilations show larger variations in linear COB', suggesting that interpretation adds some extra variability (Eagles et al., 2015).

## 2.3 Subduction and subduction margins

In this section, I briefly describe some aspects of the subduction processes that are important and relevant for microcontinent and continental fragment formation in subduction systems. Subduction is the process whereby one tectonic plate (usually oceanic in nature) moves underneath another one and sinks into the Earth's mantle (Box 2.3). In terms of global tectonics, subduction plays a crucial role by accommodating plate convergence. As such, it is also an important stage in the Wilson Cycle.

Stable, long-lasting subduction requires the down-going slab to be negatively buoyant with respect to the surrounding mantle. This negative buoyancy is provided by the cold and dense oceanic lithosphere which results in a slab pull force ($F_{SP}$) (Box 2.3).

The slab pull force is one order of magnitude larger than all other forces acting on the down going plate and is thus the main driver of subduction (Forsyth and Uyeda, 1975).

The interplay between the various forces acting on the plates controls the evolution of subduction and the deformation of the subducting and overriding lithosphere. Changes in subduction dynamics are likely to induce changes in the surrounding tectonic setting. Terrane accretion, the formation of inherited structures, and back-arc extension are of particular importance in the context of this thesis.

## **Box 4:** Forces in Subduction systems

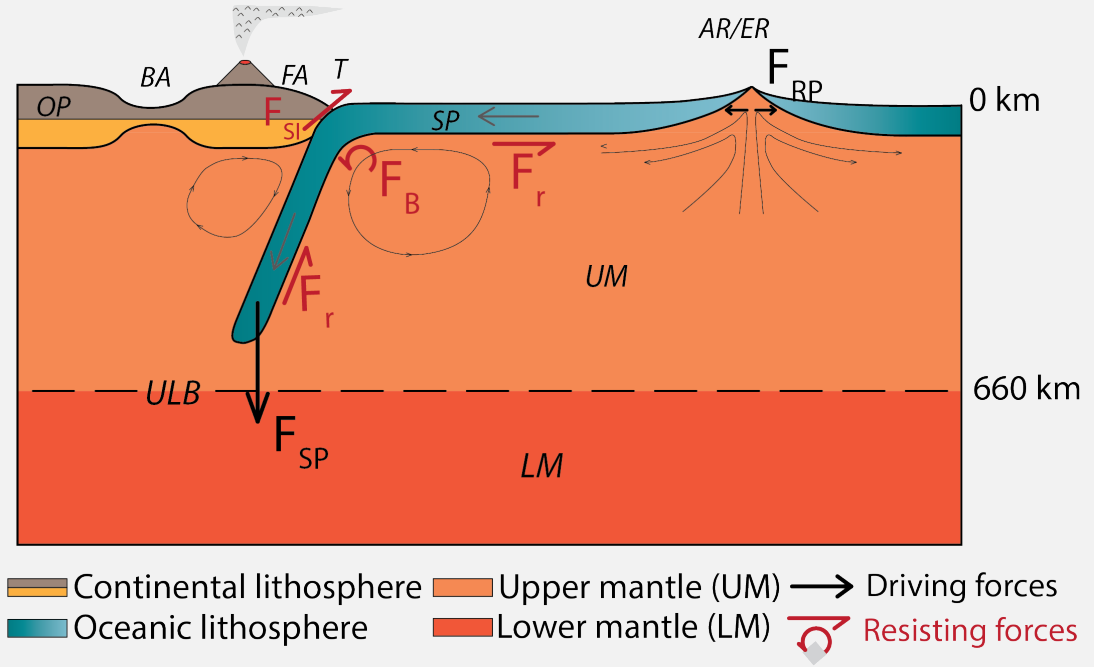


2D cartoon of an oceanic-continental subduction system. Labels depict the main forces and features relevant for this thesis. $F_{SP}$: Slab pull force; $F_{RB}$: Ridge push force; $F_r$: Viscous resistance force; $F_B$: Plate bending force; $F_{SI}$: Frictional resistance force on subduction interface; OP: Overriding plate; SP: Subducting plate; BA: Back-arc; FA: Fore-arc; T: Trench; AR/ER: Active or extinct spreading ridge; UM: Upper mantle; LM: Lower mantle; ULB: Upper-Lower mantle boundary.

Due to their large magnitude, slab pull forces are also considered to be the major driver of plate tectonics (Forsyth and Uyeda, 1975; Turcotte and Schubert, 2002). In addition to the dominant slab pull force ($F_{SP}$), ridge push forces ($F_{RP}$) also contributes positively to subduction. The elevated topography of the mid-ocean ridge creates excess potential energy. This excess energy results in a ridge push force that pushes towards the trench (Forsyth and Uyeda, 1975). Forces resisting subduction arise from the stick-slip behavior on the subduction interface ($F_{SI}$), the viscous drag due to lithosphere – mantle coupling ($F_R$) and the resistance to lithospheric bending at the trench ($F_B$).

## Terrane accretion

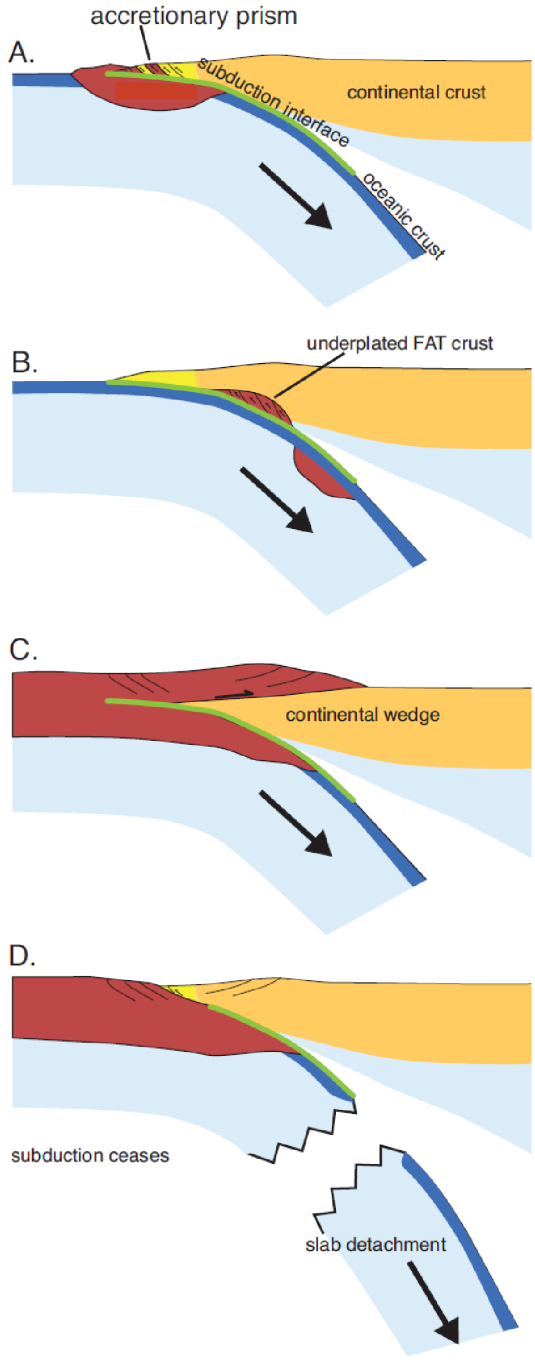


**Figure 2.4:** Schematic cartoon of various terrane accretion processes. a) Accretion of incoming fragments to the accretionary prism. b) Underplating of incoming fragments. c) 'Flake tectonics' whereby part of the incoming fragment is obducted onto the overriding plate whilst the rest is subducted. d) Docking or frontal accretion of the incoming fragment. This almost always results in slab detachment and cessation of subduction. Figure from Tetreault and Buiter (2014).

Accretion of allochtonous terranes at subduction margins is considered one of the most important process for the Earth's continental crust evolution (Stern and Scholl, 2010). Indeed, the majority of the Earth's continental crust (86%) is non-cratonic in nature and distributed heterogeneously over the Earth (Bouysse, 2014, Manuscript 1 – this thesis). These allochtonous accreting terranes can originate from a wide variety of sources. Volcanic arcs, oceanic plateaus/LIP's, seamounts, oceanic ridges and microcontinents and continental fragments (Box 5) can all be accreted to a subduction margin (Tetreault and Buiter, 2014). The exact evolution of the accreting process and the final architecture depend on the rheology and architecture of the accreting block.

Various modelling studies investigated the requirements for terrane accretion. Results clearly show that not all blocks arriving at the trench accrete to the overriding plate. When the subducting lithosphere is young, accretion of the incoming terrane is more likely (Vogt and Gerya, 2014). This is especially true when the terranes are continental in nature (Yang et al., 2018). In addition, the presence of a detachment fault in the incoming block significantly increases the probability of accretion of the incoming block to the overriding plate, and the depth of this detachment controls the volume of accreted material (Tetreault and Buiter, 2012). In line with the results from Vogt and Gerya (2014), the absence of a weak detachment layer results in the complete subduction of the incoming terrane, regardless of its buoyancy as the age of the oceanic lithosphere is this study is constant at 70 Myr (Tetreault and Buiter, 2012).

Successful terrane accretion can result in a variety of post-accretion architectures. The crust of an incoming block can shear at the subduction interface and be incor-

porated into the accretionary prism, which then grows outwards (Cloos and Shreve, 1988) (Figure 2.4a). Underplating of an incoming block is a very common way to accrete incoming terranes. In this scenario, part of the incoming block is sheared off and accreted to the bottom of the overriding plate (e.g. Tetreault and Buiter, 2012; Vogt and Gerya, 2014; Yang et al., 2018) (Figure 2.4b). This process also often results in a lateral trench relocation at the surface (Tetreault and Buiter, 2012). Flake tectonics is the process whereby the upper part of the incoming block is obducted whilst the lower part of the block enters the subduction zone (Oxburgh, 1972) (Figure 2.4c). Finally, frontal accretion or 'docking' is where a large incoming block accretes to the overriding plate. This often results in large volume additions to the continental crust. However, subduction usually ceases after accretion, followed by slab breakoff (e.g. Tetreault and Buiter, 2012; Vogt and Gerya, 2014; Yang et al., 2018) (Figure 2.4d).

These incoming allochtonous terranes not only modify the architecture of the overriding plate, they also influence the surrounding subduction evolution by changing the stress state of the subduction margin (e.g. Wallace et al., 2009).

## Formation of inherited structures

Successful terrane accretion inherently involves significant deformation of the subduction margin and channel and the incoming terrane. This deformation, whether brittle or ductile, can permanently damage the crust and/or lithosphere, forming inherited structures.

These inherited structures are weak with respect to their surroundings (e.g. Mazzotti and Gueydan, 2018)and take a long time to heal (Bercovici and Ricard, 2014, 2016). This means that upon renewed stress application, these structures will fail before the surrounding crust/lithosphere. As such, they localize deformation and play an important role in the subsequent evolution of the margin (Bercovici and Ricard, 2014; Heron et al., 2016).

### **Box 5:** Microcontinents in the final stages of the Wilson Cycle

The Wilson Cycle postulates that all (subduction) margins will, at one point or another, become incorporated into orogens via continental collision(1). This suggests that all microcontinents or continental fragments will, eventually, become incorporated into an orogen. The evolution of an orogen can then be greatly influenced by these microcontinents and continental fragments.

Whilst the study of these processes is beyond the scope of this thesis, it is worth noting that several microcontinents and/or continental fragments can be found in the modern day geological record. Known examples include the Jotun microcontinent in the Scandinavian Caledonides (Jakob et al., 2017), the Oaxaquia microcontinent that accreted to North America (Ortega-Gutierrez et al., 1995) and the Briançonnais terrane in the Alps (Handy et al., 2010; Strzerzynski et al., 2012).

(1)This does not necessarily imply that subduction only ends in collision. Inactive subduction margins can exist for long periods of time. However, at some point these inactive margins will become part of an orogen.

Terrane accretion is a common way to create inherited structures, especially in subduction margins. Examples of other inherited structure include, but are not limited to, old failed rifts (El Harfi et al., 2006; Ziegler et al., 2001), old orogenic sutures and subduction zones (Morgan et al., 1994; Schiffer et al., 2015).

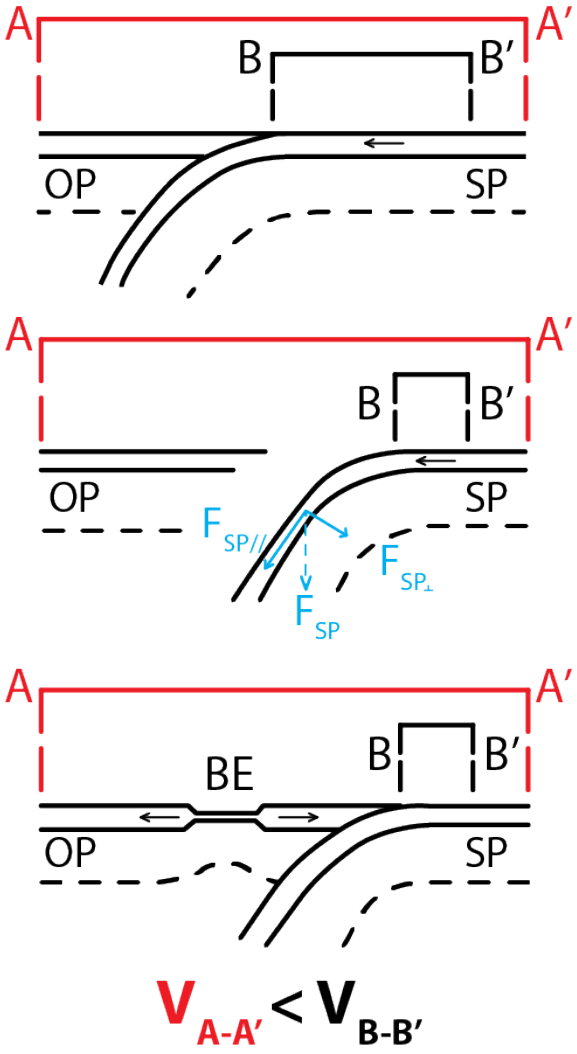


**Figure 2.5:** Schematic representation of back-arc extension kinematics. The convergence velocity (VA-A') is lower than the subduction velocity (VB-B'), resulting in back-arc extension (BE). SP: Subducting plate; OP: Overriding plate. FSP: Slab pull force.

## Back-arc extension

In addition to the convergent and sometimes collisional processes associated with terrane accretion, extensional tectonics does occur (locally) in subduction margins. Such local divergent tectonic regimes are often expressed via back-arc extension. Documented extension in an overall convergent setting shows that break-up may occur in active margins and microcontinents or continental fragments may form.

Kinematically, back-arc extension occurs when the relative convergence velocity between the subducting and overriding plate is lower than the subduction velocity (Figure 2.5). In most cases, back-arc extension is the consequence of slab rollback, which is observed for most subducting slabs on Earth (e.g. Garfunkel et al., 1986). Furthermore, observations also indicate that relatively narrow slabs ($\leq$1500 km) tend to have fast slab rollback and more significant trench curvature and are, in general, more mobile (Schellart et al., 2007). This is attributed to the fact that narrow slabs have a lower volume and thus experiences less viscous resistance.

There have been several mechanisms proposed to explain back-arc extension. One mechanism invokes suction forces nucleating from a retreating trench (Shemenda, 1993). Excess gravitational potential energy is also suggested to drive back-arc extension via gravitational collapse (Rey, 2001). Finally, subduction induced mantle flow is also suggested as a driver for back-arc extension (Chen et al., 2015, 2016; Duarte et al., 2013; Meyer and Schellart, 2013).

The variety in these proposed mechanisms and the complexity inherent to natural tectonic processes suggest that, in nature, back-arc extension is driven by an interplay between various mechanisms. Indeed, analogue modelling of the Tyrrhenian basin formation proposes that extension was initially driven by gravitational potential energy, with slab pull forces becoming more dominant later in its evolution (Faccenna et al., 1996).

# 3

# Methodology

This thesis uses a multidisciplinary approach to investigate microcontinent and continental fragment formation in subduction systems. Below I will briefly outline the methods used in the different manuscripts. For additional details regarding specific methodologies, the reader is referred to the relevant manuscript.

## 3.1 Manuscript 1: Geophysical and geological observations, plate tectonic reconstructions and seismic tomography models

In order to characterize microcontinents and/or continental fragments and to gain insight into their possible formation mechanisms in subduction zones, I used publicly available geophysical and geological data. Removing sediment thickness from measured bathymetry allows a better characterization of relevant continental margin geometries. Free air gravity anomalies are also proxies for margin geometries as well as the nature of the oceanic basin. Bouguer gravity anomalies computed by correcting for the influence of topography/bathymetry on gravitational field, provide some information about the subsurface density distribution; magnetic anomaly data offer clues about the presence of magnetized bodies and therefore can assist in identifying crustal types. Where the resolution is sufficient, I use regional or global crustal thickness models to get more clues on the nature and extend of the crust.

Using published tectonic reconstructions, I reconstruct the relevant fragments back to their pre-breakup location. This allows me to identify conjugate profiles across the margins of the specific continental fragment and its parent continent. I can then extract and compare geophysical data along these profiles to further characterize the margins. These tectonic reconstructions also allow me to track the kinematic evolution of the microcontinent or continental fragment before, during and after separation from its parent continent. In order to identify and describe the slabs associated with the relevant microcontinent or continental fragment, I extract vertical tomographic slices along sections that cross the investigated region.

Finally, I calculate the total area and volume of microcontinents and continental fragments associated with subduction systems, microcontinents formed in large-scale rifted margin settings and non-cratonic continental crust. Comparing these numbers allows

me to make inferences about the influence of microcontinents and continental fragments on the global distribution of continental crust.

## 3.2 Manuscript 2: Analogue experiments of overriding plate extension

In manuscript two I use analogue experiments to gain insight into the role of tectonic inheritance and extensional driving forces on overriding plate extension in subduction zones. Analogue experiments are typically used to investigate physical processes and properties of plate tectonics. Scaling of the models is based on principles of geometric, kinematic and dynamic similarity (Hubbert, 1937) and as such can be conducted on a variety of scales ranging from local crustal to lithospheric scale.

Similar to previous studies (e.g. Funiciello et al., 2003; Király et al., 2018), the experiments in manuscript two are on a upper mantle scale and use a two-layer, linear viscous tectonic system that represent the mantle and lithosphere. Analogue material for the overriding and subducting lithosphere consists of viscoelastic silicone putties, whereas high-viscous glucose syrup represents the mantle. In order to represent inherited structures, I create a weaker material by adding oleic acid to the continental lithosphere analogue. By varying the volume and placement of these weaker sections in the overriding plate and tracking its experimental evolution, I can make observations on the mechanisms responsible for overriding plate evolution.

## 3.3 Manuscript 3: 3D numerical experiments of overriding plate extension

In order to investigate the role of inherited weak zones and along strike variations in subduction dynamics I conduct numerical experiments using the finite element code Citcom (Moresi et al., 1996; Zhong et al., 2000). The code has been widely used by the geodynamics community to model subduction processes in 2D and 3D (e.g. Magni et al., 2017, 2012, 2014; van Hunen and Allen, 2011). After setting up the initial and boundary conditions, numerical experiments solve constitutive equations for the conservation of mass, momentum, energy and composition to produce quantitative results.

I use a Cartesian modelling domain and conduct both 2D and 3D experiments of subduction underneath a continental overriding plate. To investigate the influence of weak zone configuration on overriding plate extension, I conducted a parametric study in both 2D and 3D. I then used the weak zone configuration that produced most extension in subsequent experiments where its position and angle with respect to the trench are varied. Introducing a buoyant continental block on the subducting plate results in rotational trench kinematics. By varying the width of the incoming continental block, I can vary the induced rotational stress. I use this rotation to investigate the interplay between inherited weak zones and rotational overriding plate kinematics.

# 4

# Manuscript summaries

## 4.1 Microcontinents and continental fragments associated with subduction systems

*This manuscript was published in Tectonics in July 2020*

Manuscript 1 presents several microcontinents and continental fragments that have formed in subduction systems. This study uses geophysical and geological data (section 3.1) to unravel potential formation mechanisms and shed light on possible role of these continental pieces on larger scale plate tectonics.

We find subduction associated microcontinents and continental fragments in the Coral Sea, South China Sea, central Mediterranean and Scotia Sea regions and a 'proto-microcontinent', in the Gulf of California. All these subduction systems experienced long, complex tectonic histories, often with episodes of terrane accretion. These protracted histories are then likely to have modified the overriding plate lithosphere, introducing inherited structures.

Formation of these microcontinents and continental fragments tends to occur in back-arc settings. Separation from their parent continents is generally via rotational or oblique kinematics. Formation is generally quick (<50 Myr) and the oldest example is from the late Eocene/Paleocene. These relatively young ages and the rapid formation suggest that that microcontinents and continental fragments in subduction settings are short-lived.

The variability in microcontinent size and architecture and the tectonic setting in which they form suggest that multiple subduction-related mechanisms can produce microcontinents or continental fragments. We speculate that rapid changes in subduction dynamics are oftentimes the trigger of these mechanisms.

Although presently the amount of in-situ microcontinents –associated with both subduction and rifted margin settings– is meagre (an area of 2.5% and 1.15% of global, non-cratonic, continental crustal area and crustal volume respectively), through time microcontinents likely played an important role in the evolution and distribution of the Earth's continental crust.

## 4.2 An analogue modelling approach to investigate overriding plate extension in subduction settings

*This manuscript is currently in preparation*

Manuscript 2 uses analogue models (section 3.2) to investigate the relationship between overriding plate kinematics, inherited structures and forces driving overriding plate extension. We do this by using three sets of analogue models. In the first setup, we simulate overriding plate extension with a kinematic boundary condition (a moving wall). The second setup uses a subducting plate to induce extension. We vary the architecture of the overriding plate in our first two setups by incorporating weak zones in various configurations. In our third setup, we replace the overriding plate by a series of independently moving blocks.

Our results show that when the driving forces are shallow, extension is controlled by the lithosphere and localizes close to the origin of the stress (e.g. the moving wall). Conversely, when extension driving forces are induced by a subducting slab, the mantle exerts more control over the overriding plate evolution and extension localizes more distal from the trench. This is in accordance with previous work and matches observations of back-arc basin locations. We also observe that lateral stress transfer through the lithosphere is very important in the evolution of the overriding plate.

Introduction of a weak zone into the system results in localization of deformation in this weak zone. The position of this imposed weak zone does not matter when a moving wall drives extension. Unfortunately, due to a high viscosity on the subduction interface we were not able to study the effect of weak zone location on overriding plate extension patterns. However, we speculate that weak zone location might be more important when extension is driven by mantle flow.

## 4.3 The formation of continental fragments in subduction settings: the importance of structural inheritance and subduction system dynamics

*This manuscript was published in the Journal of Geophysical Research: Solid Earth in January 2020*

Manuscript 3 further investigates subduction-related microcontinent formation mechanisms. Using the finite element code Citcom (section 3.3), we conduct 2D and 3D numerical experiments to investigate the conditions required for localizing extension and inducing continental rifting and breakup in a continental overriding plate.

We find that an imposed/inherited structure is required to localize extension. In order to produce significant extension, this imposed weak zone must have a viscosity that is at least one order of magnitude lower than the viscosity of the surrounding lithosphere at the surface. Results also indicate that, in 3D, a narrower weak zone produces the most extension.

In addition to the imposed weak zone, we find that rotational trench kinematics are required to produce continental breakup. We generate these rotational kinematics by introducing a buoyant indenter (continental block) on the down going plate. Collision of this indenter with the overriding plate exerts a torque on the trench, resulting in trench rotation. This rotation then alters the stress state in the overriding plate and yields continental breakup and formation of a continental fragment.

Our results indicate that continental fragment formation requires the presence of a low viscosity inherited weak zone and rotational subduction kinematics. The final geometry and evolution of our experiments show a similarity to the proposed evolution of the Corsica-Sardinia block as it detached from Eurasia during the opening of the Liguro-Provençal basin. Furthermore, our results suggest that formation of microcontinents or continental fragments in an upper plate setting requires a complex and dynamic tectonic setting.

# 5

# Discussion and outlook

The main aim of this thesis was to investigate the processes and parameters that control the formation of microcontinents and continental fragments in subduction systems. Whilst microcontinents and continental fragments have been studied before, this is the first time these features are explicitly investigated in subduction settings. The results clearly show that microcontinent and continental fragments formed in subduction systems are widespread and occur globally. By drawing attention to their existence, a new perspective on subduction margins emerges.

## 5.1 Understanding formation mechanisms

Results from the global compilation indicate that formation of microcontinents and continental fragments requires complex tectonic settings and long tectonic histories. This required complexity for microcontinent/continental fragment formation is further highlighted by the results from analogue and numerical modelling. The analogue modelling results suggest that strain localization is dependent on the interplay between mantle-lithosphere coupling, inherited weak zone location and subduction induced mantle flow. Numerical experiments emphasize the importance of inherited structures and changing subduction dynamics that induce rotational trench movement. Thus, it appears that inherited structures and oblique or rotational extension kinematics are crucial ingredients for microcontinent formation.

Whilst inherited structures are, seemingly, present in all examples presented in manuscript 1, not all examples in that study formed as a result of rotational trench kinematics after collision with an incoming indenter. This, in combination with observed variations in the setting and evolution of subduction systems worldwide, strongly suggests that multiple formation mechanisms are possible. Future work can aim to explain more mechanisms such as microcontinent formation in a lower plate setting or using oblique instead of rotational extension. This would not only increases understanding of microcontinent formation, it would also increase understanding of the relationship between subduction dynamics and tectonic surface expressions.

In manuscript 3 I identified a mechanism to form continental fragments. However, although this mechanism is applicable to the initial evolution of the central Mediterranean, it does not reproduce the jump in extension to form the second oceanic basin (i.e. the Tyrrhenian basin). As such, the models does not produce a microcontinent

in sensu stricto. This raises two (related) questions; how can we produce a completely detached microcontinent and how does extension relocate?

A good place to start might be the Mediterranean itself, where several studies propose mechanisms to explain the relocation of extension to the Tyrrhenian basin. Faccenna et al. (2001) suggest that interaction from the slab with the 660 mantle discontinuity caused the jump in extension. Other studies suggest that the collision of the Calabrian trench with the African and Adriatic continents resulted in slab tearing along the continental margins and relocation of extension (Faccenna et al., 2005, 2007; Magni et al., 2014).

Another interesting avenue to explore would be the possibility of microcontinent or continental fragment formation on a subducting plate. Indeed Koptev et al. (2019) proposed that the Apulia microcontinent that accreted to Anatolia formed in a lower plate setting; they invoke a mantle plume to induce continental rifting and breakup. Whilst this mechanism is certainly plausible, the geologic setting of an impinging mantle plume is very specific. Tectonic reconstructions presented in manuscript 1 postulate that the South China Sea and Coral Sea basins opened in a lower plate position. Although this interpretation is not completely uncontroversial (e.g. Hall and Breitfeld, 2017), a mantle plume is not invoked. As such, understanding potential microcontinent/continental fragment formation in a lower plate setting merits further study.

Regardless of the exact mechanism, the complex tectonic settings associated with the examples presented in manuscript 1 and the numerical results of manuscript 3 suggest that rapid changes to subduction dynamics can lead to microcontinent or continental fragment formation. This is in accordance with results from Mallard et al. (2016) who suggested that small tectonic plates are more sensitive to readjustment of subduction systems.

## 5.2 Formation in subduction systems vs. classical rifted margins

Many conceptual and numerical models produce microcontinents via lateral relocation of extension (Nemcok et al., 2016; Peron-Pinvidic and Manatschal, 2010). This is often facilitated by periods of tectonic quiescence and cooling of the lithosphere (Abera et al., 2016; van Wijk and Cloetingh, 2002). Numerical results indicate that a cooling period of at least 20 Myr is required for lateral migration to occur (Naliboff and Buiter, 2015). Our observations of microcontinent formation in subduction systems indicates that total formation time is quick (<50 Myr, oftentimes less). This suggests that these types of mechanisms are less likely to produce microcontinent or continental fragments in rapidly changing subduction systems.

On the other hand, the prerequisite of inherited structures and rotational extension kinematics observed in this thesis is in line with analogue modelling results from Molnar et al. (2018). Despite the fact that their models use a different experimental setup and pertain to a different tectonic setting, they also require an inherited weak zone and rotational extension kinematics. The similarities between this study and my findings suggests that tectonic inheritance combined with rotational extension is a fundamentally efficient way to induce continental rifting and form a microcontinent.

Based on these comparisons, I speculate that formation mechanisms of microcontinents or continental fragments via time-insensitive or rapid formation mechanisms are applicable to both subduction and rifted margin systems.

## 5.3 Subduction associated microcontinents through geological time?

This thesis highlights (previously overlooked) microcontinents and continental fragments in subduction systems. It also increases the understanding of their architecture as well as how they form. We can use this knowledge to locate/recognize more accreted microcontinents and continental fragments in the geological record. Furthermore, as is clear from this thesis, the presence of a continental fragment or microcontinent has implications for the (pre-accretionary) tectonic setting. By better identifying microcontinents and continental fragments in the geological record we can thus also greatly improve tectonic reconstruction models.

The geological record already contains several examples of accreted microcontinents; the Jotun Microcontinent in the Scandinavian Caledonides (Jakob et al., 2019), the Oaxaquia microcontinent in North America (Ortega-Gutierrez et al., 1995) and fragments in the Variscan and Alpine orogens (von Raumer et al., 2003). Currently, microcontinents make up 2.5% of the global, non-cratonic, continental crust (Manuscript 1), but their presence in these orogens raises the question whether this percentage has evolved through time. Whilst such a quantification is challenging, the results could provide interesting insights into the evolution of plate tectonics. A quantification of microcontinents through time can also be used to better understand behavior of a subduction margin. Although terrane accretion is studied (section 2.3), these studies often neglect the complexity of such margins. The oceanic basin situated between two colliding plates is likely to be confined just before collision. This confined setting can induce changes in subduction dynamics (e.g. reduction in convergence velocities) and reduces the freedom of the oceanic plate to accommodate these changes. As a result, microcontinents and continental fragments may form. These will then complicate the margin architecture before being incorporated into the collisional orogen. By gaining more knowledge on the evolution of microcontinents through time we can thus increase our understanding of the complexity of accretionary margins.

Another line of investigation could shed light on the more fundamental issue of the evolution of plate tectonics itself. The Earth has been cooling down since its formation and it is generally proposed that plate tectonics processes are faster for a hotter Earth. Thus, it is expected that plate tectonic processes where faster in the geological past (van Hunen and van den Berg, 2008). Furthermore, based on the same principle and results from numerical modelling of plate distribution and fragmentation, Mallard et al. (2016) speculate that in the geological past there were more tectonic plates that where smaller in size. These theories suggest that in deep time microcontinents constituted a larger percentage of continental crust. We can thus potentially learn more about the Earth's geodynamic regime in the geological past by estimating/quantifying the percentage microcontinents through time.

# Bibliography


Abera, R., van Wijk, J., Axen, G., 2016. Formation of continental fragments: The Tamayo Bank, Gulf of California, Mexico. *Geology* 44, 595–598.

Andersen, T.B., Corfu, F., Labrousse, L., Osmundsen, P.T., 2012. Evidence for hyperextension along the pre-Caledonian margin of Baltica. *Journal of the Geological Society* 169, 601–612. `https://pubs.geoscienceworld.org/jgs/article-pdf/169/5/601/2795675/601.pdf`.

Bercovici, D., Ricard, Y., 2014. Plate tectonics, damage and inheritance. *Nature* 508, 513.

Bercovici, D., Ricard, Y., 2016. Grain-damage hysteresis and plate tectonic states. *Physics of the Earth and Planetary Interiors* 253, 31–47.

Berndt, C., Planke, S., Teagle, D., Huismans, R., Torsvik, T., Frieling, J., Jones, M.T., Jerram, D.A., Tegner, C., Faleide, J.I., Coxall, H., Hong, W.L., 2019. Northeast Atlantic breakup volcanism and consequences for Paleogene climate change – MagellanPlus Workshop report. *Sci. Dril.* 26, 69–85.

Bouysse, P., 2014. Geological Map of the World at 1: 35 000 000.

Brune, S., Heine, C., Clift, P.D., Pérez-Gussinyé, M., 2017. Rifted margin architecture and crustal rheology: Reviewing Iberia-Newfoundland, Central South Atlantic, and South China Sea. *Marine and Petroleum Geology* 79, 257–281.

Brune, S., Williams, S.E., Butterworth, N.P., Müller, R.D., 2016. Abrupt plate accelerations shape rifted continental margins. *Nature* 536, 201–204.

Buck, W.R., 2004. Consequences of asthenospheric variability on continental rifting. *Rheology and deformation of the lithosphere at continental margins* 62, 1–30.

Buiter, S.J.H., Torsvik, T.H., 2014. A review of Wilson Cycle plate margins: A role for mantle plumes in continental break-up along sutures? *Gondwana Research* 26, 627–653.

Chen, Z., Schellart, W.P., Duarte, J.C., 2015. Overriding plate deformation and variability of fore-arc deformation during subduction: Insight fromgeodynamic models and application to the Calabria subduction zone. *Geochemistry Geophysics Geosystems* 16, 3697–3715. `arXiv:1605.08479`.

Chen, Z., Schellart, W.P., Stark, V., Duarte, J.C., 2016. Does subduction-induced mantle flow drive backarc extension? *Earth and Planetary Science Letters* 441, 200–210.

Cloos, M., Shreve, R.L., 1988. Subduction-channel model of prism accretion, melange formation, sediment subduction, and subduction erosion at convergent plate margins: 2. Implications and discussion. *Pure and Applied Geophysics* 128, 501–545.

Dewey, J.F., Burke, K., 1974. Hot Spots and Continental Break-up: Implications for Collisional Orogeny. *Geology* 2, 57–60.

Ding, W., Franke, D., Li, J., Steuer, S., 2013. Seismic stratigraphy and tectonic structure from a composite multi-channel seismic profile across the entire Dangerous Grounds, South China Sea. *Tectonophysics* 582, 162–176.

Duarte, J.C., Schellart, W.P., Cruden, A.R., 2013. Three-dimensional dynamic laboratory models of subduction with an overriding plate and variable interplate rheology. *Geophysical Journal International* 195, 47–66.

Eagles, G., Pérez-Díaz, L., Scarselli, N., 2015. Getting over continent ocean boundaries. *Earth-Science Reviews* 151, 244–265.

El Harfi, A., Guiraud, M., Lang, J., 2006. Deep-rooted "thick skinned" model for the High Atlas Mountains (Morocco). Implications for the structural inheritance of the southern Tethys passive margin. *Journal of Structural Geology* 28, 1958–1976.

Faccenna, C., Civetta, L., Antonio, M.D., Funiciello, F., Margheriti, L., Piromallo, C., 2005. Constraints on mantle circulation around the deforming Calabrian slab. *Geophysical Research Letters* 32.

Faccenna, C., Davy, P., Brun, J.P., Funiciello, R., Giardini, D., Mattei, M., Nalpas, T., 1996. The dynamics of back-arc extension: an experimental approach to the opening of the Tyrrhenian Sea. *Geophysical Journal International* 126, 781–795.

Faccenna, C., Funiciello, F., Civetta, L., D Antonio, M., Moroni, M., Piromallo, C., 2007. Slab disruption, mantle circulation, and the opening of the Tyrrhenian basins. *Special Papers-Geological Society of America* 418, 153.

Faccenna, C., Funiciello, F., Giardini, D., Lucente, P., 2001. Episodic back-arc extension during restricted mantle convection in the Central Mediterranean. *Earth and Planetary Science Letters* 187, 105–116.

Fichter, L.S., 1996. Tectonic rock cycles. *Journal of Geoscience Education* 44, 134–148.

Forsyth, D., Uyeda, S., 1975. On the Relative Importance of the Driving Forces of Plate Motion. *Geophysical Journal International* 43, 163–200.

Franke, D., 2013. Rifting, lithosphere breakup and volcanism: Comparison of magma-poor and volcanic rifted margins. *Marine and Petroleum Geology* 43, 63–87.

Franke, D., Barckhausen, U., Baristeas, N., Engels, M., Ladage, S., Lutz, R., Montano, J., Pellejera, N., Ramos, E.G., Schnabel, M., 2011. The continent-ocean transition at the southeastern margin of the South China Sea. *Marine and Petroleum Geology* 28, 1187–1204.

Franke, D., Savva, D., Pubellier, M., Steuer, S., Mouly, B., Auxietre, J.L., Meresse, F., Chamot-Rooke, N., 2014. The final rifting evolution in the South China Sea. *Marine and Petroleum Geology* 58, 704–720.

Funck, T., Hopper, J.R., Larsen, H.C., Louden, K.E., Tucholke, B.E., Holbrook, W.S., 2003. Crustal structure of the ocean-continent transition at Flemish Cap: Seismic refraction results. *Journal of Geophysical Research: Solid Earth* 108.

Funiciello, F., Faccenna, C., Giardini, D., Regenauer-Lieb, K., 2003. Dynamics of retreating slabs: 2. Insights from three-dimensional laboratory experiments. *Journal of Geophysical Research: Solid Earth* 108, 1–16.

Gaina, C., Gernigon, L., Ball, P., 2009. Palaeocene-Recent plate boundaries in the NE Atlantic and the formation of the Jan Mayen microcontinent. *Journal of the Geological Society* 166, 601–616.

Gaina, C., Müller, R.D., Brown, B., Ishihara, T., 2003. Microcontinent formation around Australia. *Geological Society of Australia Special Publication 22* 372, 399–410.

Gaina, C., Whittaker, J.M., 2020. Microcontinents, in: Gupta, H.K. (Ed.), Encyclopaedia of Solid Earth Geophysics. Springer International Publishing.

Garfunkel, Z., Anderson, C.A., Schubert, G., 1986. Mantle circulation and the lateral migration of subducted slabs. *Journal of Geophysical Research: Solid Earth* 91, 7205–7223.

Hall, R., Breitfeld, H.T., 2017. Nature and demise of the Proto-South China Sea. *Bulletin of the Geological Society of Malaysia* 63, 61–76.

Handy, M.R., Schmid, S., Bousquet, R., Kissling, E., Bernoulli, D., 2010. Reconciling plate-tectonic reconstructions of Alpine Tethys with the geological-geophysical record of spreading and subduction in the Alps. *Earth-Science Reviews* 102, 121–158.

Heron, P.J., Pysklywec, R.N., Stephenson, R., 2016. Lasting mantle scars lead to perennial plate tectonics. *Nature Communications* 7, 11834.

Hubbert, M., 1937. Theory of scalale models as applied to the study of geologic structures. *Geological Society of America Bulletin* 48, 1459–1520.

van Hunen, J., Allen, M.B., 2011. Continental collision and slab break-off: A comparison of 3-D numerical models with observations. *Earth and Planetary Science Letters* 302, 27–37.

van Hunen, J., van den Berg, A.P., 2008. Plate tectonics on the early Earth: limitations imposed by strength and buoyancy of subducted lithosphere. *Lithos* 103, 217–235.

Jakob, J., Alsaif, M., Corfu, F., Andersen, T.B., 2017. Age and origin of thin discontinuous gneiss sheets in the distal domain of the Magma-Poor hyperextended Pre-Caledonian margin of Baltica, Southern Norway. *Journal of the Geological Society* 174, 557–571.

Jakob, J., Andersen, T.B., Kjøll, H.J., 2019. A review and reinterpretation of the architecture of the South and South-Central Scandinavian Caledonides—A magma-poor to magma-rich transition and the significance of the reactivation of rift inherited structures. *Earth-Science Reviews* 192, 513–528.

Király, A., Faccenna, C., Funiciello, F., 2018. Subduction Zones Interaction Around the Adria Microplate and the Origin of the Apenninic Arc. *Tectonics* 37, 3941–3953.

Kjøll, H.J., 2019. Neoproterozoic to Lower Paleozoic Evolution of the Pre-Caledonian Magma Rich Margin of Baltic. Phd thesis. University of Oslo.

Koptev, A., Beniest, A., Gerya, T., Ehlers, T.A., Jolivet, L., Leroy, S., 2019. Plume-Induced Breakup of a Subducting Plate: Microcontinent Formation Without Cessation of the Subduction Process. *Geophysical Research Letters* .

Leroy, S., Gente, P., Fournier, M., D'Acremont, E., Patriat, P., Beslier, M., Bellahsen, N., Maia, M., Blais, A., Perrot, J., Al-Kathiri, A., Merkouriev, S., Fleury, J., Ruellan, P., Lepvrier, C., Huchon, P., 2004. From rifting to spreading in the eastern Gulf of Aden: a geophysical survey of a young oceanic basin from margin to margin. *Terra Nova* 16, 185–192.

Lister, G.S., Etheridge, M.A., Symonds, P.A., 1986. Detachment faulting and the evolution of passive continental margins. *Geology* 14, 246–250.

Lundin, E.R., Doré, A.G., 2011. Hyperextension, serpentinization, and weakening: A new paradigm for rifted margin compressional deformation. *Geology* 39, 347–350.

Magni, V., Allen, M.B., van Hunen, J., Bouilhol, P., 2017. Continental underplating after slab break-off. *Earth and Planetary Science Letters* 474, 59–67.

Magni, V., Faccenna, C., van Hunen, J., Funiciello, F., 2014. How collision triggers backarc extension: Insight into mediterranean style of extension from 3-d numerical models. *Geology* 42, 511–514.

Magni, V., Van Hunen, J., Funiciello, F., Faccenna, C., 2012. Numerical models of slab migration in continental collision zones. *Solid Earth* 3, 293–306.

Mallard, C., Coltice, N., Seton, M., Müller, R.D., Tackley, P.J., 2016. Subduction controls the distribution and fragmentation of Earth's tectonic plates. *Nature* 535, 140–143.

Mazzotti, S., Gueydan, F., 2018. Control of tectonic inheritance on continental intraplate strain rate and seismicity. *Tectonophysics* 746, 602–610.

McKenzie, D., 1978. Some remarks on the development of sedimentary basins. *Earth and Planetary science letters* 40, 25–32.

Meyer, C., Schellart, W.P., 2013. Three-dimensional dynamic models of subducting plate-overriding plate-upper mantle interaction. *Journal of Geophysical Research: Solid Earth* 118, 775–790.

Minshull, T.A., 2009. Geophysical characterisation of the ocean–continent transition at magma-poor rifted margins. *Comptes Rendus Geoscience* 341, 382–393.

Molnar, N.E., Cruden, A.R., Betts, P.G., 2018. Unzipping continents and the birth of microcontinents. *Geology* , 1–4.

Moresi, L., Zhong, S., Gurnis, M., 1996. The accuracy of finite element solutions of Stokes's flow with strongly varying viscosity. *Physics of the Earth and Planetary Interiors* 97, 83–94.

Morgan, J.V., Hadwin, M., Warner, M.R., Barton, P.J., Morgan, R., 1994. The polarity of deep seismic reflections from the lithospheric mantle: Evidence for a relict subduction zone. *Tectonophysics* 232, 319–328.

Müller, R.D., Gaina, C., Roest, W.R., Hansen, D.L., 2001. A recipe for microcontinent formation. *Geology* 29, 203–206.

Mutter, C.Z., Mutter, J.C., 1993. Variations in thickness of layer 3 dominate oceanic crustal structure. *Earth and Planetary Science Letters* 117, 295–317.

Naliboff, J., Buiter, S.J.H., 2015. Rift reactivation and migration during multiphase extension. *Earth and Planetary Science Letters* 421, 58–67.

Nemcok, M., Sinha, S.T., Dore, A.G., Lundin, E.R., Mascle, J., Rybar, S., 2016. Mechanisms of microcontinent release associated with wrenching-involved continental break-up; a review. *Geological Society, London, Special Publications* 431, 323–359.

Nunns, A.G., 1983. Plate tectonic evolution of the greenland-scotland ridge and surrounding regions, in: Bott, M.H.P., Saxov, S., Talwani, M., Thiede, J. (Eds.), Structure and Development of the Greenland-Scotland Ridge: New Methods and Concepts. Springer US, Boston, MA, pp. 11–30.

Ortega-Gutierrez, F., Ruiz, J., Centeno-Garcia, E., 1995. Oaxaquia, a Proterozoic microcontinent accreted to North America during the late Paleozoic. *Geology* 23, 1127–1130.

Oxburgh, E.R., 1972. Flake tectonics and continental collision. *Nature* 239, 202–204.

Peron-Pinvidic, G., Manatschal, G., 2009. The final rifting evolution at deep magma-poor passive margins from Iberia-Newfoundland: A new point of view. *International Journal of Earth Sciences* 98, 1581–1597.

Peron-Pinvidic, G., Manatschal, G., 2010. From microcontinents to extensional allochthons: witnesses of how continents rift and break apart? *Petroleum Geoscience* 16, 189–197.

Peron-Pinvidic, G., Manatschal, G., Osmundsen, P.T., 2013. Structural comparison of archetypal Atlantic rifted margins: A review of observations and concepts. *Marine and Petroleum Geology* 43, 21–47.

Planke, S., Rasmussen, T., Rey, S.S., Myklebust, R., 2005. Seismic characteristics and distribution of volcanic intrusions and hydrothermal vent complexes in the Vøring and Møre basins. *Geological Society, London, Petroleum Geology Conference series* 6, 833 LP – 844.

von Raumer, J.F., Stampfli, G.M., Bussy, F., 2003. Gondwana-derived microcontinents - The constituents of the Variscan and Alpine collisional orogens. *Tectonophysics* 365, 7–22.

Reston, T.J., 2009. The structure, evolution and symmetry of the magma-poor rifted margins of the North and Central Atlantic: A synthesis. *Tectonophysics* 468, 6–27.

Rey, P., 2001. From lithospheric thickening and divergent collapse to active continental rifting. *Geological Society, London, Special Publications* 184, 77 LP – 88.

Schellart, W.P., Freeman, J., Stegman, D.R., Moresi, L., May, D., 2007. Evolution and diversity of subduction zones controlled by slab width. *Nature* 446, 308–311. t8jd4qr3m.

Schiffer, C., Stephenson, R.A., Petersen, K.D., Nielsen, S.B., Jacobsen, B.H., Balling, N., Macdonald, D.I.M., 2015. A sub-crustal piercing point for North Atlantic reconstructions and tectonic implications. *Geology* 43, 1087–1090.

Scrutton, R.A., 1976. Microcontinents and their significance. *Geodynamics: progress and prospects* 5, 177–189.

Shemenda, A.I., 1993. Subduction of the Lithosphere and Back Arc Dynamics ' Insights From Physical Modeling. *Journal of Geophysical Research : Solid Earth* 98, 16167–16185.

Sibuet, J., Tucholke, B.E., 2013. The geodynamic province of transitional lithosphere adjacent to magma-poor continental margins. *Geological Society, London, Special Publications* 369, 429 LP – 452.

Sonder, L.J., England, P.C., 1989. Effects of a temperature-dependent rheology on large-scale continental extension. *Journal of Geophysical Research: Solid Earth* 94, 7603–7619.

Stern, R.J., Scholl, D.W., 2010. Yin and yang of continental crust creation and destruction by plate tectonic processes. *International Geology Review* 52, 1–31.

Strzerzynski, P., Guillot, S., Leloup, P.H., Arnaud, N., Vidal, O., Ledru, P., Courrioux, G., Darmendrail, X., 2012. Tectono-metamorphic evolution of the Briançonnais zone (Modane-Aussois and Southern Vanoise units, Lyon Turin transect, Western Alps). *Journal of Geodynamics* 56-57, 55–75.

Svartman Dias, A.E., Lavier, L.L., Hayman, N., 2015. Conjugate rifted margins width and asymmetry: The interplay between lithospheric strength and thermomechanical processes. *Journal of Geophysical Research: Solid Earth* 120, 8672–8700.

Tetreault, J.L., Buiter, S.J., 2014. Future accreted terranes: A compilation of island arcs, oceanic plateaus, submarine ridges, seamounts, and continental fragments. *Solid Earth* 5, 1243–1275.

Tetreault, J.L., Buiter, S.J.H., 2012. Geodynamic models of terrane accretion: Testing the fate of island arcs, oceanic plateaus, and continental fragments in subduction zones. *Journal of Geophysical Research: Solid Earth* 117, 1–23.

Tetreault, J.L., Buiter, S.J.H., 2018. The influence of extension rate and crustal rheology on the evolution of passive margins from rifting to break-up. *Tectonophysics* 746, 155–172.

Tugend, J., Gillard, M., Manatschal, G., Nirrengarten, M., Harkin, C., Epin, M., Sauter, D., Autin, J., Kusznir, N., McDermott, K., 2018. Reappraisal of the magma-rich versus magma-poor rifted margin archetypes. *Geological Society, London, Special Publications* 476, SP476.9.

Turcotte, D., Schubert, G., 2002. Geodynamics. John Wiley and Sons, New York. second edition.

Vink, G.E., Morgan, W.J., Zhao, W., 1984. Preferential rifting of continents: A source of displaced terranes. *Journal of Geophysical Research: Solid Earth* 89, 10072–10076.

Vogt, K., Gerya, T.V., 2014. From oceanic plateaus to allochthonous terranes: Numerical modelling. *Gondwana Research* 25, 494–508.

Wallace, L.M., Ellis, S., Mann, P., 2009. Collisional model for rapid fore-arc block rotations, arc curvature, and episodic back-arc rifting in subduction settings. *Geochemistry, Geophysics, Geosystems* 10.

Wernicke, B., 1985. Uniform-sense normal simple shear of the continental lithosphere. *Canadian Journal of Earth Sciences* 22, 108–125.

Whitmarsh, R.B., Manatschal, G., Minshull, T.A., 2001. Evolution of magma-poor continental margins from rifting to seafloor spreading. *Nature* 413, 150–154.

van Wijk, J.W., Cloetingh, S.A.P.L., 2002. Basin migration caused by slow lithospheric extension. *Earth and Planetary Science Letters* 198, 275–288.

Wilson, J.T., 1966. Did the Atlantic close and then re-open? *Nature* 211, 676–681.

Yang, S.H., Li, Z.H., Gerya, T., Xu, Z.Q., Shi, Y.L., 2018. Dynamics of terrane accretion during seaward continental drifting and oceanic subduction: Numerical modeling and implications for the Jurassic crustal growth of the Lhasa Terrane, Tibet. *Tectonophysics* 746, 212–228.

Zhong, S., Zuber, M.T., Moresi, L., 2000. Role of temperature-dependent viscosity and surface plates in spherical shell models of mantle convection. *Journal of Geophysical Research* 105, 11063–11082.

Ziegler, P.A., 1992. Plate tectonics, plate moving mechanisms and rifting. *Tectonophysics* 215, 9–34.

Ziegler, P.A., Cloetingh, S., 2004. Dynamic processes controlling evolution of rifted basins. *Earth-Science Reviews* 64, 1–50.

Ziegler, P.A., Cloetingh, S.A.P.L., Guiraud, R., Stampfli, G.M., 2001. Peri-Tethyan platforms: constraints on dynamics of rifting and basin inversion. *Mémoire du Museum National d'Histoire Naturelle* 186, 9–49.

# Part II: Manuscripts

1

# Microcontinents and continental fragments associated with subduction systems

J. M. van den Broek and C. Gaina

*Tectonics* 39 (2020)

Tectonics

RESEARCH ARTICLE
10.1029/2020TC006063

# Microcontinents and Continental Fragments Associated With Subduction Systems

J. M. van den Broek[1] and C. Gaina[1]

[1]The Centre for Earth Evolution and Dynamics (CEED), Department of Geosciences, University of Oslo, Oslo, Norway

**Abstract** Microcontinents and continental fragments are small pieces of continental crust that are surrounded by oceanic lithosphere. Although classically associated with passive margin formation, here we present several preserved microcontinents and continental fragments associated with subduction systems. They are located in the Coral Sea, South China Sea, central Mediterranean and Scotia Sea regions, and a "proto-microcontinent," in the Gulf of California. Reviewing the tectonic history of each region and interpreting a variety of geophysical data allows us to identify parameters controlling the formation of microcontinents and continental fragments in subduction settings. All these tectonic blocks experienced long, complex tectonic histories with an important role for developing inherited structures. They tend to form in back-arc locations and separate from their parent continent by oblique or rotational kinematics. The separated continental pieces and associated marginal basins are generally small and their formation is quick (<50 Myr). Microcontinents and continental fragments formed close to large continental masses tend to form faster than those created in systems bordered by large oceanic plates. A common triggering mechanism for their formation is difficult to identify, but seems to be linked with rapid changes of complex subduction dynamics. The young ages of all contemporary pieces found in situ suggest that microcontinents and continental fragments in these settings are short lived. Although presently the amount of in-situ subduction-related microcontinents is meager (an area of 0.56% and 0.28% of global, non-cratonic, continental crustal area and crustal volume, respectively), through time microcontinents contributed to terrane amalgamation and larger continent formation.

**Key Points:**
- Microcontinents can form in association with convergent plate boundaries which experienced long and complex histories
- Formation often requires oblique or rotational kinematics as well as the presence of inherited structures in the continental crust
- Changes in slab dynamics is a potential mechanism that drives microcontinent formation in convergent settings

**Supporting Information:**
- Supporting Information S1
- Table S1

**Correspondence to:**
J. M. van den Broek,
j.v.d.broek@geo.uio.no

**Citation:**
van den Broek, J. M., & Gaina, C. (2020). Microcontinents and continental fragments associated with subduction systems. *Tectonics*, *39*, e2020TC006063. https://doi.org/10.1029/2020TC006063

Received 6 JAN 2020
Accepted 23 JUN 2020
Accepted article online 29 JUN 2020



## 1. Introduction

In the geological record, continental breakup and subsequent seafloor spreading sometimes resulted in smaller blocks being sliced and carried away from the margins of the parent continent. Changes in plate boundaries and other tectonic events moved these continental blocks back to larger continental masses and their continuously changing margins. The evolution of microcontinents is therefore an important mechanism for redistributing continental lithosphere and more information about it could shed light on various processes that affected continental margins through time. In addition, together with other scattered bathymetric features in the oceans, microcontinents played a meaningful role in paleogeography, paleo-ocean circulation, and biogeography.

Microcontinents and continental fragment formation has classically been associated with passive margin formation and accompanying divergent tectonic settings (e.g., Molnar et al., 2018; Müller et al., 2001; Nemčok et al., 2016; Péron-Pinvidic & Manatschal, 2010). However, several contemporary microcontinents and continental fragments formed in (association with) active continental margins. We aim to document these microcontinents and continental fragments and place their formation and evolution in a larger plate tectonic context. In doing so, we highlight the diversity and complexity of active continental margins and shed additional light on their evolution.

A microcontinent is defined as a piece of continental crust which has been horizontally displaced with respect to a continent, usually situated close by; it is surrounded by oceanic crust, and is smaller than the nearby/parent continent or than the smallest continent (Scrutton, 1976). Classic examples include the Jan-Mayen microcontinent in the north-east Atlantic Ocean (Gaina et al., 2009; Peron-Pinvidic et al., 2012a, 2012b) and the Seychelles in the Indian Ocean (Gaina et al., 2013; Ganerød et al., 2011; Torsvik et al., 2013). Continental fragments are defined similarly to microcontinents, with the exception that the complete separation from the parent continent did not occur (Lister et al., 1986). Examples include the Rockall and Porcupine Banks and the Galicia Bank, both in the North Atlantic (Péron-Pinvidic & Manatschal, 2010).

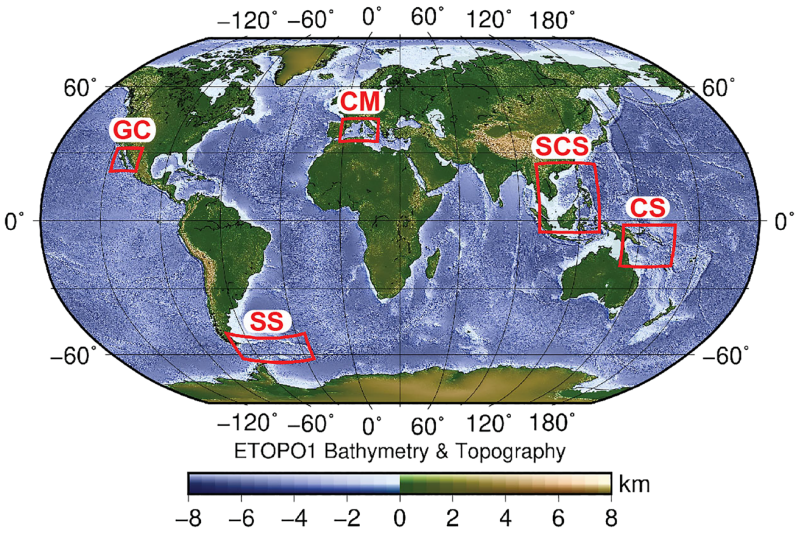


**Figure 1.** Global map with locations of the various regions studied in this work. CS = Coral Sea; SCS = South China Sea; CM = Central Mediterranean Sea; SS = Scotia Sea; GC = Gulf of California.

Various mechanisms have been proposed to explain the formation of the microcontinents and continental fragments mentioned above. One group of studies proposes microcontinent formation due to plate boundary relocations (ridge jumps) assisted by mantle heterogeneities (Abera et al., 2016; Müller et al., 2001). Other authors emphasize the role of inherited tectonic structures and the need for a strike-slip, or a rotational component in the breakup processes resulting in the isolation of a small fragment of continental crust (Molnar et al., 2018; Nemčok et al., 2016; Péron-Pinvidic & Manatschal, 2010; van den Broek et al., 2020).

An overview of continental active margins reveals the existence of small continental blocks situated in their proximity. The various continental pieces bordering the Coral Sea, NE of Australia (Gaina et al., 1999; Taylor & Falvey, 1977), the Reed and Macclesfield Banks in the South China Sea (Cullen et al., 2010; Pichot et al., 2014), the Corsica-Sardinia block in the Central Mediterranean (Advokaat et al., 2014; Faccenna et al., 2001), and various fragments in the Scotia Sea (Carter et al., 2014; Trouw et al., 1997) (Figure 1) all formed close to active continental margins and related subduction systems. In addition, rifting and spreading in the Gulf of California is separating the Baja California microplate from the North-American continent (Sutherland et al., 2012; Umhoefer, 2011), a process connected to the subduction of the Farallon plate under the North American plate.

The formation of microcontinents and continental fragments formed in convergent and/or subduction systems is an overlooked aspect of active margin evolution. To address this deficiency, we present a global catalogue of microcontinents and continental fragments associated to convergent margins. First, we review the overall tectonic setting and history of these microcontinents. Second, we reevaluate their present-day structure based on available geological and geophysical data. By studying patterns in their rifted margin morphology, we search for clues revealing potential mechanisms and/or parameters that controlled their formation. We then attempt to place microcontinent formation in subduction systems into a larger geodynamic context and asses its influence on global, non-cratonic, continental crust evolution.

For simplicity we group microcontinents and continental fragments associated with subduction and refer to them as microcontinents for the remainder of this paper. We define “proto-microcontinents” as pieces of continental lithosphere that are likely to (partially) separate from their parent continents in the future.

## 2. A Review of the Tectonic History of Microcontinents and Continental Fragments Associated With Subduction

We investigate microcontinents in regions affected by subduction in the following locations: (1) the Coral Sea; (2) the South China Sea; (3) the central Mediterranean Sea; (4) the Scotia Sea; and (5) the Gulf of

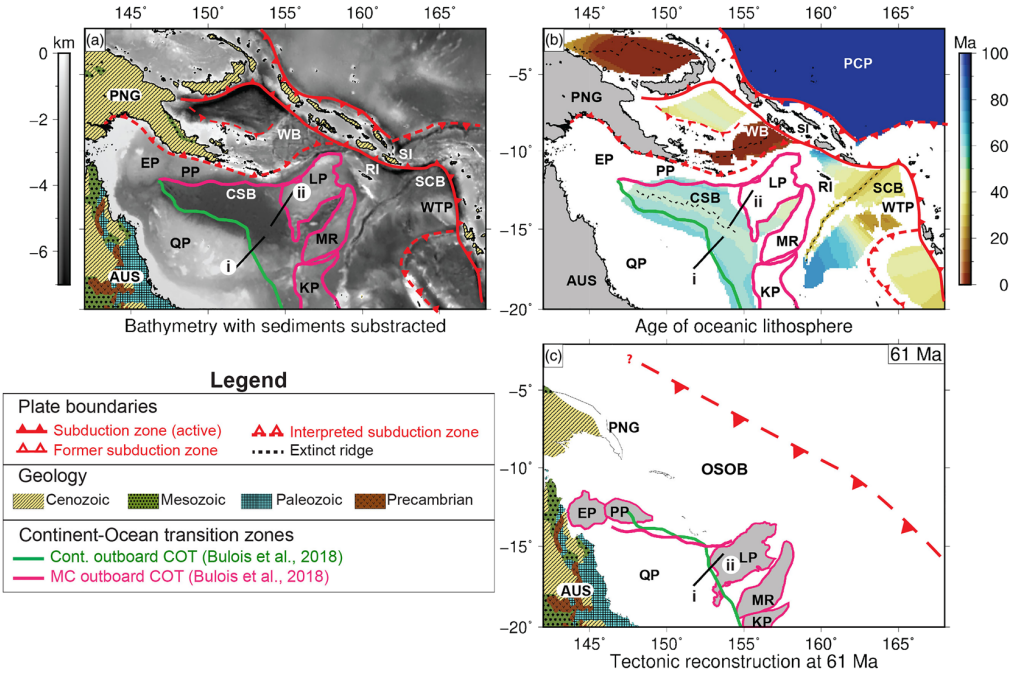


**Figure 2.** Geological models and bathymetric observations for the Coral Sea. (a) Bathymetry with sediments subtracted (no backstripping) and onshore geology. (b) Oceanic age grid of the various basins in the Coral Sea region. (c) Tentative tectonic reconstruction to the pre-Coral Sea breakup configuration. MC = microcontinent; LP = Louisiade Plateau; MR = Mellish Rise; KP = Kenn Plateau; WTP = West Torres Plateau; SCB = Santa Cruz Basin; RI = Rennel Island; WB = Woodlark Basin; PP = Papuan Plateau; EP = Eastern Plateau; PNG = Papua New Guinea; AUS = Australia; QP = Queensland Plateau; CSB = Coral Sea Basin; PCP = Pacific Plate; OSOB = Owen Stanley Oceanic Basin.

California (Figure 1). In the following we will review the tectonic evolution of each region with a focus on the relevant oceanic basins and the microcontinent(s).

In order to highlight the morphology of continental margins, we create a "no-sediment" bathymetry by subtracting the total sediment thickness estimation from the global bathymetric grid. Note that we do not preform backstripping, but simply remove the sediment thickness without compensating for depth adjustments. For bathymetry we use the ETOPO1 global relief model (Amante & Eakins, 2009). Sediment thickness in the Mediterranean region is from the EPcrust model (Molinari & Morelli, 2011), while for all other regions we utilize the GlobSed model from Straume et al. (2019). First-order onshore geological provinces from the third edition of the World Geological Map (Bouysse, 2014) are shown together with the offshore "no-sediment bathymetry" maps and on tectonic reconstruction maps in order to provide basic information about on-shore geology.

Kinematic reconstructions and oceanic age grids provide insight into the tectonic evolution of a region. Interpreted ages of oceanic crust are provided by the global oceanic age grid from Müller et al. (2008), while the location of spreading ridges are either reinterpreted for this study or taken from Müller et al. (2016). Tectonic reconstructions are produced with the open source software GPlates (http://www.gplates.org). The pre-breakup configurations and present-day microcontinent locations, together with the age of surrounding oceanic lithosphere (age grids), are presented in Figures 2–6. Additional kinematic reconstructions, mainly documenting plate boundary relocations that led to complete isolation of the microcontinents, are in the supporting information. Reconstructions for the Mediterranean region are from Advokaat et al. (2014) and van Hinsbergen et al. (2014). The pre-breakup reconstruction of the Coral Sea was created using the model of Seton et al. (2016), which is based on Gaina et al. (1999). Reconstruction parameters for the Scotia Sea are from Eagles and Jokat (2014). Both the South China Sea and the Gulf of California where reconstructed according to Matthews et al. (2016).

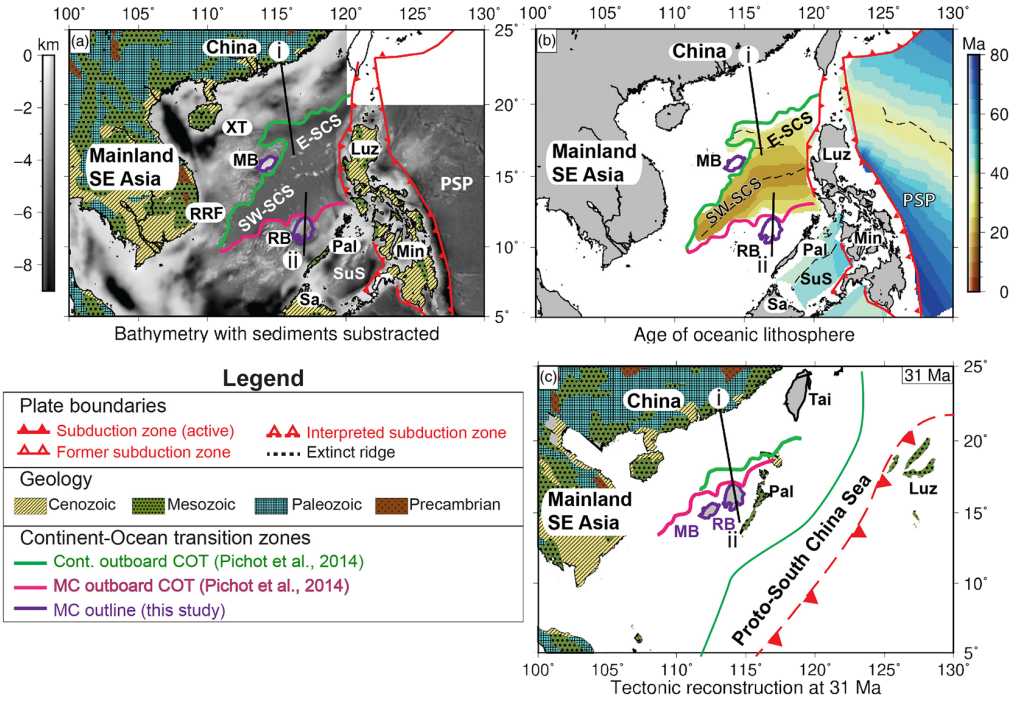


**Figure 3.** Geological models and bathymetric observations for the South China Sea. (a) Bathymetry with sediments subtracted (no backstripping) and onshore geology. (b) Oceanic age grid of the various basins in the South China Sea region. (c) Tentative tectonic reconstruction of the pre-breakup configuration of the South China Sea. XT = Xisha Through; MB = Macclesfield Bank; RB = Reed Bank; RRF = Red River Fault; SW-SCS = South West subbasin; E-SCS = Eastern subbasin; Luz = Luzon; PSP = Philippine Sea Plate; Min = Mindoro; Pal = Palawan; SuS = Sulawesi Sea; Tai = Taiwan.

### 2.1. The Coral Sea

The SW Pacific and the neighboring northeast margin of Australia are complex regions which have been shaped in the Cenozoic by various subduction episodes that resulted from changes in relative plate motions of the Australian and Pacific plates (Figure 2). The eastern margin of Australia/Gondwanaland was a long-lived convergent margin since at least the Cambrian (Glen, 2005) up until mid-Cretaceous times (Laird & Bradshaw, 2004). During this long-lived convergent margin setting, the NE Australian region experienced two rifting phases as recorded in the present-day sedimentary record (Bulois et al., 2018). The first rifting stage occurred in the Triassic and may have exploited crustal scale heterogeneities already present on the edge of the Australian craton (Bulois et al., 2018; Van Wyck & Williams, 2002). A subsequent rifting episode from the Jurassic to Lower Cretaceous exploited and reactivated these structures (Bulois et al., 2018). During this extension episode, new rift basins were created and this extended margin was considered to be the southern margin of the postulated "Owen Stanley Oceanic Basin" (Figure 2c) (Bulois et al., 2018). The existence of an older oceanic basin NE of Australia is inferred from the presence of supra-subduction zone ophiolites and ultramafic strata accreted in the Papuan fold and thrust belts (Bulois et al., 2018; Lus et al., 2004; Webb et al., 2014). This basin was supposedly formed as a back-arc basin due to a retreating Pacific slab.

The subduction configuration of the Pacific plate north and northeast of Australia probably changed around mid-Cretaceous time (Laird & Bradshaw, 2004), but the exact architecture of this region is difficult to reconstruct as subsequent tectonic episodes have overprinted its Cretaceous fabric (i.e., Seton et al., 2016). However, available geological evidence combined with plate circuit modeling suggests that west-dipping subduction continued from late Cretaceous to early Cenozoic, albeit at a slower pace. Associated back-arc basin opening occurred from the mid-upper Cretaceous to the early Eocene (Matthews et al., 2015). This last rifting episode of NE Australian margin in the upper Cretaceous ended with continental breakup and seafloor spreading along an axis that cross-cut the trends of the previous two rift systems. Note that the

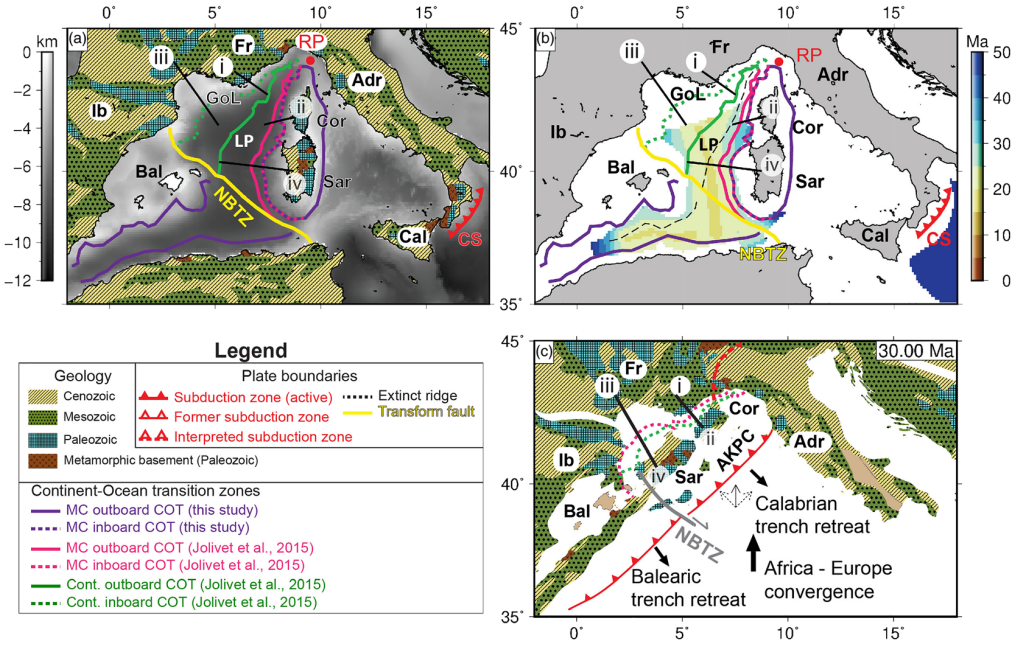


**Figure 4.** Geological models and bathymetric observations for the Central Mediterranean region. (a) Bathymetry with sediments subtracted (no backstripping) and onshore geology. (b) Oceanic age grid of the various basins in the Central Mediterranean. Note that this age grid is incorrect. (c) Tectonic reconstruction of the pre-breakup situation of the Central Mediterranean. Ib = Iberian Peninsula; GoL = Gulf of Lyon; Fr = France; Adr = Adria; CS = Calabrian Subduction Zone; Cal = Calabria; Cor = Corsica; Sar = Sardinnia; NBTZ = North Balearic Transfer Zone; RP = Rotation pole of the Liguro-Provençal basin; Bal = Balearic Islands; AKPC = AlKaPeCa terrane.

opening of the Coral Sea may have been associated to either NE subduction of the Australian plate under the Pacific plate (i.e., Whattam et al., 2008), or a SW subduction of the Pacific plate under the Australian plate. Geological evidences favor the first scenario, whereas slab remnants in the mantle can be invoked by both hypotheses (see section 3 and supporting information). Oceanic accretion in the Coral Sea started in the middle Paleocene and lasted until early Eocene (Figure 2b) (Gaina et al., 1999; Weissel & Watts, 1979).

Opening of the Coral Sea detached the Kenn, Louisiade and Papuan plateaus, and the Melish Rise from the NE Australian margin (Figure 2). The Eastern Plateau is still attached to the NE Australian margin via extended crust (Figure 2b). Cessation of Coral Sea seafloor spreading around 52 Ma has been attributed to changes in absolute plate motion direction (Eagles et al., 2004; Matthews et al., 2015; Schellart et al., 2006), or to the influence of subduction north and east of the basin along the Papuan-Rennel-New Caledonian trench system (Gaina et al., 1999). Subsequent subduction and back-arc basin formation resumed northeast of Coral Sea (Figure 2) (Matthews et al., 2015; Seton et al., 2016), and closure and accretion of oceanic (back-arc) basins onto Papua New Guinea occurred to the northwest (Lus et al., 2004).

### 2.2. The South China Sea

Southeast Asia is a complex amalgamation of terranes, continental fragments, island arcs, and associated marginal and back-arc basins (Figure 3) resulted from the interaction of the Pacific, Eurasian, and Australian plates (Ding et al., 2016; Wu et al., 2016; Zahirovic et al., 2014). Several authors proposed a north-west dipping, Andean type, subduction of the Paleo-Pacific plate below mainland SE Asia from the Middle Jurassic to Middle/late Cretaceous or early Eocene (Figure 3c) (Hall & Breitfeld, 2017; Taylor & Hayes, 1983; Zahirovic et al., 2014). This convergence potentially accreted various pieces of continental and island arc material to the margin (Breitfeld et al., 2017; Hennig et al., 2017; Pubellier et al., 2003). Around Paleocene times, roll back of the Paleo-Pacific plate resulted in the separation of the south Palawan block from the south Chinese paleo margin and the formation of the so called Proto South China Sea (Zahirovic et al., 2014). The subsequent Cenozoic evolution of the region is controversial.

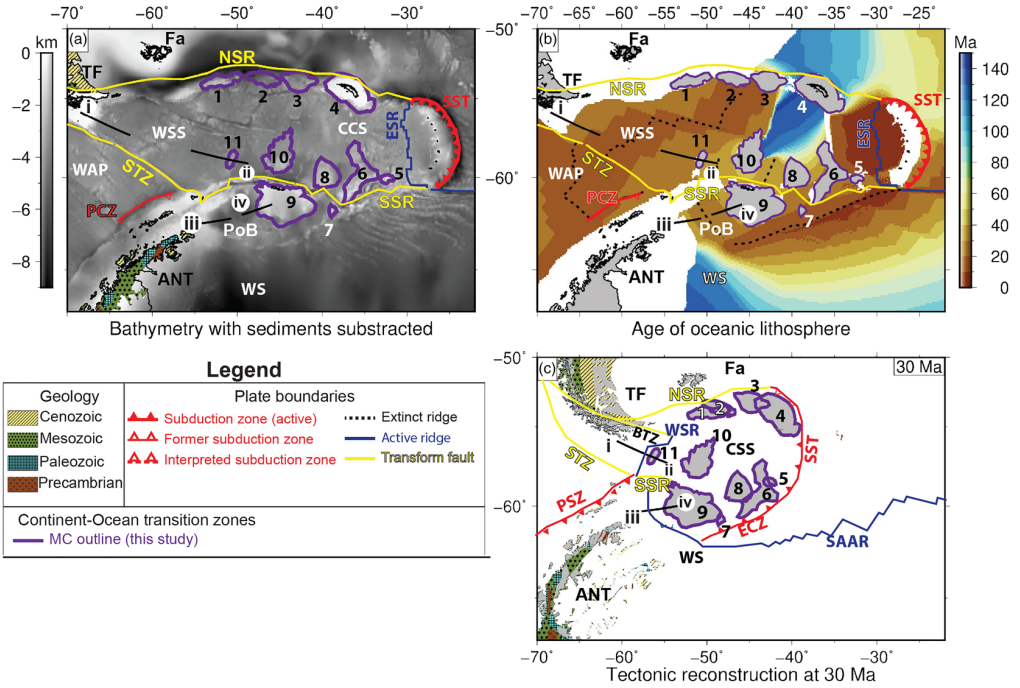


**Figure 5.** Geological models and bathymetric observations for the Scotia Sea. (a) Bathymetry with sediments subtracted (no backstripping) and onshore geology. (b) Oceanic age grid of the various basins in the Scotia Sea. (c) Tentative tectonic reconstruction of the pre-breakup configuration of the Scotia Sea. Microcontinents: 1 = Davis Bank; 2 = Barker Bank; 3 = Shag Rocks; 4 = South Georgia Microcontinent; 5 = Herdman Bank; 6 = Discovery Bank; 7 = Jane Bank; 8 = Bruce Bank; 9 = South Orkney Microcontinent; 10 = Pirie Bank; 11 = Terror Rise; Other abbreviations: ANT = Antarctica; WS = Weddel Sea; ESR = East Scoti a Ridge; NSR = North Scotia Ridge; SSR = South Scotia Ridge; TF = Tierra del Fiego; Fa = Falkand Islands; STZ = Shackelton Fractue Zone; WAP = West Antarctic Plate; PSZ = Pacific Subduction Zone; BTZ = Burdwood Transform Fault; WSR = West Scotia Ridge; CCS = Central Scotia Sea; ECZ = Endurance Subduction Zone; SST = South Sandwich Trench.

Some authors suggest that northwest to north directed subduction continued, but extension relocated and resulted in back-arc opening to the south China Sea (Sibuet et al., 2016; Wu et al., 2016). Other authors proposed that the Proto South China Sea subducted southward beneath NE Borneo and Palawan and the South China Sea basin opened NW of it (Figure 3c) (Bai et al., 2015; Zahirovic et al., 2014). No conclusive evidence for either model exists, but observations and dating on Borneo point to a southward directed Paleogene subduction (Hall & Breitfeld, 2017). However, more data are needed to better understand these scenarios.

The South China Sea experienced three phases of rifting since the late Cretaceous, two of which occurred during the Cenozoic (Cullen et al., 2010). Rifting from Paleocene to Eocene was widespread, as documented by the structure of the South China Sea margins (Cullen et al., 2010; Franke et al., 2014). Subsequent rifting from the late Eocene to early Miocene was more localized, and resulted in continental breakup and initiation of seafloor spreading in the South China Sea basin (Cullen et al., 2010; Franke et al., 2014; Li et al., 2014; Sibuet et al., 2016).

The present-day South China Sea has two main subbasins: the east and southwest subbasins (Figure 3) (Li et al., 2014). Recent IODP drilling, detailed analysis of deep tow magnetic data, and interpretation of seismic reflection data indicate that breakup in the (northern) east subbasin occurred in early Oligocene times (Franke et al., 2014; Li et al., 2014). Extension propagated westward, as evidenced by continental rifting in the Xisha trough (Figure 3a) (Sibuet et al., 2016). In late Oligocene–early Miocene times, a southward ridge jump occurred in the east subbasin which terminated the extension in the Xisha trough and spreading along the northern margin (Figure 3b) (Li et al., 2014; Sibuet et al., 2016) and initiated seafloor spreading in the southwestern subbasin (Li et al., 2014; Sibuet et al., 2016). This mid-ocean ridge further propagated in a south-westerly direction, creating the distinctive V-shape of the South China Sea southwest subbasin

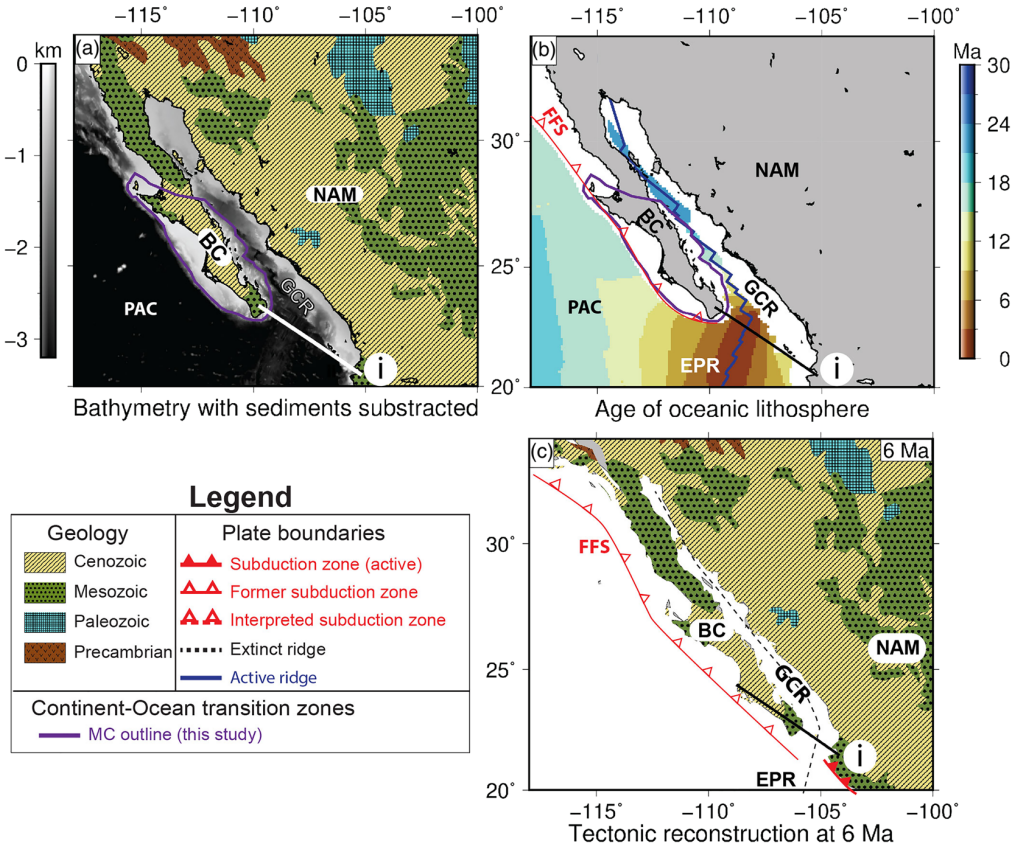


**Figure 6.** Geological models and bathymetric observations for Gulf of California region. (a) Bathymetry with sediments subtracted (no backstripping) and onshore geology. (b) Oceanic age grid of the various basins in the Gulf of California region. (c) Tentative tectonic reconstruction of the pre-breakup configuration of the Gulf of California. NAM = North American plate; BC = Baja California; GCR = Gulf of California Ridge; EPR = East Pacific Rise; FFS = Farallon Subduction zone; PAC = Pacific plate.

(Franke et al., 2014; Sibuet et al., 2016). Opening of the South China Sea detached the Reed Bank, Dangerous grounds, and a continental block comprised of NE Palawan and SW Mindoro from the South Chinese Margin (Figure 3). During its lifetime, extension and spreading directions in the South China Sea rotated from N175°, via N165° to N145° (Sibuet et al., 2016). Spreading in the South China Sea ceased in the middle Miocene (Figure 3b) and this event is often correlated with the choking of the Proto South China Sea subduction zone by a block with thick crust (e.g., NE Palawan and SW Mindoro) (Hall & Breitfeld, 2017; Sibuet et al., 2016; Yumul et al., 2003).

### 2.3. The Central Mediterranean Sea

The Mediterranean Sea region has experienced a long and complex tectonic evolution since the Paleozoic. The opening and closing of various oceanic basins resulted in an amalgamation of terranes with different ages and compositions (Figure 4) (Dewey & Sengör, 1979; Vissers et al., 2013; von Raumer et al., 2003).

The Africa-Eurasia/Iberia convergence played the main role in the Cenozoic evolution of this region. Convergence of Iberia with Eurasia resulted in the formation of the Pyrenean orogeny which, at the time, extended eastward into southern France as evidenced by basement thrusting (Lacombe & Jolivet, 2005). Further east, convergence between the Adriatic microplate and Eurasia created the Alps (Schmid et al., 2017; Turco et al., 2012).

Around Oligocene times, the northward subducting African slab segmented into the Calabrian and Balearic slabs which started to rollback independently (Figure 4c) (Faccenna et al., 2001; Seton et al., 2012;

van Hinsbergen et al., 2014). During this period of slab rollback the continental Corsica-Sardinia block was detached from Eurasia and the Liguro-Proven_x004AB;al back-arc basin was formed (Advokaat et al., 2014; Gattacceca et al., 2007; Seranne et al., 1999). Just before continental breakup between Eurasia and the Corsica-Sardinia block, the Adriatic microplate was colliding with the southern Eurasian margin, resulting in simultaneous subduction of oceanic and continental material (Figure 4) (Turco et al., 2012; van Hinsbergen et al., 2014). This may have triggered or contributed to continental breakup of the southern Eurasian margin and subsequent seafloor spreading in the Liguro-Proven_x004AB;al basin in early Miocene time (Figure 4b) (Faccenna et al., 1997). As a consequence, the Corsica-Sardinia block rotated counterclockwise ca. 45–50° around an Euler pole located just north of Corsica (Figure 4) (Advokaat et al., 2014; Gattacceca et al., 2007). Seafloor spreading in the Liguro-Provençal basin was active from early (21 Ma) to middle Miocene (Faccenna et al., 1997). After a 6 Myr quiet period, at 10 Ma the extension relocated east of the Corsica-Sardinia microcontinent, initiating the formation of the Tyrrhenian basin (Faccenna et al., 2001). This relocation of extension terminated the relative motion of the Corsica-Sardinia microcontinent with respect to Eurasia, leaving it isolated in the Central Mediterranean in its present-day position.

### 2.4. The Scotia Sea

The Scotia Sea region is situated between the Antarctic Peninsula and the southern tip of South America. Its Cenozoic evolution has been controlled by the interaction between the Antarctic and South American plates. Although the tectonic evolution of the region is still debated, several scenarios have been proposed (Dalziel et al., 2013; Eagles & Jokat, 2014).

The pre-breakup setting of the region is controversial (Brown et al., 2006; Eagles & Jokat, 2014; Müller et al., 2008). Dalziel et al. (2013) suggest that the South Georgia microcontinent was located south of Tierra del Fuego from Jurassic to Cenozoic times. In contrast, Eagles (2010a) proposed that it was located in a more internal part of Gondwana and that the formation of the Central Scotia Sea oceanic crust was associated with Gondwana breakup. According to Eagles (2010), the South Georgia microcontinent was located adjacent to the Falkland Islands in early Eocene times (Figure 5). At that time interval, the continental fragments that are presently distributed along the South Scotia Ridge (Figure 5) were clustered north of the South Orkney microcontinent, and are considered to have been part of the East Antarctic Plate (Eagles & Jokat, 2014). East of this assemblage, the Endurance subduction zone was active since the early Paleocene (Barker et al., 1991; Eagles, 2010b), subducting oceanic lithosphere from the northwest Weddell sea beneath the South Orkney microcontinent (Figure 5c).

During middle Eocene times, a rotation of the South American-Antarctica plate system drove southeast-directed trench retreat of the Endurance trench and/or changes along the Burwood transform zone. This resulted in the initiation of rifting in the Powel Basin (King & Barker, 1988), between the Antarctic Peninsula and the South Orkney microcontinent, and spreading between the Pirie and Bruce Banks (Figure 5) (Barker et al., 2013; Eagles et al., 2006).

At the start of Oligocene times, the extension relocated westward between the Pirie Bank and the Terror Rise (Figure 5) (Eagles & Jokat, 2014). In the middle Oligocene extension once again relocated westward to the West Scotia Ridge, between Tierra del Fuego and the Terror Rise (Figure 5) (Eagles et al., 2006). Also in the middle Oligocene, breakup occurred in the Powell basin and the Endurance subduction zone lengthened northward toward South Georgia (Figure 5c) (Barker, 1995; Eagles & Jokat, 2014). This led to the abandonment of the Burwood transfer zone in favor of the North Scotia Ridge and the formation of microcontinents by the transfer of the various northern continental fragments from the South American plate to the Scotia plate (Eagles & Jokat, 2014).

Collision of ridge segments from the South American-Antarctic ridge system with the Endurance subduction zone resulted in the cessation of spreading along the Powell ridge around early Miocene (Figure 5b) (Barker, 1995; Eagles & Livermore, 2002). This resulted in the formation of the South Scotia Ridge, which acted as a plate boundary between the Scotia Sea and Antarctic plates. After this reorganization, the South Orkney microcontinent and the Bruce bank started to diverge from the Jane and Discovery banks as the Proto-East Scotia Ridge and associated Sandwich plate were established in a back-arc setting (Figure 5b) (Vanneste & Larter, 2002). Collision of the South American-Antarctic Ridge with the South

Sandwich trench ended the extension along the southern part of the Proto-East Scotia Ridge (Eagles & Jokat, 2014). The newly formed Sandwich plate quickly accommodated the eastward directed trench roll-back of the South Sandwich trench. Spreading along the East Scotia Ridge resulted in a cessation of extension along the West Scotia Ridge in the late Miocene (Figure 5b) (Eagles et al., 2005). Back-arc spreading along the East Scotia Ridge is still active today, accommodating the eastward trench retreat of the South Sandwich Trench (Smalley et al., 2007).

### 2.5. The Gulf of California

The western margin of the North American plate was a long-lived convergent margin since the Jurassic and experienced an amalgamation of numerous terranes (e.g., Wright et al., 2016). When the active mid-ocean ridge between the Pacific and Farallon plates reached this convergent margin, a transtensional motion followed by ridge propagation into the continental margin led to the gradual detachment of Baja California from North American plate (Atwater, 1970; Atwater & Severinghaus, 1989).

The exact evolution of Gulf of California system (Figure 6) from a convergent to an extensional system has been the subject of numerous studies. The classical view is that continental rifting in the Gulf of California initiated in the middle Miocene and quickly transitioned to seafloor spreading during the late Miocene–early Pliocene (Lizarralde et al., 2007; Umhoefer, 2011). It is thought that this quick transition from continental rifting to breakup was due to the combination of an already existing hot and weak crust between the two strong crustal blocks of the Baja California and the Mexican mainland, and relatively rapid and very oblique plate motions between the North American and Pacific plates (Umhoefer, 2011).

Recently, Ferrari et al. (2018) suggested an alternative scenario postulating that extension in the region initiated in the middle Eocene via a wide continental rift adjacent to the southern Basin and Range province. The initiation of rifting was tentatively connected to the decrease in the North-American-Farallon convergence rates and the presence of slab windows in the mantle (Ferrari et al., 2018). This plate velocity decrease led to changes in plate boundary forces and the availability of fertile mantle beneath the Gulf of California. From the early to middle Miocene, extension localized in a narrow rift at the approximate location of the present-day Gulf of California (Ferrari et al., 2018). In middle Miocene time, cessation of subduction west of Baja California led to a change in the stress state that resulted in transtension/extension of the Gulf of California.

The available tectonic models agree that continental breakup occurred in the southern Gulf of California during the Pliocene (Lizarralde et al., 2007; Umhoefer, 2011). The transtensional rifting was diachronous and varied along strike from narrow to wide rifts (Lizarralde et al., 2007). Although the Baja Californian microcontinent has yet to detach from the North-American mainland, the continued activity in the Gulf of California suggests that separation might occur in the future. As such, Baja California can be considered a “proto-microcontinent.”

## 3. Present-Day Microcontinent Structure From Geophysical Data and Geological Models

Each region described in the previous section hosts one or more microcontinents that formed in association with a subduction system. In order to understand the formation of these microcontinents we need a comprehensive overview of their present-day structure, especially their rifted margins and the parent-continent conjugate margins. In the following, we will present a characterization of the rifted margins of selected microcontinents based on publicly available geophysical and geological data and models.

We use free-air gravity anomalies from Sandwell et al. (2014) and Bouguer gravity anomalies from the World Gravity Map (Balmino et al., 2012; Bonvalot et al., 2012) to investigate the margin architectures. Both data sets have a 1° spatial resolution. For inspecting magnetic anomalies, we use the gridded magnetic data from the NGDC marine trackline database (http://geomag.org/models/wdmam.html). These data are line-leveled and projected to sea-level according to the procedure described by Paterson and Reeves (1985). Where possible, published models of crustal thickness are also considered. In the Mediterranean we utilize EPcrust model (Molinari & Morelli, 2011), and in the Gulf of California CRUST1.0 is used (Laske et al., 2012). For all other regions, (global) crustal thickness models have an inadequate resolution. Instead, we use various local seismic studies to constrain crustal thickness where possible.

We also inspect few tomographic models for visually identifying the subducted slabs that may have been connected to subduction processes that led to microcontinent formation. Slab sinking velocities in the upper mantle are generally considered to be slightly less or equal to the Stokes sinking velocity of a sinking slab, which are around 2–7 cm/year (Capitanio et al., 2007). A simple calculation suggests that a slab sinking at 5 cm/year will arrive at the 660 km discontinuity about 13 Myr after the slab starts sinking. Due to the increased viscosity in the lower mantle, sinking velocities of slabs in the lower mantle are significantly slower at roughly 1.2 cm/year (Goes et al., 2008). Note that slabs may also deform and stall at the transition zone between upper and lower mantle, and a slab thickening by a factor of 2–3 in the viscous lower mantle is also expected (Gaherty & Hager, 1994).

Since all microcontinents discussed in this study formed in the Cenozoic time, and most of them in the last 30 Ma (see section 2), we expect to see the slabs in the upper mantle and upper lower mantle. For a qualitative inspection of the subducted slabs, and without the intention to assign exact ages to identified slabs, we have chosen the UU-P07 seismic tomographic model by Amaru (2007). The UU-P07 model has a good resolution in the upper mantle (0.4° laterally). The model was obtained by the use of 3-D reference models which are based on travel time residuals and independent models based on surface waves, normal models, and long period body waves. Other tomographic (DETOX-P3, Hosseini et al., 2019; MITP08, Li et al., 2008; and TX2019slab, Lu et al., 2019) are shown for comparison in the supporting information (Figures S2–S6).

We inspect the microcontinent margins and their conjugates and attempt to characterize the transition from continental to oceanic domain (continent-ocean boundary or transitional domain, COB or COT) expressed in geophysical data along selected profiles perpendicular on these margins. We consider the inboard COT location, where transitional crust starts to replace extensional continental crust, as the outer boundary of the relevant microcontinent. Where available, we show previously published COB/COTs, and adopt their outboard (where oceanic crust starts) COTs or COB interpretation if no inboard COT is available. Although identification of COBs based on potential field data may be less precise (Eagles et al., 2015), it does allow us to make a rough first order estimation of the microcontinent size and constrain a first order margin architecture. By tentatively identifying the first magnetic anomaly associated with sea-floor spreading, we obtain a first order estimate of the outboard limit of interpreted transitional crust. The conjugated profiles and identified COB/COTs are subsequently reconstructed to pre-breakup positions, allowing us to identify the symmetry (or lack of) of the margin morphology. Finally, we gather information and make a rough estimation of the continental crust volumes detached from active margins due to subduction processes.

### 3.1. Microcontinents in the Coral Sea

Located off the northeastern margin of Australia (Figures 1 and 2), the Louisiade Plateau is one of several pieces of continental lithosphere originally attached to this margin (see section 2.1). It is roughly 270 × 470 km in size and is separated from the Australian margin by the Coral Sea oceanic crust (Figure 2). While the Louisiade Plateau is submerged, the crustal nature of this microcontinent is inferred from geophysical data. Seismic reflection data show a similar structure as the conjugate continental Queensland plateau situated on NE Australian margin (Ewing et al., 1970; Feary et al., 1993; Taylor & Falvey, 1977). Dredged rocks from various plateaus in the NE Coral Sea basin support this continental nature (Hoffmann & Exon, 2008) and tectonic reconstructions indicate their origin from NE Australia (Figure 2c) (Gaina et al., 1999).

Continent-Ocean boundaries for the Coral Sea have been published and are included on the maps in Figures 2 and 6. The COBs of the Coral Sea and neighboring Rennell and Louisiade troughs are mainly interpreted based on gravity and magnetic anomaly data, and we have adopted the microcontinents outline from Seton et al. (2016) which is partially based on Gaina et al. (1999). This interpretation seems to hold against global geophysical data shown in our maps (Figure 7).

The Louisiade Plateau margin shows a smooth geometry (Figure 7e, profile ii). Both the Queensland plateau (Figure 7e, profile i) and the Louisiade plateau (Figure 7e, profile ii) margins have a subtle shelf break around the COB. The Queensland Plateau has a slightly steeper gradient in the “no-sediment bathymetry” and gravity data when compared to the conjugate Louisiade Plateau. This could indicate a slight asymmetry in the conjugate margins for these two selected locations. There appears to be a roughly 50 km wide gap between the interpreted COB of the Louisiade plateau and the first interpreted seafloor magnetic anomaly

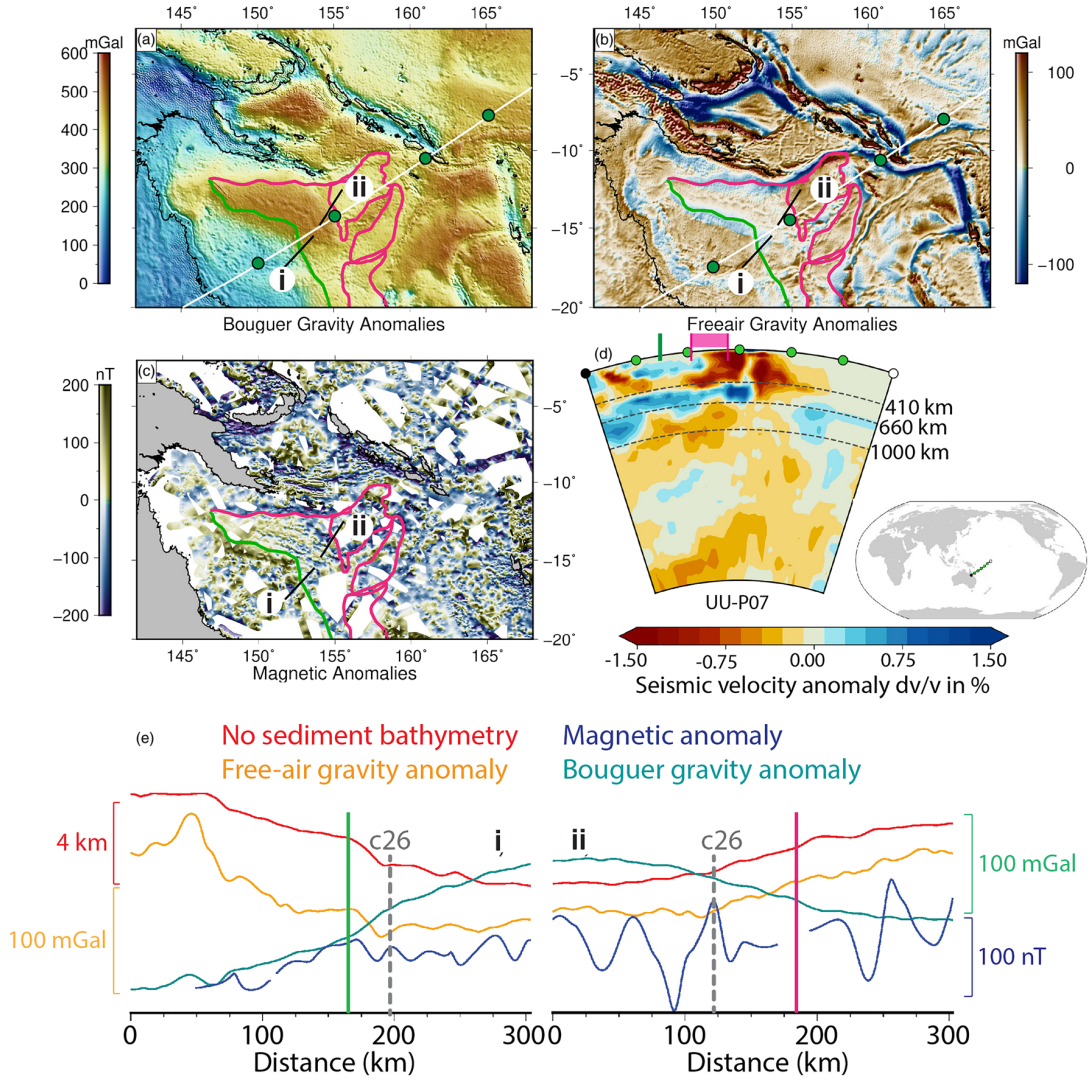


**Figure 7.** Geophysical data and models for the Coral Sea region. Legend as in Figure 2. Note the COB of the Coral Sea basin and the various microcontinents. The white line in panels (a) and (b) represents the profile along which the tomographic section is extracted. (a) Bouguer Gravity Anomalies. (b) Free-air Gravity Anomalies. (c) Magnetic anomalies, first spreading anomalies based on Gaina et al. (1999). (d) Seismic tomography section from UU-P07 crossing the Coral Sea region. (e) Profiles of geophysical data extracted along profiles i and ii. See Figures 2 and 7a–7c for location (black thin lines).

in this region (C26), and a distance of about 30 km between the COB and identified seafloor magnetic anomalies on the conjugate Queensland plateau (Figure 7e). Taking into account the uncertainties in identified COBs, we consider that the seafloor spreading at this specific location may have started slightly before C26. Following continental breakup, the formation of conjugate oceanic flanks was relatively symmetric.

Vintage seismic refraction data as well as gravity data and modeling suggest that the crustal thickness of the Louisiade plateau is around 20 km (Ewing et al., 1970). The conjugate Queensland plateau has a crustal thickness of around 25–28 km and the oceanic crust flooring the Coral Sea is around 7 km thick (Taylor & Falvey, 1977). Crustal thickness data for the Mellish Rise and the Kenn Plateau are poorly constrained. The regional crustal model from Segev et al. (2012) and Crust1.0 (Laske et al., 2012) indicate these plateaus have crustal thickness of around 7–11 km. The values for the Bouguer gravity anomalies on the various submerged plateaus are only slightly lower than the anomalies in the oceanic Coral Sea Basin (Figure 7a). This could indicate that the continental crust there is relatively thin.

**Table 1**
*(a) Table Detailing the Data Used in Calculations of Total Continental Crustal Area and Volume; (b) Global Continental Crustal Area and Volume and Total Continental Crustal Area and Volume for Each Region Described in This Paper; (c) The Amounts of Continental Crust in Classic and Subduction Associated Microcontinents, Normalized to Global non-Cratonic Continental Crust Area and Volume*

| (a) | Crustal area and volume for each MC-CF | | | | | |
|---|---|---|---|---|---|---|
| | Region | MC-CF | Area ($km^2$) | Thickness (km) | Source | Volume ($km^3$) |
| | California | Baja California Microplate | 1.70E + 05 | 18 | 6 | 3.10E + 06 |
| | Coral Sea | Louisiade Plateau | 1.29E + 05 | 20 | 1 | 2.57E + 06 |
| | | Mellish Rise | 8.10E + 04 | 10 | 2 | 8.10E + 05 |
| | | West Torres Plateau | 4.40E + 04 | 11 | 2 | 4.84E + 05 |
| | | Kenn Plateau | 7.33E + 04 | 11 | 2 | 8.07E + 05 |
| | South China | Macclessfield bank | 9.39E + 03 | 16 | 1 | 1.50E + 05 |
| | | Reed Bank | 2.00E + 04 | 24 | 1 | 4.79E + 05 |
| | Scotia | Barker Bank | 1.90E + 04 | 18 | 4 | 3.42E + 05 |
| | | Bruce Bank | 2.45E + 04 | 18 | 4 | 4.40E + 05 |
| | | Davis Bank | 2.12E + 04 | 17 | 4 | 3.60E + 05 |
| | | Discovery Bank | 2.07E + 03 | 25 | 5 | 5.17E + 04 |
| | | Herdman Bank | 3.37E + 03 | 18 | 4 | 6.06E + 04 |
| | | Jane Bank | 2.07E + 03 | 18 | 4 | 3.72E + 04 |
| | | Pirie Bank | 3.75E + 04 | 18 | 1 | 6.75E + 05 |
| | | South Georgia Microcontinent | 6.63E + 04 | 19 | 4 | 1.26E + 06 |
| | | South Orkney Microcontinet | 7.31E + 04 | 24 | 1 | 1.75E + 06 |
| | | Shag Rocks | 2.78E + 04 | 18 | 4 | 5.00E + 05 |
| | | Terror Rise | 5.14E + 03 | 17 | 4 | 8.74E + 04 |
| | Mediterranean | Corsic-Sardinia | 1.11E + 05 | 22 | 3 | 2.42E + 06 |
| **b)** | **Cont. Crust area and volume—Global** | | | | | |
| | | | **Area ($km^2$)** | **Volume ($km^3$)** | | |
| | Total continental crust | | 1.93E + 08 | 6.96E + 09 | | |
| | Cratonic crust | | 2.80E + 07 | 1.10E + 09 | | |
| | Non-cratonic continental crust | | 1.65E + 08 | 5.86E + 09 | | |
| | Classic microcontinents | | 3.22E + 06 | 5.08E + 07 | | |
| | **Crustal area and volume for each region** | | | | | |
| | **Region** | | **Area ($km^2$)** | **Volume ($km^3$)** | | |
| | California | | 1.70E + 05 | 3.10E + 06 | | |
| | Coral Sea | | 3.27E + 05 | 4.67E + 06 | | |
| | South China Sea | | 2.93E + 04 | 6.29E + 05 | | |
| | Scotia Sea | | 2.82E + 05 | 5.57E + 06 | | |
| | Mediterranean | | 1.11E + 05 | 2.42E + 06 | | |
| | **Crustal area and volume per MC type** | | | | | |
| | **Type** | | **Area ($km^2$)** | **Volume ($km^3$)** | | |
| | Microcontinent | | 6.09E + 05 | 1.02E + 07 | | |
| | Cont. fragment | | 1.40E + 05 | 3.05E + 06 | | |
| | Proto MC-CF | | 1.70E + 05 | 3.10E + 06 | | |
| | **Total** | | **9.19E + 05** | **1.64E + 07** | | |
| **c)** | **Percentage of non-cratonic continental crust** | | | | | |
| | **Feature** | | **Area (%)** | **Volume (%)** | | |
| | Classic microcontinents | | 1.95 | 0.87 | | |
| | Subduction microcontinents | | 0.56 | 0.28 | | |
| | All microcontinents | | **2.51** | **1.15** | | |

*Note.* (a) See the text for details regarding the calculation. Sources for crustal thickness assumptions are provided. Data sources: 1 = Seismic refraction data; 2 = Crust1.0 (Laske et al., 2012); 3 = EPcrust (Molinari & Morelli, 2011); 4 = S wave velocity model; 5 = Surface wave tomography; 6 = Seismic receiver functions.

Utilizing the published COBs and microcontinent outlines, we find that the total area of the microcontinent-like submerged plateaus offshore NE of Australia (Louisiade, Kenn and West Torrest Plateaus, and the Mellish Rise) is ~$3.27 \times 10^5$ $km^2$. Using a thickness of 20 km for the Louisiade Plateau and 11 km for the other microcontinents, we find a total crustal volume of microcontinents in the Coral Sea region of ~$4.75 \times 10^6$ $km^3$. A detailed overview of the areas, thicknesses, and volumes of each microcontinent can be found in Table 1.

A vertical profile extracted from the selected seismic tomography model shows a fast anomaly below Australia and the Coral Sea situated between 410 and 660 km (Figures 7d and S2). The slab appears to be

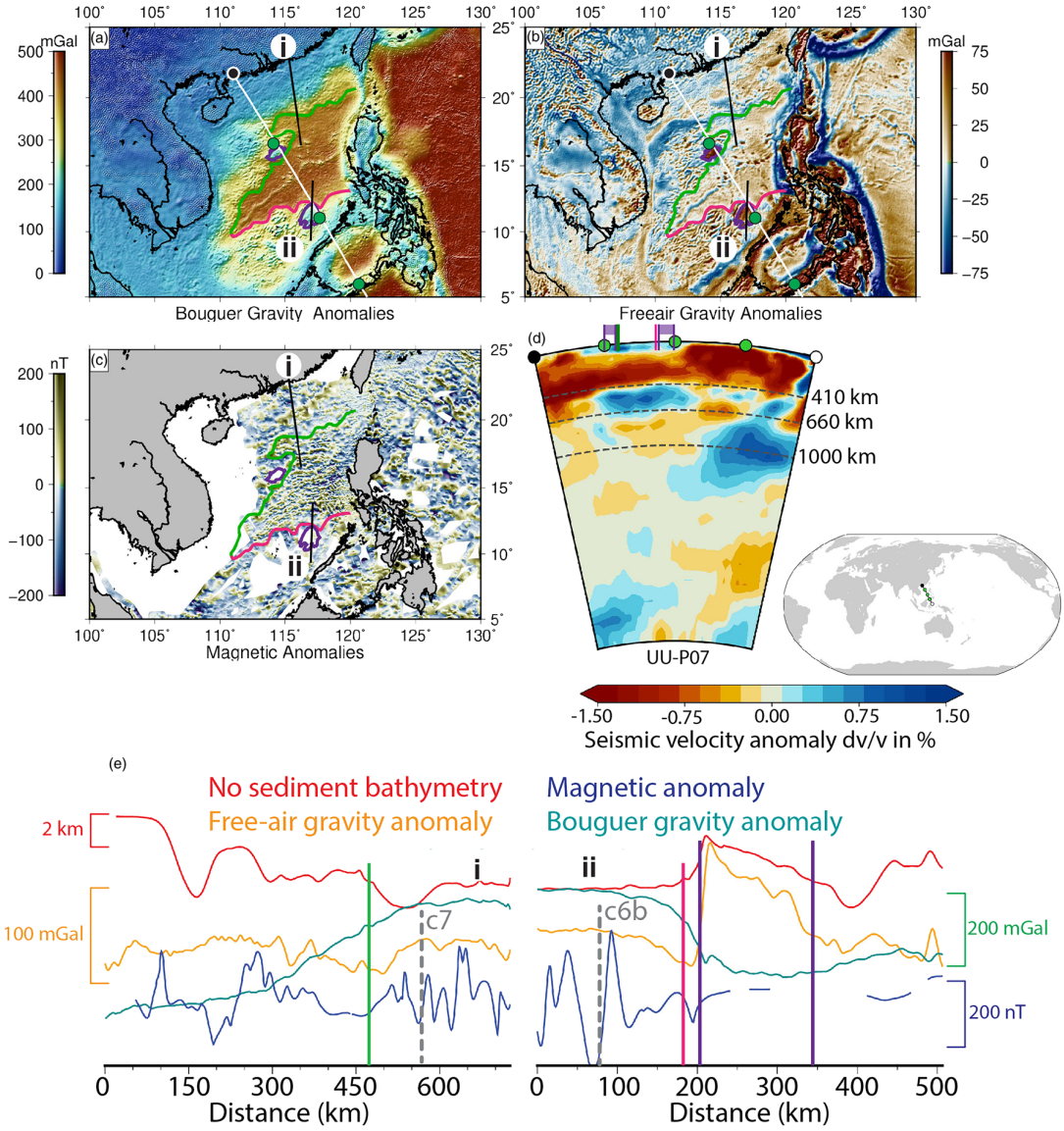


**Figure 8.** Geophysical data and models for the South China Sea region. Legend as in Figure 3. Note the COB of the South China Sea basin and the various microcontinents. The white line in panels (a) and (b) represents the profile along which the tomographic section is extracted. (a) Bouguer Gravity Anomalies. (b) Free-air Gravity Anomalies. (c) Magnetic anomalies, first spreading anomalies based on Barckhausen and Roeser (2004). (d) Seismic tomography section from UU-P07 crossing the South China Sea region. (e) Profiles of geophysical data extracted along profiles i and ii. See Figures 3 and 8a–8c for location (black thin lines).

detached from the surface and partially draped on the 660 km discontinuity toward the Australian continent. It underlies the Coral Sea basin, indicating a southwestward subduction that may have caused the formation of this basin. Below NE Australia the slab appears to penetrate into the lower mantle which may point to an older age of the slab, early Cenozoic or late Cretaceous. However, if the Coral Sea formed due to a NE oriented subduction (i.e., Whattam et al., 2008), another steeper, detached slab is visible in the upper lower mantle under the Pacific plate. Another slab dipping southward under the Australian continent could be identified in the lower mantle below 1,000 km, indicating episodic subduction under this continent at least since the Cretaceous time (Figure 7d).

### 3.2. Microcontinents in the South China Sea

During the opening of the South China Sea basin, the submerged Reed bank in the NE Palawan and SW Mindoro continental blocks detached from the Chinese mainland (Figure 3) (Bai et al., 2015; Sibuet et al., 2016; Taylor & Hayes, 1980). The submerged Macclesfield bank is still attached to the Chinese continental margin via extended continental crust (Figures 3 and 8). The Reed and Macclesfield banks have an approximate size of 160 × 80 and 200 × 130 km, respectively. Evidence for their continental nature is provided by various seismic refraction experiments (Hutchison, 2004; Pichot et al., 2014) as well as ODP drilling (Shipboard Scientific Party, 2000) and dredging (Kudrass et al., 1986).

Due to its high hydrocarbon potential, the South China Sea has been extensively surveyed. Consequently, several COB interpretations exist and the margin architecture is relatively well known. We utilize the South China Sea COB identification from Pichot et al. (2014), which is shown on the maps in Figure 3. This interpretation is primarily based on seismic reflection and refraction data (Franke et al., 2014; Pichot et al., 2014). Our COB interpretation based on available geophysical data agrees with published COBs based on seismic data (Figure 8). While a full set of COT boundaries for the entire South China Sea has not been published yet, there is a general consensus in the literature that a COT is relatively narrow (~30 km) in comparison with the width of the rifted margins themselves (400–800 km).

Due to the fact that South China Sea sits on a lower plate that subducts southeastward, the exact extent of its southern margin is unclear. However, the northern continental rifted margin is preserved and shows lateral variation in width (Figures 3a and 8). The eastern part of the northern rifted margin has a width of around 400 km, while south of Hainan the rifted margin is almost 800 km wide (Pichot et al., 2014) (Figures 3a and 8). Free-air gravity anomalies show a relatively smooth trend for the northern margin of the eastern subbasin, while the South China Sea's southern margin and the northern margin of the SW subbasin show a shorter wavelength variation, which may be correlated to brittle surface faults (Franke et al., 2014) (Figure 8b).

Geophysical data extracted along the profiles crossing the Chinese continental margin and the Reed bank show clear shelf breaks toward the oceanic South China Sea basin (Figure 8e). Toward the southern end of the Reed bank, the gradients in the geophysical data are less steep and the sharp northern boundary is not seen in the south. This suggests that the sharp transition from continental to oceanic crust is related to the process that localized extension during continental breakup.

Although the COT is interpreted to be abrupt, the magnetic data extracted along the profiles shows a ca. 100 km wide zone between the interpreted COB and first magnetic anomaly (C6b) (Figure 8e). Other authors observed a similar wide COT in NW Palawan, where it was interpreted to be related to magma starved extension resulting in mantle exhumation (Franke et al., 2011). The northern South China Sea margin also has a transitional region of 75 km wide (Figure 8e). The formation of these transitional zones may be related to a slow-down in extension after breakup or a period of mantle exhumation that may have preceded the formation of normal oceanic crust in the South China Sea.

Crustal thickness of continental blocks in South China Sea is constrained by wide-angle seismic refraction data and suggests values of around 24 km for the Reed Bank (Ruan et al., 2011) and 16 km for the Macclesfield bank (Huang et al., 2019). The conjugate northern margin has a crustal thickness of around 20–24 km, inferred from seismic refraction data (Pichot et al., 2014; Wang et al., 2006; Wu et al., 2012). Using the published COB from Pichot et al. (2014), we find that the total crustal area of the Reed and Macclesfield Banks is ~$2.93 \times 10^4$ km$^2$. A crustal thickness of 24 and 16 km for the Reed and Macclesfield banks, respectively, yields a total crustal volume ~$6.29 \times 10^5$ km$^3$ for the microcontinents found in the South China Sea region. A detailed overview of the areas, thicknesses, and volumes of South China Sea microcontinents can be found in Table 1.

Seismic tomography along a vertical profile crossing the South China Sea shows a fast anomaly between 410 and 660 km, and another wider anomaly to the south in the upper lower mantle below the Celebes Sea basin (Figures 8d and S3). Both anomalies could be linked to the two stages opening of the South China Sea (see section 2). The fast anomaly in the shallow lower mantle could be the detached proto-South China Sea slab, but the complex history of this region cannot rule out a different interpretation (Figure 8d).

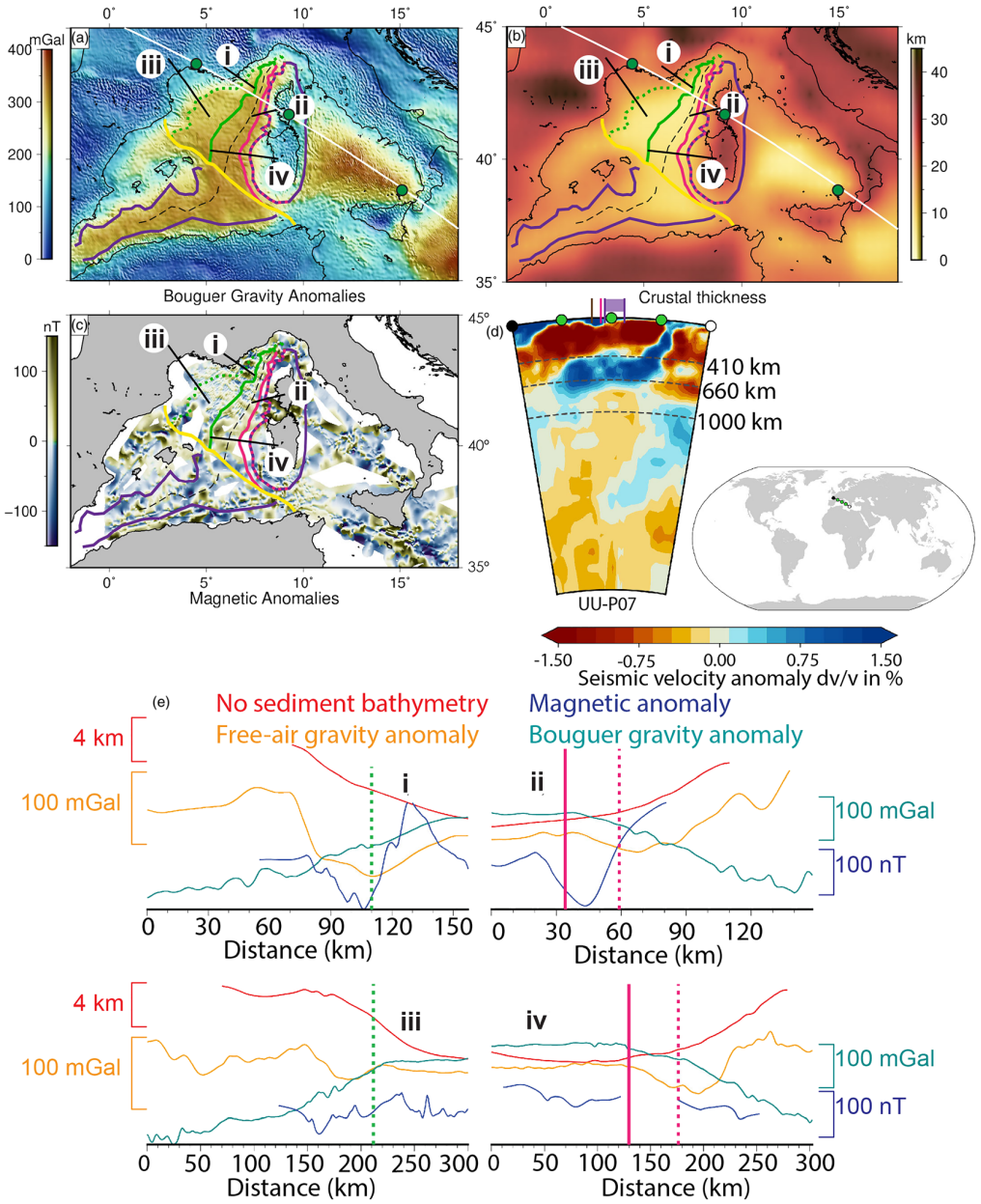


**Figure 9.** Geophysical data and models for the Central Mediterranean region. Note the COB of the Liguro-Provençal basin and the Corsica-Sardinia block. Legend as in Figure 4. The white line in panels (a) and (b) represents the profile along which the tomographic section is extracted. (a) Bouguer Gravity Anomalies. (b) Crustal thickness from EPCrust. (c) Magnetic anomalies. (d) Seismic tomography section from UU-P07 crossing the Central Mediterranean region. (e) Profiles of geophysical data extracted along profiles i, ii, iii, and iv. See Figures 4 and 9a–9c for location (black thin lines).

### 3.3. Microcontinents in the Central Mediterranean Sea

An excellent bathymetric fit of the margins (Bache et al., 2010), paleomagnetic constraints (Advokaat et al., 2014; Gattacceca et al., 2007), and onshore Hercynian and Alpine geology (di Rosa et al., 2017; Faccenna et al., 2004; Gueydan et al., 2017; Rossi et al., 2009) prove the continental origin of the Corsica-Sardinia block which detached from the southern margin of France after opening of the Liguro-Provençal basin (see also section 2.3). This continental block is roughly 230 × 470 km in size, is flanked

by the Liguro-Provençal basin to the west and the Tyrrhenian basin to the east, and toward the north is attached to the Adriatic microplate via extended, submerged, continental crust (Figure 9).

Based on seismic reflection data, in combination with gravity and magnetic observations, Rollet et al. (2002) published a map delineating the complete continent-ocean transition zone (COT) with both inboard and outboard COT boundaries for the Ligurian basin (Figures 4 and 9). These where subsequently expanded upon by Jolivet et al. (2015) who used a new seismic reflection profile. As these COT interpretations are well constrained and in agreement with our selected geophysical data, we utilize them in Figures 4 and 9. As the available COT interpretation does not cover the entire Corsica-Sardinia block, we have extended this interpretation of inboard COT by using the geophysical data described previously in the manuscript (Figures 4a and 9). The high amplitude magnetic anomalies are likely related to volcanic intrusions, as also suggested by Rollet et al. (2002) (Figure 9c).

The margins of the Corsica-Sardinia and their Eurasian conjugates have been extensively studied using seismic reflection and wide-angle refraction data (Gailler et al., 2009; Jolivet et al., 2015; Rollet et al., 2002). Both the Eurasian and Corsica-Sardinia margins show a progression of crustal types from a thinned continental margin to transitional crust which changes into a typical oceanic material in the center of the basin (Gailler et al., 2009). Geometrically, however, the Liguro-Provençal basin as well as its margins are asymmetric (Figures 4a and 9).

General asymmetry of the Liguro-Provençal basin is visible in the eastward lateral offset of the high Bouguer gravity anomalies (Figure 9a). The margin in the Gulf of Lyon is around 150 km wide, while the Sardinian margin is around 100 km wide (Bache et al., 2010; Gailler et al., 2009). The Corsican margin is roughly 70 km wide and the Ligurian margin has a width of circa 40 km. The Ligurian COT is around 40 km while the Corsican COT is around 50 km (Contrucci et al., 2001; Rollet et al., 2002). Note that the available age grid for the Central Mediterranean is not accurate (Figure 4). We suggest that our new interpretation of COT and tentative location of an extinct mid-ocean ridge can be used in the future to amend the existent age grid.

Crustal thickness from EP crust is around 5 km or less in both the Liguro-Provençal and Tyrrhenian basins. The Corsica-Sardinia block crustal thickness is as high as 30–35 km (Figure 9b). This is confirmed by various seismic refraction and receiver function studies and gravity inversion modeling (Bethoux et al., 1999; Chamot-Rooke et al., 1999). Based upon the same types of data, crustal thickness below Sardinia is around 25 km (Gailler et al., 2009). Coverage of magnetic data in the Liguro-Provençal basin is incomplete and a clear extinct ridge is difficult to identify (Figure 9c). We tentatively interpreted one (Figures 4b and 9), primarily based on the Bouguer gravity data.

The continental crust of the Corsica-Sardinia block covers an area of ~$1.11 \times 10^5$ km$^2$ (Table 1). Using the crustal thickness below the Corsica-Sardinia block from 0.5° resolution EPcrust model from Molinari and Morelli (2011), we calculate a total crustal volume of ~$2.42 \times 10^6$ km$^3$ for the Corsica-Sardinia block (Table 1).

A vertical profile through the selected seismic tomographic model shows a distinct high velocity anomaly in the upper mantle below the central Mediterranean which is interpreted as the Calabrian slab (Figures 9d and S4). The slab is still connected to the surface and has a subvertical dip down toward the 660 km discontinuity on which it has draped during SE directed trench-retreat.

### 3.4. Microcontinents in the Scotia Sea

The Scotia Sea region, located between the Antarctic Peninsula and the southernmost tip of South America (Figures 1 and 5), contains many small basins. It is bounded by an active trench to the east, the Shackleton Fracture Zone to the west, and the North and South Scotia Ridges to the north and south. These ridges contain multiple microcontinents (see section 2.4), however we will mainly focus on the South Orkney Microcontinent and the Terror Rise and their conjugates on the Antarctic and South American margins (Figure 5). The South Orkney Microcontinent is the largest microcontinent along the South Scotia Ridge (250 × 350 km) and the Terror Rise (180 × 70 km) represents the site of the most recent breakup between Tierra del Fuego and the microcontinents along the South Scotia Ridge.

The continental nature of the various microcontinents that line the South and North Scotia Ridges is established via their seismic signature in both refraction and reflection experiments, (Bry et al., 2004; Eagles

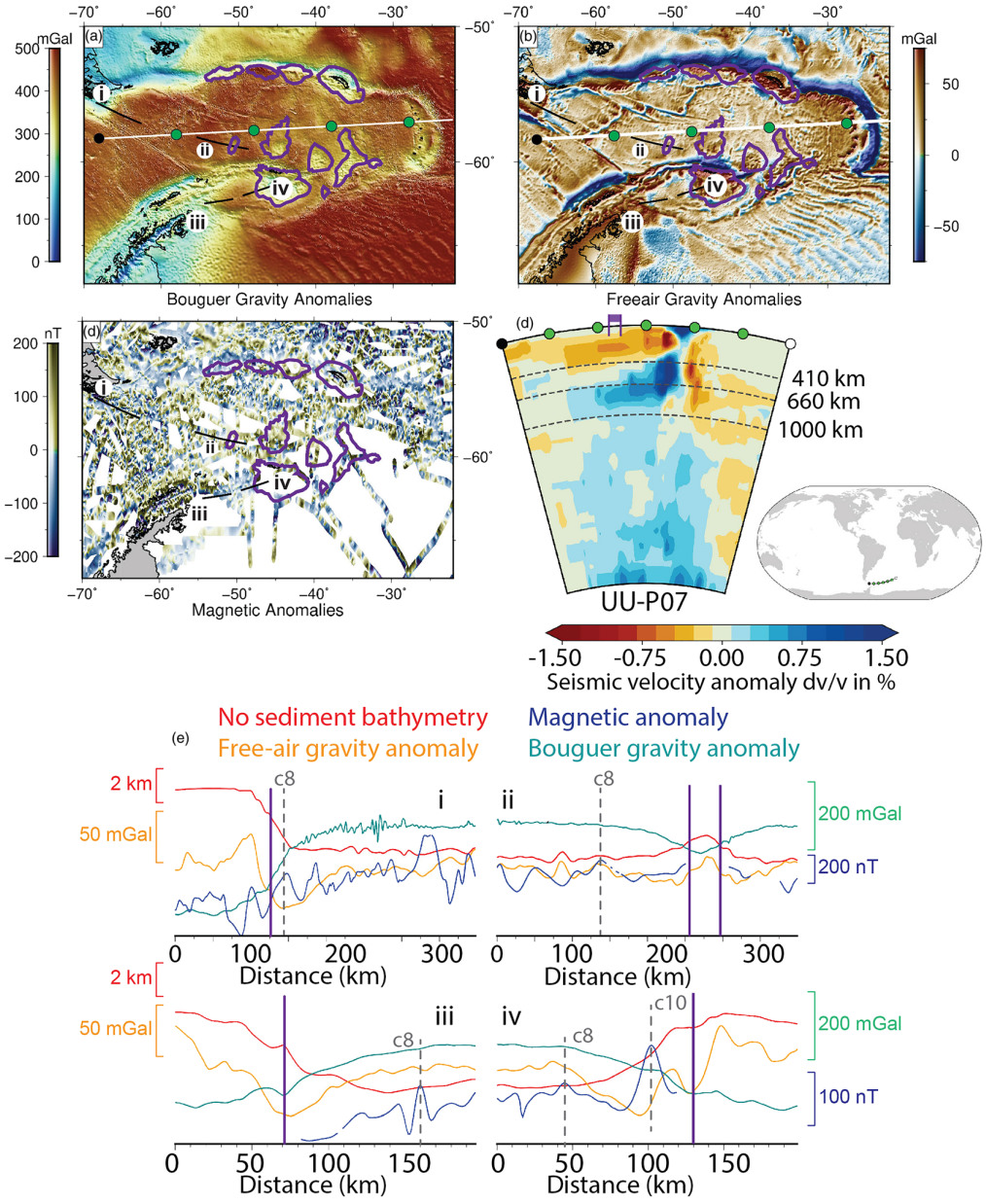


**Figure 10.** Geophysical data and models for the Scotia Sea region. Note the COB of the various microcontinents. Legend as in Figure 5. The white line in panels (a) and (b) represents the profile along which the tomographic section is extracted. (a) Bouguer Gravity Anomalies. (b) Free-air Gravity Anomalies. (c) Magnetic anomalies, first spreading anomalies based on Eagles and Livermore (2002) and Eagles et al. (2005). (d) Seismic tomography section from UU-P07 crossing the Scotia Sea region. (e) Profiles of geophysical data extracted along profiles i, ii, iii, and iv. See Figures 5 and 10a–10c for location (black thin lines).

et al., 2006; Pandey et al., 2010), their magnetic signature (Eagles et al., 2006), and their conjugate position to the Tierra del Fuego margin (Eagles et al., 2006; Eagles & Jokat, 2014). Outcropping continental rock on the South Georgia and South Orkney Islands (Carter et al., 2014; Dalziel et al., 1981; Trouw et al., 1997) also provide undisputable evidence for their continental nature.

As there is no published COB available, nor any indication of the COB in seismic data, we tentatively interpret the extent of the various microcontinents from potential field data (Figures 5 and 10). The lateral transforms of the North and South Scotia Ridges have strong signatures in the geophysical data, hindering the

delineation of various microcontinents (Figure 10). However, by using bathymetric data as a starting point and combining it with free air and Bouguer gravity anomalies we tentatively interpret the extent of the various microcontinents in the region.

Along the Southern Scotia Ridge, the outline of the South Orkney Microcontinent is clearly visible in all gravity and bathymetric data (Figures 5a and 10). Some of the smaller southern banks (Terror Rise, Pirie, and Jane Banks) have a less pronounced signature (Figures 5a and 10), likely due to their extended continental nature. The various sedimentary basins in between the Terror Rise, Pirie Bank, and Bruce Bank have also a distinct signature in the Bouguer gravity field (Figure 10a), aiding in the interpretation of these microcontinents.

The Terror Rise COB interpreted on the selected profile lies at ca. 100 km landward from magnetic anomaly C8 (Figure 10e). On the South American side, this distance is around 20 km. The magnetic anomalies along the South Orkney Microcontinent-Antarctica profiles have very low amplitude variations, which may show either high sediment thickness or possibly the presence of lower magnetic crust, like serpentinized exhumed mantle. Nonetheless, we interpret a distance of roughly 90 km between the Antarctic COB and the C8 anomaly and 30 km between the C10 anomaly and the South Orkney Microcontinent COB (Figure 10e).

Profiles crossing the margins of both the South American-Terror Rise and the South Orkney Microcontinent-Antarctica conjugates show a distinct difference between the two margin sets (Figure 10d). The South American margin has a clear and distinct shelf break and transition into the oceanic domain, primarily observable in the Bouguer gravity anomalies. Amplitudes of the geophysical data are much less pronounced on the Terror Rise, but as the profile crosses the entire Terror Rise, its extent is clear (Figure 10e).

Based on seismic reflection data, Coren et al. (1997) interpreted transitional crust on the two conjugate margins of the Powel basin which is about 60 km wide on the Antarctic side and approximately 20 km wide on the side of the South Orkney Microcontinent. The profiles crossing the margins of Antarctica and the South Orkney Microcontinent have much a smoother signature and the aforementioned COTs cannot be recognized (Figure 10e). The margin of the South Orkney Microcontinent appears to be slightly steeper, matching the potential asymmetry postulated above.

Seismic refraction data indicate that crustal thickness of the South Orkney Microcontinent is around 22–25 km (King & Barker, 1988). While we did not find any refraction experiments that cross the Terror Rise in the literature, we did find refraction data on its southeastern conjugate, the Pirie Bank, which has a crustal thickness of ~18 km (King & Barker, 1988). The crustal thickness beneath the Discovery bank is in the range of 23–28 km (Vuan et al., 2005) as inferred from surface wave tomography. *S* wave velocity models indicate a Moho depth of between 17 and 20 km below the South Scotia Ridge (Vuan et al., 1999). As these data are all roughly within the same range and the Terror Rise appears to be formed by extended continental crust, we assign a continental crustal thickness for this block of 17 km. Crustal thickness below thus the North Scotia Ridge is, between 16 and 19 km according to *S* wave velocity models (Vuan et al., 1999).

Using our tentative interpretations for the extent of the microcontinents in the Scotia Sea region, we find that they constitute a total area of ~$2.82 \times 10^5$ km$^2$. Using published crustal thickness data, we ascertain a total crustal volume of microcontinents in the Scotia Sea region of ~$5.57 \times 10^6$ km$^3$. An overview of the areas, thicknesses, and volumes of Scotia Sea microcontinents is presented in Table 1.

Seismic tomography profile across the Scotia Sea shows a thin fast anomaly extending from the surface to 410 km where it becomes wider and almost subvertical up to the 660 km discontinuity (Figure 10d). The fast anomaly seems to continue with a horizontal, wider anomaly along and below the 660 km discontinuity. Other tomographic models show either a very weak vertical fast anomaly or one that lies flat on the 660 km discontinuity (Figure S5). We interpret this fast anomaly as the subducting South American oceanic lithosphere. Faster anomalies are observed in the lower mantle, but if they are slabs, they may be connected with older episodes of subduction (Figure 10d).

### 3.5. Microcontinents in the Gulf of California

Originally attached to the North-American plate, the Baja California started to detach following breakup occurred in the Gulf of California (Stock & Hodges, 1989). As it is not completely separated from the North American continent (Figure 6), Baja California can be considered a proto-microcontinent.

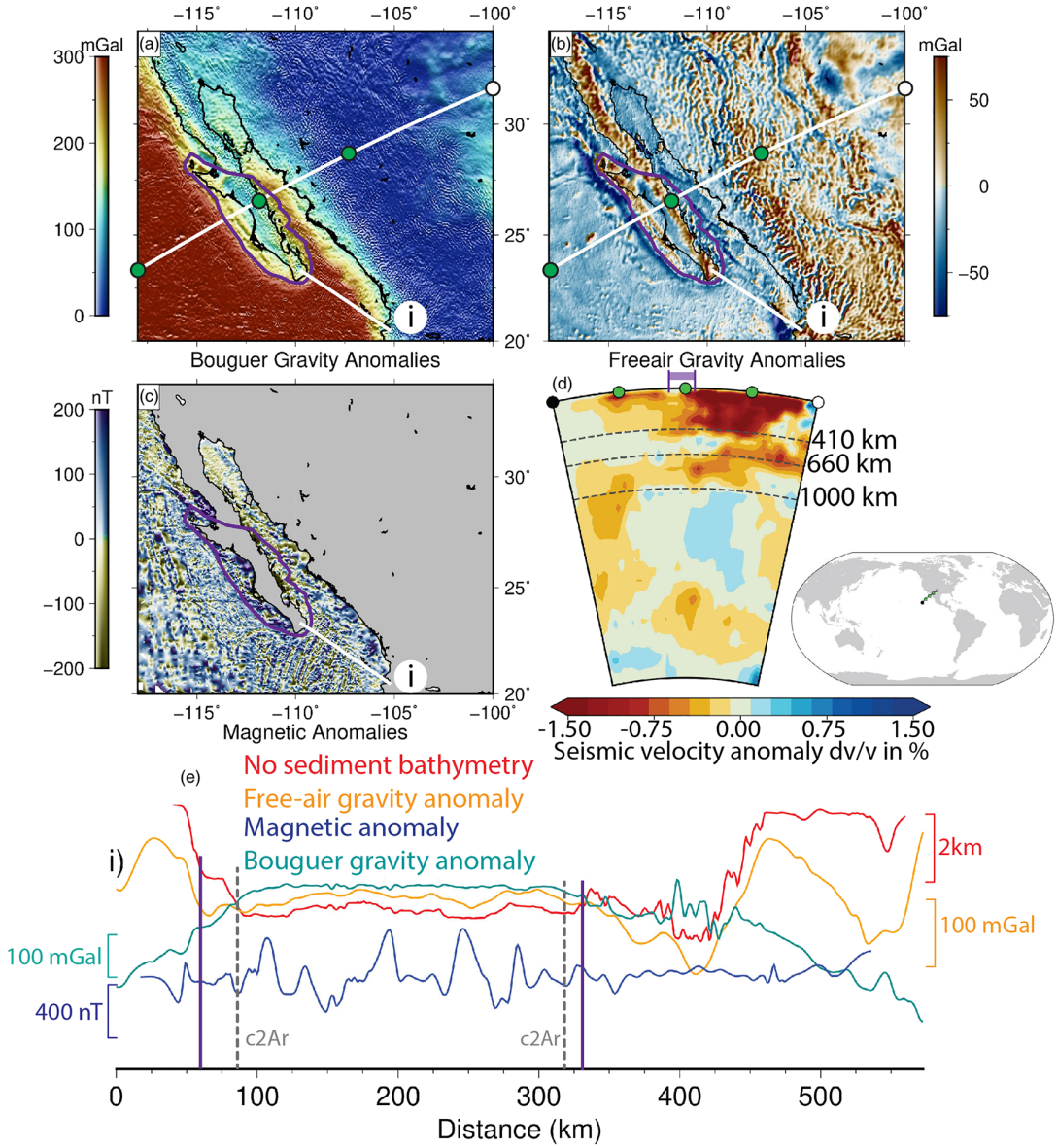


**Figure 11.** Geophysical data and models for the Gulf of California region. Legend as in Figure 6. The white line in panels (a) and (b) represents the profile along which the tomographic section is extracted. (a) Bouguer Gravity Anomalies. (b) Free-air Gravity Anomalies. (c) Magnetic anomalies, first spreading anomalies based on Ness et al. (1991). (d) Seismic tomography section from UU-P07 crossing the South China Sea region. (e) Section of geophysical data extracted along profile i. See Figure 6 and 11a–11c for location (black thin lines).

Separated from the Mexican mainland by the Gulf of California, Baja California is around 200 km long and its length (up to the northernmost part of Gulf of California) is approximately 1,000 km. To the west, it is bounded by the Guadalupe and Magdalena oceanic microplates, which are thought to be remnants of the Farallon plate. The continental nature of the Baja California is indicated by seismic refraction experiments and receiver function analysis (Lizarralde et al., 2007; Persaud et al., 2007).

A full set of continent ocean boundaries or transition zone location is lacking, but Sutherland et al. (2012) did interpret a COT on a seismic reflection/refraction line across the southern part of the Gulf of Mexico. Based on their interpretation, conjugate COT widths differ by about 5 km, with a 14 km wide COT on the Baja California side and a 19 km wide COT for the conjugate North-American margin (Figure 11e). Using the

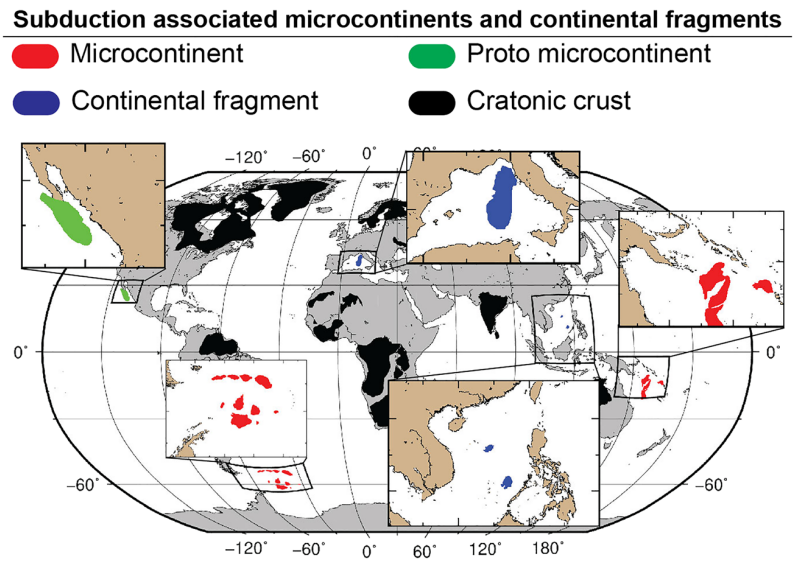


**Figure 12.** Overview of the extent various microcontinents and continental fragments associated with subduction systems discussed in this paper as well as the area and volume. The black area represents cratonic continental crust and is neglected in the calculations. See the text for details on area and volumetric calculations.

selected geophysical data in this study, we tentatively identify the extent of the Baja California proto-microcontinent (Figures 6a and 11). The western boundary is delineated by the paleo plate-boundary of the subduction zone. Although Baja California is still attached to the North-American continent, we interpret a northern boundary around 27.5° north which coincides with changes in the Bouguer gravity anomalies signature (Figure 11a), changes in the crustal thickness (Figure 11b), and with the northern extent of >250 mGal Bouguer gravity anomaly in the Gulf of California basin (Figure 11a).

Along the extracted profile (Figure 11e, profile i), we identify a region of roughly 50 km between the interpreted COB of Baja California and the C2Ar magnetic anomaly that could be related to oceanic spreading. On the conjugate North American side, this region is around 10 km wide (Figure 11e). Crustal thickness of the Baja California block is variable, with a 29–34 km thick crust beneath the western side of the peninsula, and a thinner 24–27 km thick crust underneath the eastern side (López-Pineda et al., 2007; Persaud et al., 2007). Crustal thickness in the conjugate North-American plate is also variable, with a thickness of 18 km in the south to 32 km in the north (López-Pineda et al., 2007).

Using the identified extent of the Baja California proto-microcontinent, we find a total area of ~$1.7 \times 10^5$ km$^2$. A crustal volume for the Baja California proto-microcontinent of ~$3.1 \times 10^6$ km$^3$ is calculated using crustal thickness from Crust1.0 from Laske et al. (2012).

A rather diffuse fast anomaly can be observed in the upper mantle below the Gulf of California between 410 and 660 km depth (Figures 11d and S6), and probably unlikely to be the Farallon slab. A larger, almost vertical fast anomaly is observed in the lower mantle, below 1,000 km. Previous tomographic studies suggest the Farallon plate traveled a longer distance to the east and is now located in the lower mantle (van der Meer et al., 2010).

The interaction of the subducting Farallon-Pacific active mid-ocean ridge and the continental North America led to the fragmentation of the Farallon plate in two smaller plates, the Magdalena and Guadalupe microplates, and the formation of a slab window. Recent studies based on denser seismological data were able to image these subducted microplates and the slab window in the upper mantle below the Gulf of California (Paulssen & de Vos, 2017). A high-velocity anomaly of 40 to 60 km thickness situated at depths of 115 to 135 km has been imaged below southern and central Baja California; this anomaly does not continue to the north implying the presence of a slab window. Paulssen and de Vos (2017) suggest that the subducted slab remnants cause coupling between Baja California and Pacific which influence the slow detachment of the proto-microcontinent.

## 4. Observed Patterns in Microcontinent Formation in Subduction Systems

In this paper we have identified and described various microcontinents that formed in (association with) subduction systems worldwide (Figure 12) where extension in the upper or lower plate is linked to the dynamics of subducted slabs and surrounding mantle. Guided by our chosen examples and previously proposed mechanisms for microcontinent formation in extensional settings, our goal is to identify possible links between the structure of preserved microcontinents, of surrounding oceanic basins, and identified subducted slabs. These causal links may give clues of how active continental margins were affected by subduction in geological time.

### 4.1. Potential Microcontinent Formation Mechanisms

Mechanisms that explain microcontinent formation can be roughly divided into two categories. The first category proposes that plate boundary relocations (ridge jumps) assisted by mantle heterogeneities can lead to microcontinent formation (Abera et al., 2016; Müller et al., 2001). A second category emphasizes the role of inherited tectonic structures and the need for a strike-slip motion, or a rotational component in the breakup processes resulting in the isolation of a small fragment of continental crust (Molnar et al., 2018; Nemčok et al., 2016; Péron-Pinvidic & Manatschal, 2010; van den Broek et al., 2020). The microcontinents described in this paper appear to have mainly formed via mechanisms of the second category.

#### 4.1.1. Rotational Kinematics and Inherited Structures

All basins that separate microcontinents from their parent continents experienced a diachronous breakup and propagating mid-ocean ridges. This was caused by either rotational development of the system, such as in the Mediterranean Sea, or by oblique plate motions, such as those present in the Gulf of California. Furthermore, most of the microcontinents described here have formed in a back-arc setting with a retreating slab. The notable exception to this are the microcontinents in the South China Sea where the South China Sea basin was in a lower plate position with respect to the trench (Figure 3) (Hall & Breitfeld, 2017). Coral Sea opening could also have been triggered by a northward subducted slab, but this scenario is still debated (i.e., Whattam et al., 2008).

Another aspect that all subduction-associated microcontinents have in common is a long and complex tectonic history. The preextensional tectonic settings of all examples discussed above, except the Scotia Sea, are characterized by long-lived accretionary margins. Such margins tend to display crustal growth during their lifetime, usually resulting from the accretion of allochtonous terranes to the overriding plate (Cawood et al., 2009; Stern & Scholl, 2010; Tetreault & Buiter, 2012). The accretion or subduction of such terranes is dependent on the rheological and geometrical structure of the incoming terrane (Tetreault & Buiter, 2012), however any accreted fragments likely result in the formation of lithospheric scale inherited structures as they are transferred from the lower to the upper plate.

Recent analogue and numerical work indicates that this combination of rotational kinematics with inherited structures is a requirement for continental rifting and microcontinent formation (Molnar et al., 2018; van den Broek et al., 2020). The differential motion applied to different segments of the crust induces differential stress, which then localizes in an inherited weak zone. Formation of the Corsica-Sardinia block is likely to be the result of this kind of mechanism (van den Broek et al., 2020).

#### 4.1.2. Hot, Thick Crust and Oblique Rifting

In addition to inherited tectonic structures, the initial thermal configuration of the crust can also play an important role in the evolution of rifting. The increasing temperatures result in decreased crust-mantle coupling, profoundly influencing margin evolution (Brune et al., 2017). However, as different initial configurations can yield similar results, it is difficult to draw any conclusions about the preextension configuration based on the final rift architecture (Brune et al., 2017).

Both the South China Sea and the Gulf of California where characterized by long-lived accretionary margins that likely resulted in a hot and thick crust in the preextensional overriding plate. Both regions also experienced rifting over large areas before strain localization resulted in continental breakup and oceanic basin formation. Finally, both regions show a distinct slow velocity anomaly in the upper mantle (Figures 8 and 11). A similar situation might have occurred in the Coral Sea, but we lack data to make any further inferences.

Formation of (proto-)microcontinents in the South China Sea and the Gulf of California suggest that hot and thick convergent margins that have a heterogeneous architecture are prime locations for microcontinent formation in a subduction setting. While the exact mechanism responsible for formation of the microcontinents in the South China Sea remains enigmatic at this time, the Gulf of California provides some more clues.

In the Gulf of California, continental breakup occurred after detachment of an oceanic slab, possibly formed by the fragmentation of the Farallon slab. However, as evidenced by the Mexican Basin and Range province, the North-American upper plate was already experiencing (back-arc) extension prior to the oceanic slab breakoff (Ferrari et al., 2018). As the subducting slab was very young, it may have subducted with a shallow dip. This shallow slab dip likely inhibited the formation of a back-arc basin that requires steeper slabs with a dip greater than 50° (Lallemand et al., 2005).

Present-day spreading in the Gulf of California is also highly oblique (Figures 6 and 11), likely related to the highly diachronous subduction of the oceanic plate. Furthermore, results from numerical modeling indicate that oblique rifting is energetically favorable to continental breakup (Brune et al., 2012). We thus speculate that the oceanic slab breakoff may have altered the stress state of the upper plate enhancing the breakup started by the highly oblique propagation of the mid-ocean ridge into North American continent.

#### 4.1.3. Continental Crust Fragmentation

We are missing a clear mechanism explaining the formation of microcontinents in the Coral and Scotia Sea regions. Both regions show some interesting similarities: (1) a high number of smaller scattered continental blocks (Table S1/Figure 7), and (2) a location at the junction between large tectonic plates.

The Scotia Sea region is sandwiched between the South American and Antarctic plates whereas the Coral Sea was close to the interaction of the Australian, Pacific, and Eurasian plates (Figures 2 and 5). Such large plates are strong and long lived. Modeling of global mantle convection suggests that their size is controlled by large-scale mantle flow patterns and their lifespan is related to the reorganization of mantle flow (Mallard et al., 2016). These authors suggest that the fragmentation in smaller plates is driven by subduction geometry (Mallard et al., 2016). Indeed, the cessation of spreading in the Coral Sea has previously been related to changes in absolute plate motion vectors (Schellart et al., 2006). We thus speculate that the episodes of crust fragmentation and the formation of microcontinents in the Scotia and Coral sea regions are likely related to (larger) changes in the subduction system at the junction of large tectonic plates.

Microcontinents and continental fragment formed in active margin settings may also have played an important role in the tectonic evolution of the margins studied here. Observations on geophysical data collected from the eastern segment of the South Scotia Ridge suggests that, due to its weaker nature, continental crust localizes deformation (Galindo-Zaldívar et al., 2002). Dynamic subduction systems induce rapid changes in the stress field. The deformation of continental material would then accommodate these changes, showing the importance of microcontinents or continental fragments in subduction systems and shaping the active margins.

### 4.2. Rapid Microcontinent Formation

The duration of rifting/seafloor spreading connected to various microcontinents in subduction settings may also indicate a link to the subduction dynamics. Rifting between Eurasia and the Corsica-Sardinia block lasted only 9 Myr and seafloor spreading lasted around 8 Myr (Gattacceca et al., 2007; Jolivet & Faccenna, 2000). In the Scotia Sea, rifting in between the Discovery and Pirie banks and between the Pirie Bank and Terror Rise lasted 20 Myr altogether (Eagles & Jokat, 2014) (Table 1).

On the other hand, rifting in the Coral Sea region is thought to have taken 50 Myr (Bulois et al., 2018), whereas rifting in the South China Sea region took around 30 Myr (Franke et al., 2014). Seafloor spreading in these regions lasted 8 and 18 Myr, respectively (Table S1). The Gulf of California experienced a 28 Myr long rifting episode preceding breakup (Ferrari et al., 2018) (Table S1).

From these comparisons it follows that microcontinents formed in the short-lived rift and drift systems tend to be surrounded by, or are in proximity of, larger continental masses. They are, in a sense, formed in a more confined setting. Longer lived microcontinent formation tends to occur in (relatively) unconfined systems which are bounded on one side by (large) subducting oceanic plates (e.g., the South China Sea and the Coral Sea).

The formation of microcontinents in unconfined subduction systems might have longer rifting episodes as changes in subduction dynamics might be more easily accommodated in the neighboring oceanic domain without affecting too much the of the continental margins. Conversely, microcontinent formation in a confined system has shorter rift and spreading episodes. The proximity of such (large volumes of) buoyant continental material could result in limited space, which combined with dynamically changing subduction forces, induce rapid continental rifting, and microcontinent formation.

All microcontinents presented in this study formed during Cenozoic time and, to our knowledge, no Mesozoic or older subduction associated microcontinents are preserved in situ. This suggests that microcontinents formed in subduction settings have a relatively short life span. It seems likely that this is due to the fact that these microcontinents can be easily incorporated into orogenic and accretionary systems during subsequent basin closure. As such it follows that many subduction associated microcontinents are to be found in the geological record although subsequent deformation and metamorphism might complicate their recognition as such.

This observation of rapid formation and short lifespans is in agreement with recent work described by Mallard et al. (2016). These authors suggest that small plates can rapidly adjust to changes in subduction systems and that they form in tens of millions of years. Note that their 3-D modeling of mantle convection results in tectonic-plate like upper lid configuration and plate boundary dynamics, but no continental domains. However, numerical modeling and our observations may suggest that events of microcontinent formation in subduction settings can be potentially used as a proxy for identifying episodes of dynamic changes in subduction systems.

### 4.3. A Relation Between Microcontinent Formation Time and COT Width?

Regions of transitional or unconstrained crustal nature between the identified COB and the first magnetic anomaly associated with seafloor spreading vary between 10 (Gulf of California margin) and 150 km (margin of the Gulf of Lyon), but averaging around 50–75 km (Figures 7–11, S1, Table S1). The existence of transitional crust along these margins as well as the absence of clear syn-breakup volcanic eruptions and Seward Dipping Reflectors (SDRs) suggests that all discussed microcontinents probably formed in a magma-poor rifted margin setting.

The widest of these interpreted areas of transitional crust are located along the Terror Rise margin in the Scotia Sea region (100 km wide) and along the margin of the Gulf of Lyon in the central Mediterranean (150 km wide). Widths of this transitional crust in the more unconfined regions are generally around 50–75 km (Table S1). Microcontinents formed in the confined settings thus have wider zones of transitional crust when compared with microcontinents formed in unconfined settings. The wider regions of transitional crust in the confined settings might be the result of a low magma supply as also observed in passive margins studies (i.e., Buck, 2004), which in the cases analyzed here is pointing to a stalled or very slow subduction regime.

## 5. Microcontinents and Global Continental Crust Evolution

Throughout geological history microcontinents and continental ribbons played a crucial role in transferring continental crust across oceans and contributing to large continental mass formation. For example, Oaxaquia was a Proterozoic microcontinent that accreted to North America during the late Paleozoic (Ortega-Gutierrez et al., 1995). A myriad of "continental ribbons" originated from northern Gondwana and accreted to Eurasia during closure of the Paleo- and Neo-Tethys, forming the Variscan and Alpine collisional orogens (von Raumer et al., 2003). From present-day area extent of known continental crust area, ca. 14% represent old cratonic area (according to the World Geological Map published by Bouysse, 2014) (Table 1, Figure S11). The remaining crust was formed in oceanic domains as island arcs and microcontinents.

The microcontinents discussed in this paper are situated offshore and are (partially) submerged, therefore they can be easily neglected when assessing the global volume of continental crust. A first order quantification of the area and volume of these tectonic blocks shows that an area of $9.19 \times 10^5$ km$^2$ and a total crustal volume of $1.64 \times 10^7$ km$^3$ (see Table 1 for details) have formed due to subduction-related continental breakup. This is about 0.56% of the global non-cratonic continental crustal area and 0.28% of the global

non-cratonic continental crustal volume; values that can be higher as many other submerged, continental pieces in SW Pacific may be considered in the subduction-related microcontinent category.

If we add to this calculation the area and volume of in-situ preserved microcontinents associated with passive margin formation (i.e., Gaina & Whittaker, 2020) (Table 1, Figure S11), we conclude that about 2.5% of present-day extent of non-cratonic continental crust (and 1.15% of its volume) is found away from the main continental masses. While 2.5% seems low, results from 3-D mantle convection numerical models suggests that fragmentation of tectonic plates may have decreased through the geological time due to Earth's cooling (Mallard et al. 2016). This seems reasonable as the present-day age and structure of continental crust is heterogeneous. We therefore conclude that the formation of microcontinents as inferred from preserved present-day examples may have been important in the crustal formation and redistribution process in the deep time.

## 6. Conclusions

This study reviewed various in-situ microcontinents that formed in active continental margin settings. Our examples show that microcontinents and continental fragments affiliated with subduction settings occur worldwide. They tend to form in regions with a complex tectonic history, are often associated with back-arc regions, and are frequently bordered by small marginal basins. Their total area covers ca $9.19 \times 10^5$ km$^2$ although individual microcontinents or continental fragments are generally small ($<17 \times 10^4$ km$^2$). The active margins from which they detach often contain inherited structures. Reactivation of these structures appears to be a major factor in the formation of microcontinents and continental fragments.

We identify various common characteristics that may point to their potential formation mechanisms. Some microcontinents form in a rotational kinematic setting, while others form in an obliquely rifting setting, and both types require the presence inherited structures. Finally, formation mechanisms for the systems with multiple microcontinents are difficult to identify, but multiple plate boundary relocations within the margins of larger continental masses may be explained by the weakness of continental crust that is preferentially exploited when changes in plate motions and therefore stress redistribution occur.

Rifting and subsequent seafloor spreading in confined basins, located in close proximity of large continental masses (e.g., the Mediterranean Sea), tends to be reduced when compared to back-arc basins that form next to larger oceanic basins (e.g., the Coral Sea). We speculate that this discrepancy stems from different responses to changes in subduction dynamics.

Although differences in formation time exist, their formation is generally quick. Furthermore, all discussed subduction associated microcontinents and continental fragments have formed in the Cenozoic and no older microcontinents or continental fragments associated with active margins can be found in situ today. This is in agreement with modeling results that suggest that small subduction systems can rapidly adjust to dynamic changes. We thus suggest that formation of microcontinents in subduction systems can be used as a proxy for such changes to subduction dynamics.

**Acknowledgments**
We thank the Editor, the Associate Editor, an anonymous reviewer, and Alexander Cruden for their constructive reviews. Their excellent comments and suggestions substantially improved our manuscript. Both authors acknowledge support from the Research Council of Norway through its Centers of Excellence funding scheme, project 223272. They also acknowledge funding from the Horizon2020 Marie Sklodowska Curie Initial Training Network grant 674899—SUBITOP. Maps in Figures 1–12 were made using Generic Mapping Tools (GMT; Wessel et al., 2013). We have used the free application GPlates (gplates.org) for tectonic reconstructions. Seismic tomography section was constructed using the SubMachine web application (Hosseini et al., 2018). In order to avoid distortion of data we utilized perceptually uniform color schemes (Crameri, 2018a, 2018b).

## References

Abera, R., van Wijk, J., & Axen, G. (2016). Formation of continental fragments: The Tamayo Bank, Gulf of California, Mexico. *Geology*, *44*(8), 595–598. https://doi.org/10.1130/G38123.1

Advokaat, E. L., van Hinsbergen, D. J. J., Maffione, M., Langereis, C. G., Vissers, R. L. M., Cherchi, A., et al. (2014). Eocene rotation of Sardinia, and the paleogeography of the western Mediterranean region. *Earth and Planetary Science Letters*, *401*, 183–195. https://doi.org/10.1016/j.epsl.2014.06.012

Amante, C., & Eakins, B. W. (2009). ETOPO1 arc-minute global relief model: Procedures. *NESDIS NGDC-24*, *NOAA Technical Memorandum*, Boulder, CO: NOAA.

Amaru, M. L. (2007). *Global travel time tomography with 3-D reference models* (Vol. 274). Utrecht, The Netherlands: Utrecht University.

Atwater, T., & Severinghaus, J. (1989, January 1). Tectonic maps of the Northeast Pacific. In Winterer, Hussong, & Decker (Eds.). The Eastern Pacific Ocean and Hawaii.

Atwater, T. (1970). Implications of plate tectonics for the Cenozoic tectonic evolution of Western North America. *GSA Bulletin*, *81*(12), 3513–3536. https://doi.org/10.1130/0016-7606(1970)81[3513:IOPTFT]2.0.CO;2

Bache, F., Olivet, J. L., Gorini, C., Aslanian, D., Labails, C., & Rabineau, M. (2010). Evolution of rifted continental margins: The case of the Gulf of Lions (Western Mediterranean Basin). *Earth and Planetary Science Letters*, *292*(3–4), 345–356. https://doi.org/10.1016/j.epsl.2010.02.001

Bai, Y., Wu, S., Liu, Z., Müller, R., Williams, S., Zahirovic, S., & Dong, D. (2015). Full-fit reconstruction of the South China Sea conjugate margins. *Tectonophysics*, *661*, 121–135. https://doi.org/10.1016/j.tecto.2015.08.028
Balmino, G., Vales, N., Bonvalot, S., & Briais, A. (2012). Spherical harmonic modelling to ultra-high degree of Bouguer and isostatic anomalies. *Journal of Geodesy*, *86*(7), 499–520. https://doi.org/10.1007/s00190-011-0533-4
Barckhausen, U., & Roeser, H. A. (2004). Seafloor Spreading Anomalies in the South China Sea Revisited. In P. Clift W. Kuhnt P. Wang & D. Hayes (Eds.), *Continent-Ocean Interactions Within East Asian Marginal Seas*, *Geophysical Monograph Series* (Vol. 149, pp. 121–125). Washington, DC: AGU.
Barker, P. (1995). Tectonic framework of the East Scotia Sea. In B Taylor (Ed.), *Backarc basins: Tectonics and magmatism* (pp. 281–314). New York, NY: Plenum. https://doi.org/10.1007/978-1-4615-1843-3_7
Barker, P., Dalziel, I. W. D., & Storey, B. C. (1991). Tectonic development of the Scotia arc region. *The geology of Antarctica* (215–248). Oxford, UK: Clarendon.
Barker, P., Lawver, L., & Larter, R. (2013). Heat-flow determinations of basement age in small oceanic basins of the southern central Scotia Sea. *Geological Society, London, Special Publications*, *381*(1), 139–150. https://doi.org/10.1144/SP381.3
Bethoux, N., Bertrand, E., Contrucci, I., Sosson, M., & Ferrandini, J. (1999). The deep structure of Corsica as inferred by a broad band seismological profile. *Geophysical Research Letters*, *26*(17), 2661–2664. https://doi.org/10.1029/1999GL005360
Bonvalot, S., Balmino, G., Briais, A., Kuhn, M., Peyrefitte, A., Vales, N., et al. (2012). World gravity map. In *Bureau Gravimetrique International (BGI), Map, CGMW-BGI-CNES728*. Paris: IRD.
Bouysse, P. (2014). *Geological Map of the World at 1: 35 000 000* (3rd ed.). Paris: CCGM.
Breitfeld, H., Hall, R., Galin, T., Forster, M., & BouDagher-Fadel, M. (2017). A Triassic to Cretaceous Sundaland–Pacific subduction margin in West Sarawak, Borneo. *Tectonophysics*, *694*, 35–56. https://doi.org/10.1016/j.tecto.2016.11.034
Brown, B., Gaina, C., & Müller, D. (2006). Circum-Antarctic palaeobathymetry: Illustrated examples from Cenozoic to recent times. *Palaeogeography, Palaeoclimatology, Palaeoecology*, *231*(1-2), 158–168. https://doi.org/10.1016/j.palaeo.2005.07.033
Brune, S., Heine, C., Clift, P., & Pérez-Gussinyé, M. (2017). Rifted margin architecture and crustal rheology: Reviewing Iberia-Newfoundland, central South Atlantic, and South China Sea. *Marine and Petroleum Geology*, *79*, 257–281. https://doi.org/10.1016/j.marpetgeo.2016.10.018
Brune, S., Popov, A., & Sobolev, S. (2012). Modeling suggests that oblique extension facilitates rifting and continental break-up. *Journal of Geophysical Research*, *117*, B08402. https://doi.org/10.1029/2011JB008860
Bry, M., White, N., Singh, S., England, R., & Trowell, C. (2004). Anatomy and formation of oblique continental collision: South Falkland basin. *Tectonics*, *23*, TC4011. https://doi.org/10.1029/2002TC001482
Buck, W. (2004). Consequences of asthenospheric variability on continental rifting. In Karner, G. D. Taylor, B. Driscoll, N. W. & Kohlstedt, D. L. (Eds.), *Rheology and Deformation of the Lithosphere at Continental Margins* (Vol. 62, pp. 1–30). New York, NY: Columbia University Press.
Bulois, C., Pubellier, M., Chamot-Rooke, N., & Delescluse, M. (2018). Successive rifting events in marginal basins: The example of the Coral Sea region (Papua New Guinea). *Tectonics*, *37*, 3–29. https://doi.org/10.1002/2017TC004783
Capitanio, F., Morra, G., & Goes, S. (2007). Dynamic models of downgoing plate-buoyancy driven subduction: Subduction motions and energy dissipation. *Earth and Planetary Science Letters*, *262*(1–2), 284–297. https://doi.org/10.1016/j.epsl.2007.07.039
Carter, A., Curtis, M., & Schwanethal, J. (2014). Cenozoic tectonic history of the South Georgia microcontinent and potential as a barrier to Pacific-Atlantic through flow. *Geology*, *42*(4), 299–302. https://doi.org/10.1130/G35091.1
Cawood, P., Kröner, A., Collins, W., Kusky, T., Mooney, W., & Windley, B. (2009). Accretionary orogens through Earth history. *Geological Society, London, Special Publications*, *318*(1), 1–36. https://doi.org/10.1144/SP318.1
Chamot-Rooke, N., Gaulier, J., & Jestin, F. (1999). Constraints on Moho depth and crustal thickness in the Liguro-Provençal basin from a 3D gravity inversion: Geodynamic implications. *Geological Society, London, Special Publications*, *156*(1), 37–61. https://doi.org/10.1144/GSL.SP.1999.156.01.04
Contrucci, I., Nercessian, A., Béthoux, N., Mauffret, A., & Pascal, G. (2001). A Ligurian (Western Mediterranean Sea) geophysical transect revisited. *Geophysical Journal International*, *146*(1), 74–97. https://doi.org/10.1046/j.0956-540X.2001.01418.x
Coren, F., Ceccone, G., Lodolo, E., Zanolla, C., Zitellini, N., Bonazzi, C., & Centonze, G. (1997). Morphology, seismic structure and tectonic development of the Powell Basin, Antarctica. *Journal of the Geological Society*, *154*(5), 849–862. https://doi.org/10.1144/gsjgs.154.5.0849
Crameri, F. (2018a). Geodynamic diagnostics, scientific visualisation and StagLab 3.0. *Geoscientific Model Development*, *11*(6), 2541–2562. https://doi.org/10.5194/gmd-11-2541-2018
Crameri, F. (2018b). *Scientific colour-maps*. Retrieved from https://doi.org/10.5281/zenodo.1243862
Cullen, A., Reemst, P., Henstra, G., Gozzard, S., & Ray, A. (2010). Rifting of the South China Sea: New perspectives. *Petroleum Geoscience*, *16*(3), 273–282. https://doi.org/10.1144/1354-079309-908
Dalziel, I., Elliot, D., Jones, D., Thomson, J., Thomson, M., Wells, N., & Zinsmeister, W. (1981). The geological significance of some Triassic microfossils from the South Orkney Islands, Scotia Ridge. *Geological Magazine*, *118*(1), 15–25. https://doi.org/10.1017/S0016756800024766
Dalziel, I., Lawver, L., Norton, I., & Gahagan, L. (2013). The Scotia Arc: Genesis, evolution, global significance. *Annual Review of Earth and Planetary Sciences*, *41*(1), 767–793. https://doi.org/10.1146/annurev-earth-050212-124155
Dewey, J., & Sengör, A. (1979). Aegean and surrounding regions: Complex multiplate and continuum tectonics in a convergent zone. *Geological Society of America Bulletin*, *90*(1), 84–92. https://doi.org/10.1130/0016-7606(1979)90<84:AASRCM>2.0.CO;2
di Rosa, M., de Giorgi, A., Marroni, M., & Vidal, O. (2017). Syn-convergence exhumation of continental crust: Evidence from structural and metamorphic analysis of the Monte Cecu area, Alpine Corsica (northern Corsica, France). *Geological Journal*, *52*(6), 919–937. https://doi.org/10.1002/gj.2857
Ding, W., Li, J., & Clift, P. (2016). Spreading dynamics and sedimentary process of the southwest sub-basin, South China Sea: Constraints from multi-channel seismic data and IODP Expedition 349. *Journal of Asian Earth Sciences*, *115*, 97–113. https://doi.org/10.1016/j.jseaes.2015.09.013
Eagles, G. (2010a). South Georgia and Gondwana's Pacific Margin: Lost in translation? *Journal of South American Earth Sciences*, *30*(2), 65–70. https://doi.org/10.1016/j.jsames.2010.04.004
Eagles, G. (2010b). The age and origin of the central Scotia Sea. *Geophysical Journal International*, *183*(2), 587–600. https://doi.org/10.1111/j.1365-246X.2010.04781.x
Eagles, G., Gohl, K., & Larter, R. (2004). High-resolution animated tectonic reconstruction of the South Pacific and West Antarctic Margin. *Geochemistry, Geophysics, Geosystems*, *5*, Q07002. https://doi.org/10.1029/2003GC000657

Eagles, G., & Jokat, W. (2014). Tectonic reconstructions for paleobathymetry in Drake Passage. *Tectonophysics*, *611*, 28–50. https://doi.org/10.1016/j.tecto.2013.11.021
Eagles, G., & Livermore, R. (2002). Opening history of Powell Basin, Antarctic Peninsula. *Marine Geology*, *185*(3-4), 195–205. https://doi.org/10.1016/S0025-3227(02)00191-3
Eagles, G., Livermore, R., Fairhead, J., & Morris, P. (2005). Tectonic evolution of the west Scotia Sea. *Journal of Geophysical Research*, *110*, B02401. https://doi.org/10.1029/2004JB003154
Eagles, G., Livermore, R., & Morris, P. (2006). Small basins in the Scotia Sea: The Eocene Drake Passage gateway. *Earth and Planetary Science Letters*, *242*(3-4), 343–353. https://doi.org/10.1016/j.epsl.2005.11.060
Eagles, G., Pérez-Díaz, L., & Scarselli, N. (2015). Getting over continent ocean boundaries. *Earth-Science Reviews*, *151*, 244–265. https://doi.org/10.1016/j.earscirev.2015.10.009
Ewing, M., Hawkins, L., & Ludwig, W. (1970). Crustal structure of the Coral Sea. *Journal of Geophysical Research*, *75*(11), 1953–1962. https://doi.org/10.1029/JB075i011p01953
Faccenna, C., Becker, T., Lucente, F., Jolivet, L., & Rossetti, F. (2001). History of subduction and back-arc extension in the Central Mediterranean. *Geophysical Journal International*, *145*(3), 809–820. https://doi.org/10.1046/j.0956-540x.2001.01435.x
Faccenna, C., Funiciello, F., Giardini, D., & Lucente, P. (2001). Episodic back-arc extension during restricted mantle convection in the Central Mediterranean. *Earth and Planetary Science Letters*, *187*(1–2), 105–116. https://doi.org/10.1016/S0012-821X(01)00280-1
Faccenna, C., Mattei, M., Funiciello, R., & Jolivet, L. (1997). Styles of back-arc extension in the Central Mediterranean. *Terra Nova*, *9*(3), 126–130. https://doi.org/10.1046/j.1365-3121.1997.d01-12.x
Faccenna, C., Piromallo, C., Crespo-blanc, A., & Jolivet, L. (2004). Lateral slab deformation and the origin of the western Mediterranean arcs. *Tectonics*, *23*(1). https://doi.org/10.1029/2002TC001488
Feary, D., Champion, D., Bultitude, R., & Davies, P. (1993). 37 Igneous and metasedimentary basement lithofacies of the Queensland plateau (Sites 824 and 825). In *Proceedings of the Ocean Drilling Program Drilling Program Scientific Results* (Vol. 133, pp. 535–540). College Station, TX.
Ferrari, L., Orozco-Esquivel, T., Bryan, S., López-Martínez, M., & Silva-Fragoso, A. (2018). Cenozoic magmatism and extension in western Mexico: Linking the Sierra Madre Occidental silicic large igneous province and the Comondú Group with the Gulf of California rift. *Earth-Science Reviews*, *183*(April), 115–152. https://doi.org/10.1016/j.earscirev.2017.04.006
Franke, D., Barckhausen, U., Baristeas, N., Engels, M., Ladage, S., Lutz, R., et al. (2011). The continent-ocean transition at the southeastern margin of the South China Sea. *Marine and Petroleum Geology*, *28*(6), 1187–1204. https://doi.org/10.1016/j.marpetgeo.2011.01.004
Franke, D., Savva, D., Pubellier, M., Steuer, S., Mouly, B., Auxietre, J.-L., et al. (2014). The final rifting evolution in the South China Sea. *Marine and Petroleum Geology*, *58*, 704–720. https://doi.org/10.1016/j.marpetgeo.2013.11.020
Gaherty, J. B., & Hager, B. H. (1994). Compositional vs. thermal buoyancy and the evolution of subducted lithosphere. *Geophysical Research Letters*, *21*(2), 141–144. https://doi.org/10.1029/93GL03466
Gailler, A., Klingelhoefer, F., Olivet, J.-L., & Aslanian, D. (2009). Crustal structure of a young margin pair: New results across the Liguro-Provencal Basin from wide-angle seismic tomography. *Earth and Planetary Science Letters*, *286*(1–2), 333–345. https://doi.org/10.1016/j.epsl.2009.07.001
Gaina, C., Gernigon, L., & Ball, P. (2009). Palaeocene-Recent plate boundaries in the NE Atlantic and the formation of the Jan Mayen microcontinent. *Journal of the Geological Society*, *166*(4), 601–616. https://doi.org/10.1144/0016-76492008-112
Gaina, C., Müller, R. D., Royer, J.-Y., & Symonds, P. (1999). Evolution of the Louisiade triple junction. *Journal of Geophysical Research*, *104*(B6), 12927–12939. https://doi.org/10.1029/1999JB900038
Gaina, C., Torsvik, T. H., van Hinsbergen, D. J. J., Medvedev, S., Werner, S. C., & Labails, C. (2013). The African plate: A history of oceanic crust accretion and subduction since the Jurassic. *Tectonophysics*, *604*, 4–25. https://doi.org/10.1016/j.tecto.2013.05.037
Gaina, J. M., & Whittaker, C. (2020). Microcontinents. In H. K. Gupta (Ed.), *Encyclopedia of Solid Earth Geophysics*, Berlin: Springer International Publishing.
Galindo-Zaldívar, J., Balanyá, J. C., Bohoyo, F., Jabaloy, A., Maldonado, A., Martínez-Martínez, J. M., et al. (2002). Active crustal fragmentation along the Scotia–Antarctic plate boundary east of the South Orkney Microcontinent (Antarctica). *Earth and Planetary Science Letters*, *204*(1-2), 33–46. https://doi.org/10.1016/S0012-821X(02)00959-7
Ganerød, M., Torsvik, T. H., van Hinsbergen, D. J. J., Gaina, C., Corfu, F., Werner, S., et al. (2011). Palaeoposition of the Seychelles microcontinent in relation to the Deccan Traps and the Plume Generation Zone in late Cretaceous-early Palaeogene time. *Geological Society, London, Special Publications*, *357*(1), 229–252. https://doi.org/10.1144/SP357.12
Gattacceca, J., Deino, A., Rizzo, R., Jones, D. S., Henry, B., Beaudoin, B., & Vadeboin, F. (2007). Miocene rotation of Sardinia: New paleomagnetic and geochronological constraints and geodynamic implications. *Earth and Planetary Science Letters*, *258*(3–4), 359–377. https://doi.org/10.1016/j.epsl.2007.02.003
Glen, R. A. (2005). The Tasmanides of eastern Australia. *Special Publication-Geological Society of London*, *246*(1), 23–96. https://doi.org/10.1144/GSL.SP.2005.246.01.02
Goes, S., Capitanio, F. A., & Morra, G. (2008). Evidence of lower-mantle slab penetration phases in plate motions. *Nature*, *451*(7181), 981–984. https://doi.org/10.1038/nature06691
Gueydan, F., Brun, J.-P., Phillippon, M., & Noury, M. (2017). Sequential extension as a record of Corsica Rotation during Apennines slab roll-back. *Tectonophysics*, *710-711*, 149–161. https://doi.org/10.1016/j.tecto.2016.12.028
Hall, R., & Breitfeld, H. T. (2017). Nature and demise of the Proto-South China Sea. *Bulletin. Geological Society of Malaysia*, *63*(63), 61–76. https://doi.org/10.7186/bgsm63201703
Hennig, J., Breitfeld, H. T., Hall, R., & Surya Nugraha, A. M. (2017). The Mesozoic tectono-magmatic evolution at the Paleo-Pacific subduction zone in West Borneo. *Gondwana Research*, *48*, 292–310. https://doi.org/10.1016/j.gr.2017.05.001
Hoffmann, K. L., Exon, N., Quilty, P. G., & Findlay, C. S. (2008). *Mellish Rise and adjacent deep water plateaus off northeast Australia: new evidence for continental basement from Cenozoic micropalaeontology and sedimentary geology* (pp. 317–323). Sydney: PESA Eastern Australian Basins Symposium III.
Hosseini, K., Matthews, K. J., Sigloch, K., Shephard, G. E., Domeier, M., & Tsekhmistrenko, M. (2018). SubMachine: Web-based tools for exploring seismic tomography and other models of Earth's deep interior. *Geochemistry, Geophysics, Geosystems*, *19*, 1464–1483. https://doi.org/10.1029/2018GC007431
Hosseini, K., Sigloch, K., Tsekhmistrenko, M., Zaheri, A., Nissen-Meyer, T., & Igel, H. (2019). Global mantle structure from multifrequency tomography using P, PP and P-diffracted waves. *Geophysical Journal International*, *220*(1), 96–141. https://doi.org/10.1093/gji/ggz394

Huang, H., He, E., Qiu, X., Guo, X., Fan, J., & Zhang, X. (2019). Insights about the structure and development of Zhongsha Bank in the South China Sea from integrated geophysical modelling. *International Geology Review*, *62*(7-8), 1070–1080. https://doi.org/10.1080/00206814.2019.1653798

Hutchison, C. S. (2004). Marginal basin evolution: The southern South China Sea. *Marine and Petroleum Geology*, *21*(9), 1129–1148. https://doi.org/10.1016/j.marpetgeo.2004.07.002

Jolivet, L., & Faccenna, C. (2000). Mediterranean extension and the Africa-Eurasia collision. *Tectonics*, *19*(6), 1095–1106. https://doi.org/10.1029/2000TC900018

Jolivet, L., Gorini, C., Smit, J., & Leroy, S. (2015). Continental breakup and the dynamics of rifting in back-arc basins: The Gulf of Lion margin. *Tectonics*, *34*, 662–679. https://doi.org/10.1002/2014TC003570

King, E. C., & Barker, P. F. (1988). The margins of the South Orkney microcontinent. *Journal of the Geological Society (London)*, *145*(2), 317–331. https://doi.org/10.1144/gsjgs.145.2.0317

Kudrass, H. R., Wiedicke, M., Cepek, P., Kreuzer, H., & Müller, P. (1986). Mesozoic and Cainozoic rocks dredged from the South China Sea (Reed Bank area) and Sulu Sea and their significance for plate-tectonic reconstructions. *Marine and Petroleum Geology*, *3*(1), 19–30. https://doi.org/10.1016/0264-8172(86)90053-X

Lacombe, O., & Jolivet, L. (2005). Structural and kinematic relationships between Corsica and the Pyrenees-Provence domain at the time of the Pyrenean orogeny. *Tectonics*, *24*, 1–20. https://doi.org/10.1029/2004TC001673

Laird, M. G., & Bradshaw, J. D. (2004). The break-up of a long-term relationship: The Cretaceous separation of New Zealand from Gondwana. *Gondwana Research*, *7*(1), 273–286. https://doi.org/10.1016/S1342-937X(05)70325-7

Lallemand, S., Heuret, A., & Boutelier, D. (2005). On the relationships between slab dip, back-arc stress, upper plate absolute motion, and crustal nature in subduction zones. *Geochemistry, Geophysics, Geosystems*, *6*, Q09006. https://doi.org/10.1029/2005GC000917

Laske, G., Masters, G., Ma, Z., & Pasyanos, M. (2012). *CRUST1. 0: An updated global model of the Earth's crust* (Vol. 14). Vienna: EGU General Assembly.

Li, C., van der Hilst, R. D., Engdahl, E. R., & Burdick, S. (2008). A new global model for P wave speed variations in Earth's mantle. *Geochemistry, Geophysics, Geosystems*, *9*, Q05018. https://doi.org/10.1029/2007GC001806

Li, C.-F., Xu, X., Lin, J., Sun, Z., Zhu, J., Yao, Y., et al. (2014). Ages and magnetic structures of the South China Sea constrained by deep tow magnetic surveys and IODP Expedition 349. *Geochemistry, Geophysics, Geosystems*, *15*, 4958–4983. https://doi.org/10.1002/2014GC005567

Lister, G. S., Etheridge, M. A., & Symonds, P. A. (1986). Detachment faulting and the evolution of passive continental margins. *Geology*, *14*(3), 246–250. https://doi.org/10.1130/0091-7613(1986)14<246:DFATEO>2.0.CO;2

Lizarralde, D., Axen, G. J., Brown, H. E., Fletcher, J. M., González-Fernández, A., Harding, A. J., et al. (2007). Variation in styles of rifting in the Gulf of California. *Nature*, *448*(7152), 466–469. https://doi.org/10.1038/nature06035

López-Pineda, L., Rebollar, C. J., & Quintanar, L. (2007). Crustal thickness estimates for Baja California, Sonora, and Sinaloa, Mexico, using disperse surface waves. *Journal of Geophysical Research*, *112*, B04308. https://doi.org/10.1029/2005JB003899

Lu, C., Grand, S. P., Lai, H., & Garnero, E. J. (2019). TX2019slab: A New P and S Tomography Model Incorporating Subducting Slabs. *Journal of Geophysical Research: Solid Earth*, *124*, 11,549–11,567. https://doi.org/10.1029/2019JB017448

Lus, W. Y., McDougall, I., & Davies, H. L. (2004). Age of the metamorphic sole of the Papuan Ultramafic Belt ophiolite, Papua New Guinea. *Tectonophysics*, *392*(1-4), 85–101. https://doi.org/10.1016/j.tecto.2004.04.009

Mallard, C., Coltice, N., Seton, M., Dietmar Müller, R., & Tackley, P. J. (2016). Subduction controls the distribution and fragmentation of Earth's tectonic plates. *Nature*, *535*(7610), 140–143. https://doi.org/10.1038/nature17992

Matthews, K. J., Maloney, K. T., Zahirovic, S., Williams, S. E., Seton, M., & Dietmar Müller, R. (2016). Global plate boundary evolution and kinematics since the late Paleozoic. *Global and Planetary Change*, *146*, 226–250. https://doi.org/10.1016/j.gloplacha.2016.10.002

Matthews, K. J., Williams, S. E., Whittaker, J. M., Müller, R. D., Seton, M., & Clarke, G. L. (2015). Geologic and kinematic constraints on late Cretaceous to mid Eocene plate boundaries in the southwest Pacific. *Earth-Science Reviews*, *140*, 72–107. https://doi.org/10.1016/j.earscirev.2014.10.008

Molinari, I., & Morelli, A. (2011). EPcrust: A reference crustal model for the European plate. *Geophysical Journal International*, *185*(1), 352–364. https://doi.org/10.1111/j.1365-246X.2011.04940.x

Molnar, N. E., Cruden, A. R., & Betts, P. G. (2018). Unzipping continents and the birth of microcontinents. *Geology*, 1–4. https://doi.org/10.1130/g40021.1

Müller, R. D., Gaina, C., Roest, W. R., & Hansen, D. L. (2001). A recipe for microcontinent formation. *Geology*, *29*(3), 203–206. https://doi.org/10.1130/0091-7613

Müller, R. D., Sdrolias, M., Gaina, C., & Roest, W. R. (2008). Age, spreading rates, and spreading asymmetry of the world's ocean crust. *Geochemistry, Geophysics, Geosystems*, *9*, Q04006. https://doi.org/10.1029/2007GC001743

Müller, R. D., Seton, M., Zahirovic, S., Williams, S. E., Matthews, K. J., Wright, N. M., et al. (2016). Ocean basin evolution and global-scale plate reorganization events since Pangea breakup. *Annual Review of Earth and Planetary Sciences*, *44*(1), 107–138. https://doi.org/10.1146/annurev-earth-060115-012211

Nemčok, M., Sinha, S. T., Doré, A. G., Lundin, E. R., Mascle, J., & Rybár, S. (2016). Mechanisms of microcontinent release associated with wrenching-involved continental break-up: A review. *Geological Society, London, Special Publications*, *431*(1), 323–359. https://doi.org/10.1144/SP431.14

Ness, G. E., Lyle, M. W., & Couch, R. W. (1991). Marine magnetic anomalies and oceanic crustal isochrons of the Gulf and Peninsular Province of the Californias. *American Association of Petroleum Geologists Memoir*, *47*, 47–69.

Ortega-Gutierrez, F., Ruiz, J., & Centeno-Garcia, E. (1995). Oaxaquia, a Proterozoic microcontinent accreted to North America during the late Paleozoic. *Geology*, *23*(12), 1127–1130. https://doi.org/10.1130/0091-7613(1995)023<1127:OAPMAT>2.3.CO;2

Pandey, A., Parson, L., & Milton, A. (2010). Geochemistry of the Davis and Aurora Banks: Possible implications on evolution of the North Scotia Ridge. *Marine Geology*, *268*(1-4), 106–114. https://doi.org/10.1016/j.margeo.2009.10.025

Paterson, N. R., & Reeves, C. V. (1985). Applications of gravity and magnetic surveys: The state-of-the-art in 1985. *Geophysics*, *50*(12), 2558–2594. https://doi.org/10.1190/1.1441884

Paulssen, H., & de Vos, D. (2017). Slab remnants beneath the Baja California peninsula: Seismic constraints and tectonic implications. *Tectonophysics*, *719*, 27–36. https://doi.org/10.1016/j.tecto.2016.09.021

Peron-Pinvidic, G., Gernigon, L., Gaina, C., & Ball, P. (2012a). Insights from the Jan Mayen system in the Norwegian-Greenland Sea-I. Mapping of a microcontinent. *Geophysical Journal International*, *191*(2), 413–435. https://doi.org/10.1111/j.1365-246X.2012.05623.x

Peron-Pinvidic, G., Gernigon, L., Gaina, C., & Ball, P. (2012b). Insights from the Jan Mayen system in the Norwegian-Greenland Sea-II. Architecture of a microcontinent. *Geophysical Journal International*, *191*(2), 413–435. https://doi.org/10.1111/j.1365-246X.2012.05623.x

Péron-Pinvidic, G., & Manatschal, G. (2010). From microcontinents to extensional allochthons: Witnesses of how continents rift and break apart? *Petroleum Geoscience*, *16*(3), 189–197. https://doi.org/10.1144/1354-079309-903

Persaud, P., Pérez-Campos, X., & Clayton, R. W. (2007). Crustal thickness variations in the margins of the Gulf of California from receiver functions. *Geophysical Journal International*, *170*(2), 687–699. https://doi.org/10.1111/j.1365-246X.2007.03412.x

Pichot, T., Delescluse, M., Chamot-Rooke, N., Pubellier, M., Qiu, Y., Meresse, F., et al. (2014). Deep crustal structure of the conjugate margins of the SW South China Sea from wide-angle refraction seismic data. *Marine and Petroleum Geology*, *58*, 627–643. https://doi.org/10.1016/j.marpetgeo.2013.10.008

Pubellier, M., Ego, F., Chamot-Rooke, N., & Rangin, C. (2003). The building of pericratonic mountain ranges: Structural and kinematic constraints applied to GIS-based reconstructions of SE Asia. *Bulletin de la Societe Geologique de France*, *174*(6), 561–584. https://doi.org/10.2113/174.6.561

Rollet, N., Déverchère, J., Beslier, M.-O., Guennoc, P., Réhault, J.-P., Sosson, M., & Truffert, C. (2002). Back arc extension, tectonic inheritance, and volcanism in the Ligurian Sea, Western Mediterranean. *Tectonics*, *21*(3), 6-1–6-23. https://doi.org/10.1029/2001TC900027

Rossi, P., Oggiano, G., & Cocherie, A. (2009). A restored section of the "southern Variscan realm" across the Corsica-Sardinia microcontinent. *Comptes Rendus Geoscience*, *341*(2–3), 224–238. https://doi.org/10.1016/j.crte.2008.12.005

Ruan, A.-G., Niu, X.-W., Qiu, X.-L., Li, J.-B., Wu, Z.-L., Zhao, M.-H., & Wei, X.-D. (2011). A wide angle ocean bottom seismometer experiment across Liyue Bank, the southern margin of the South China Sea. *Chinese Journal of Geophysics*, *54*(6), 1033–1044. https://doi.org/10.1002/cjg2.1682

Sandwell, D. T., Müller, R. D., Smith, W. H. F., Garcia, E., & Francis, R. (2014). New global marine gravity model from CryoSat-2 and Jason-1 reveals buried tectonic structure. *Science*, *346*(6205), 65–67. https://doi.org/10.1126/science.1258213

Schellart, W. P., Lister, G. S., & Toy, V. G. (2006). A late Cretaceous and Cenozoic reconstruction of the Southwest Pacific region: Tectonics controlled by subduction and slab rollback processes. *Earth-Science Reviews*, *76*(3–4), 191–233. https://doi.org/10.1016/j.earscirev.2006.01.002

Schmid, S. M., Kissling, E., Diehl, T., van Hinsbergen, D. J. J., & Molli, G. (2017). Ivrea mantle wedge, arc of the Western Alps, and kinematic evolution of the Alps–Apennines orogenic system. *Swiss Journal of Geosciences*, *110*(2), 581–612. https://doi.org/10.1007/s00015-016-0237-0

Scrutton, R. A. (1976). Microcontinents and their significance. In *Geodynamics: Progress and Prospects* (Vol. 5, pp. 177–189). Washington, DC: AGU.

Segev, A., Rybakov, M., & Mortimer, N. (2012). A crustal model for Zealandia and Fiji. *Geophysical Journal International*, *189*(3), 1277–1292. https://doi.org/10.1111/j.1365-246X.2012.05436.x

Séranne, M. (1999). The Gulf of Lion continental margin (NW Mediterranean) revisited by IBS: An overview. *Geological Society, London, Special Publications*, *156*(1), 15–36. https://doi.org/10.1144/gsl.sp.1999.156.01.03

Seton, M., Müller, R. D., Zahirovic, S., Gaina, C., Torsvik, T., Shephard, G., et al. (2012). Global continental and ocean basin reconstructions since 200 Ma. *Earth-Science Reviews*, *113*(3–4), 212–270. https://doi.org/10.1016/j.earscirev.2012.03.002

Seton, M., Mortimer, N., Williams, S., Quilty, P., Gans, P., Meffre, S., et al. (2016). Melanesian back-arc basin and arc development: Constraints from the eastern Coral Sea. *Gondwana Research*, *39*, 77–95. https://doi.org/10.1016/j.gr.2016.06.011

Shipboard Scientific Party (2000). Leg 184 Summary: Exploring the Asian Monsoon through Drilling in the South China Sea. In P. Wang, W. L. Prell, & P. Blum (Eds.), *Proceedings of the Ocean Drilling Program, Initial Reports* (Vol. 184, pp. 1–77). TX: ODP College Station.

Sibuet, J.-C., Yeh, Y.-C., & Lee, C.-S. (2016). Geodynamics of the South China Sea. *Tectonophysics*, *692*, 98–119. https://doi.org/10.1016/j.tecto.2016.02.022

Smalley, R., Dalziel, I. W. D., Bevis, M. G., Kendrick, E., Stamps, D. S., King, E. C., et al. (2007). Scotia arc kinematics from GPS geodesy. *Geophysical Research Letters*, *34*, L21308. https://doi.org/10.1029/2007GL031699

Stern, R. J., & Scholl, D. W. (2010). Yin and yang of continental crust creation and destruction by plate tectonic processes. *International Geology Review*, *52*(1), 1–31. https://doi.org/10.1080/00206810903332322

Stock, J. M., & Hodges, K. V. (1989). Pre-Pliocene extension around the Gulf of California and the transfer of Baja California to the Pacific Plate. *Tectonics*, *8*(1), 99–115. https://doi.org/10.1029/TC008i001p00099

Straume, E. O., Gaina, C., Medvedev, S., Hochmuth, K., Gohl, K., Whittaker, J. M., et al. (2019). GlobSed: Updated total sediment thickness in the world's oceans. *Geochemistry, Geophysics, Geosystems*, *20*, 1756–1772. https://doi.org/10.1029/2018GC008115

Sutherland, F. H., Kent, G. M., Harding, A. J., Umhoefer, P. J., Driscoll, N. W., Lizarralde, D., et al. (2012). Middle Miocene to early Pliocene oblique extension in the southern Gulf of California. *Geosphere*, *8*(4), 752–770. https://doi.org/10.1130/GES00770.1

Taylor, B., & Hayes, D. E. (1980). The tectonic evolution of the South China Basin. D. Hayes In *The Tectonic and Geologic Evolution of Southeast Asian Seas and Islands*, *Geophysical Monographs Series* (Vol. 23, (Figure 1), pp. 89–104). Washington, DC: AGU.

Taylor, B., & Hayes, D. E. (1983). Origin and history of the South China Sea basin. D. Hayes In *The Tectonic and Geologic Evolution of Southeast Asian Seas and Islands: Part 2*, *Geophysical Monograph Series* (Vol. 27, pp. 23–56). Washington, DC: AGU.

Taylor, L., & Falvey, D. (1977). Queensland Plateau and Coral Sea Basin; stratigraphy, structure and tectonics. *The APPEA Journal*, *17*(1), 13. https://doi.org/10.1071/AJ76002

Tetreault, J. L., & Buiter, S. J. H. (2012). Geodynamic models of terrane accretion: Testing the fate of island arcs, oceanic plateaus, and continental fragments in subduction zones. *Journal of Geophysical Research*, *117*, B08403. https://doi.org/10.1029/2012JB009316

Torsvik, T. H., Amundsen, H., Hartz, E. H., Corfu, F., Kusznir, N., Gaina, C., et al. (2013). A Precambrian microcontinent in the Indian Ocean. *Nature Geoscience*, *6*(3), 223–227. https://doi.org/10.1038/ngeo1736

Trouw, R. A. J., Passchier, C. W., Simões, L. S. A., Andreis, R. R., & Valeriano, C. M. (1997). Mesozoic tectonic evolution of the South Orkney Microcontinent, Scotia arc, Antarctica. *Geological Magazine*, *134*(3), 383–401. https://doi.org/10.1017/S0016756897007036

Turco, E., Macchiavelli, C., Mazzoli, S., Schettino, A., & Pierantoni, P. P. (2012). Kinematic evolution of Alpine Corsica in the framework of Mediterranean mountain belts. *Tectonophysics*, *579*, 193–206. https://doi.org/10.1016/j.tecto.2012.05.010

Umhoefer, P. J. (2011). Why did the Southern Gulf of California rupture so rapidly?—Oblique divergence across hot, weak lithosphere along a tectonically active margin. *GSA Today*, *21*(11), 4–10. https://doi.org/10.1130/G133A.1

van den Broek, J. M., Magni, V., Gaina, C., & Buiter, S. J. H. (2020). The formation of continental fragments in subduction settings: The importance of structural inheritance and subduction system dynamics. *Journal of Geophysical Research: Solid Earth*. https://doi.org/10.1029/2019JB018370

van der Meer, D. G., Spakman, W., van Hinsbergen, D. J. J., Amaru, M. L., & Torsvik, T. H. (2010). Towards absolute plate motions constrained by lower-mantle slab remnants. *Nature Geoscience*, *3*(1), 36–40. https://doi.org/10.1038/ngeo708

van Hinsbergen, D. J. J., Vissers, R. L. M., & Spakman, W. (2014). Origin and consequences of western Mediterranean subduction, rollback, and slab segmentation. *Tectonics*, *33*, 393–419. https://doi.org/10.1002/2013TC003349

Van Wyck, N., & Williams, I. S. (2002). Age and provenance of basement metasediments from the Kubor and Bena Bena Blocks, central Highlands, Papua New Guinea: Constraints on the tectonic evolution of the northern Australian cratonic margin. *Australian Journal of Earth Sciences*, *49*(3), 565–577. https://doi.org/10.1046/j.1440-0952.2002.00938.x

Vanneste, L. E., & Larter, R. D. (2002). Sediment subduction, subduction erosion, and strain regime in the northern South Sandwich forearc. *Journal of Geophysical Research*, *107*(B7), 2149. https://doi.org/10.1029/2001JB000396

Vissers, R. L. M., van Hinsbergen, D. J. J., Meijer, P. T., & Piccardo, G. B. (2013). Kinematics of Jurassic ultra-slow spreading in the Piemonte Ligurian Ocean. *Earth and Planetary Science Letters*, *380*, 138–150. https://doi.org/10.1016/j.epsl.2013.08.033

von Raumer, J. F., Stampfli, G. M., & Bussy, F. (2003). Gondwana-derived microcontinents—The constituents of the Variscan and Alpine collisional orogens. *Tectonophysics*, *365*(1–4), 7–22. https://doi.org/10.1016/S0040-1951(03)00015-5

Vuan, A., Cazzaro, R., Costa, G., Russi, M., & Panza, G. F. (1999). S-wave velocity models in the Scotia Sea region, Antarctica, from nonlinear inversion of Rayleigh waves dispersion. *Pure and Applied Geophysics*, *154*(1), 121–139. https://doi.org/10.1007/s000240050224

Vuan, A., Lodolo, E., Panza, G. F., & Sauli, C. (2005). Crustal structure beneath Discovery Bank in the Scotia Sea from group velocity tomography and seismic reflection data. *Antarctic Science*, *17*(1), 97–106. https://doi.org/10.1017/S0954102005002488

Wang, T. K., Chen, M.-K., Lee, C.-S., & Xia, K. (2006). Seismic imaging of the transitional crust across the northeastern margin of the South China Sea. *Tectonophysics*, *412*(3–4), 237–254. https://doi.org/10.1016/j.tecto.2005.10.039

Webb, L. E., Baldwin, S. L., & Fitzgerald, P. G. (2014). The Early-Middle Miocene subduction complex of the Louisiade Archipelago, southern margin of the Woodlark Rift. *Geochemistry, Geophysics, Geosystems*, *15*, 4024–4046. https://doi.org/10.1002/2014GC005500

Weissel, J. K., & Watts, A. B. (1979). Tectonic evolution of the Coral Sea Basin. *Journal of Geophysical Research*, *84*(B9), 4572–4582. https://doi.org/10.1029/JB084iB09p04572

Wessel, P., Smith, W. H. F., Scharroo, R., Luis, J., & Wobbe, F. (2013). Generic mapping tools: Improved version released. *Eos, Transactions American Geophysical Union*, *94*(45), 409–410. https://doi.org/10.1002/2013EO450001

Whattam, S. A., Malpas, J., Ali, J. R., & Smith, I. E. M. (2008). New SW Pacific tectonic model: Cyclical intraoceanic magmatic arc construction and near-coeval emplacement along the Australia-Pacific margin in the Cenozoic. *Geochemistry, Geophysics, Geosystems*, *9*, Q03021. https://doi.org/10.1029/2007GC001710

Wright, N. M., Seton, M., Williams, S. E., & Dietmar Müller, R. (2016). The late Cretaceous to recent tectonic history of the Pacific Ocean basin. *Earth-Science Reviews*, *154*, 138–173. https://doi.org/10.1016/j.earscirev.2015.11.015

Wu, J., Suppe, J., Lu, R., & Kanda, R. (2016). Philippine Sea and East Asian plate tectonics since 52 Ma constrained by new subducted slab reconstruction methods. *Journal of Geophysical Research: Solid Earth*, *121*, 4670–4741. https://doi.org/10.1002/2016JB012923

Wu, Z. L., Li, J. B., Ruan, A. G., Lou, H., Ding, W. W., Niu, X. W., & Li, X. B. (2012). Crustal structure of the northwestern sub-basin, South China Sea: Results from a wide-angle seismic experiment. *Science China Earth Sciences*, *55*(1), 159–172. https://doi.org/10.1007/s11430-011-4324-9

Yumul, G. P., Dimalanta, C. B., Tamayo, R. A., & Maury, R. C. (2003). Collision, subduction and accretion events in the Philippines: A synthesis. *The Island Arc*, *12*(2), 77–91. https://doi.org/10.1046/j.1440-1738.2003.00382.x

Zahirovic, S., Seton, M., & Müller, R. D. (2014). The Cretaceous and Cenozoic tectonic evolution of Southeast Asia. *Solid Earth*, *5*(1), 227–273. https://doi.org/10.5194/se-5-227-2014

3

# The Formation of Continental Fragments in Subduction Settings: The Importance of Structural Inheritance and Subduction System Dynamics

J. M. van den Broek, V. Magni, C. Gaina and S. J. H. Buiter

*Journal of Geophysical Research: Solid Earth* 125 (2020)

JGR Solid Earth

RESEARCH ARTICLE
10.1029/2019JB018370

# The Formation of Continental Fragments in Subduction Settings: The Importance of Structural Inheritance and Subduction System Dynamics

**J.M. van den Broek[1], V. Magni[1], C. Gaina[1], and S.J.H. Buiter[1,2]**

[1]The Centre for Earth Evolution and Dynamics, Department of Geosciences, University of Oslo, Oslo, Norway, [2]Team for Solid Earth Geology, Geological Survey of Norway, Trondheim, Norway

**Key Points:**
- Microcontinents and continental fragments may form next to wide continental collision zones due to rotational stress in the upper plate
- An inherited continental weak zone combined with lateral stress gradients along-trench result in upper plate continental fragment formation
- Extension also localizes in the upper plate if the weak zone is not trench parallel, wider weak zones extending less than narrow ones

**Supporting Information:**
- Supporting Information S1

**Correspondence to:**
J. M. van den Broek,
j.v.d.broek@geo.uio.no

**Citation:**
van den Broek, J. M., Magni, V., Gaina, C., & Buiter, S. J. H. (2020). The formation of continental fragments in subduction settings: The importance of structural inheritance and subduction system dynamics. *Journal of Geophysical Research: Solid Earth*, *125*, e2019JB018370. https://doi.org/10.1029/2019JB018370

Received 12 JUL 2019
Accepted 24 DEC 2019
Accepted article online 30 DEC 2019



**Abstract** Microcontinents and continental fragments are pieces of continental lithosphere, formed by extension and breakup, followed by plate boundary relocations. Microcontinents or continental fragments affiliated with passive margins are well documented, but those close to active margins are less studied. We use dynamic two- and three-dimensional numerical experiments to investigate how preexisting weaknesses within a continental upper plate affect extension and the possible formation of continental fragments. Our parametric study of the configuration (width and viscosity) of this imposed weakness indicates that stress localization and breakup of the upper plate are most efficient for narrow weak zones and a viscosity contrast between the weak zone and the surrounding crust of at least 1 order of magnitude. Moreover, upper plate extension and breakup occurs only if extension has a rotational component, here caused by the presence of a continental indenter on the downgoing plate. The width of the indenter relative to oceanic part of the downgoing plate controls differential slab pull that triggers trench retreat and upper plate deformation. A downgoing plate with a relatively large continental indenter yields large enough slab rotation to detach a continental block from the overriding plate and form wide back-arc basins. Variations in the weak zone angle with respect to the trench result in different basin geometries. We successfully modeled the first step in breakup of active continental margins and determined the settings that may facilitate microcontinent formation in a subduction framework.

## 1. Introduction

### 1.1. The Formation of Microcontinents and Continental Fragments

Microcontinents are small pieces of continental lithosphere, situated above or below sea level, that are almost completely surrounded by oceanic crust. Continental fragments are similarly defined but are still attached to their parent continent via thinned continental crust (Scrutton*, 1976*). This continental connection distinguishes continental fragments from microcontinents. The advent of modern, high-resolution geophysical data has yielded a significant increase in the number of identified microcontinents and continental fragments in recent years (see, e.g., Tetreault & Buiter, 2014 for a review). Most in situ preserved microcontinents and continental fragments formed in divergent tectonic settings as part of continental breakup processes. In the context of this paper, we take into account both "microcontinents," which are defined as pieces of continental lithosphere completely surrounded by oceanic crust, and "continental fragments" which are not completely detached from their parent continent by oceanic crust, but may be in an incipient stage of microcontinent formation or a failed one.

Classic examples of microcontinents include the Jan-Mayen microcontinent in the north-east Atlantic Ocean (Gaina et al., 2009; Peron-Pinvidic et al., 2012a, 2012b), various microcontinents around Australia (Gaina et al., 2003), the Seychelles microcontinent in the Indian Ocean (Gaina et al., 2013; Ganerød et al., 2011; Torsvik et al., 2013; Figure 1a). A variety of mechanisms have been proposed to explain microcontinent formation in extensional settings. In a review of several cases of microcontinent formation around the globe, Müller et al. (2001) inferred that a mantle plume impinging on continental lithosphere adjacent to an active spreading ridge weakens the continental lithosphere and induces rifting followed by continental breakup. The nearby active spreading ridge is then abandoned in favor of the new mid-ocean ridge, isolating a fragment of the passive margin as a microcontinent. This scenario could apply to the Jan-Mayen microcontinent in the NE Atlantic. Peron-Pinvidic and Manatschal (2010) revised the structure and setting of continental

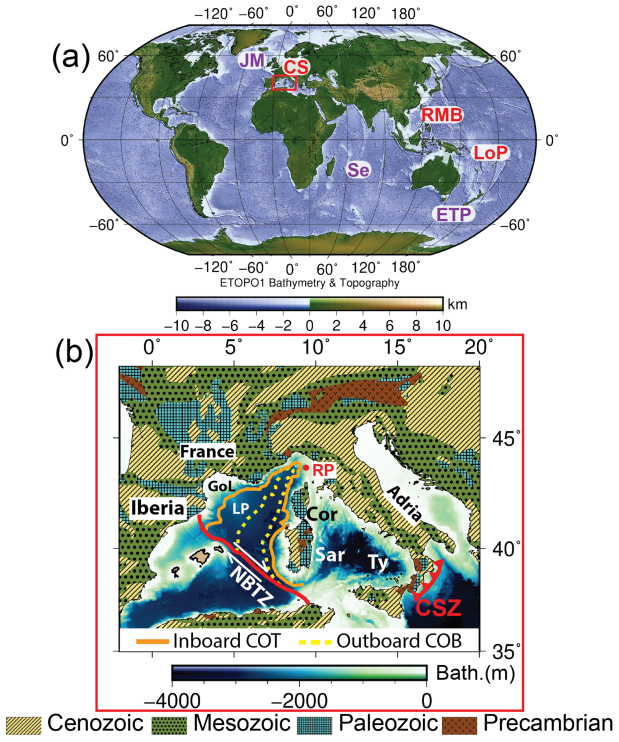


**Figure 1.** (a) Global map with selected locations of microcontinents and continental fragments formed in divergent settings (purple) and those associated with subduction systems (red). CS = Corsica-Sardinia block, ETP = East Tasman Plateau, JM = Jan-Mayen microcontinent, LoP = Louisiade Plateau, RMB = Reed and Macclesfield Banks, Se = Seychelles. (b) Regional map of the central Mediterranean showing the first order onshore geology and era ages of the various terranes. Geological age data from UNESCO World Geological map (Bouysse, 2014). Cor = Corsica, GoL = Gulf of Lion, LP = Liguro-Provençal basin, CSZ = Calabrian Subduction Zone, NBTZ = North Balearic Transform Zone, Sar = Sardinia, Ty = Tyrrhenian Sea, RP = rotational pole of LP basin opening, COT = Continent-Ocean transition zone, COB = Continent-Ocean Boundary.

allochthons in the Atlantic Ocean and postulated that differential thinning of preexisting structures during continental margin formation may form microcontinents and continental fragments by competing rift propagation within weak lithosphere. Examples of such continental fragments are found of the western coast of Ireland. Analogue modeling by Molnar et al. (2018) demonstrated that rotational extension applied to a continental margin in combination with inherited lithospheric weaknesses facilitates microcontinent formation. Competing strike-slip faults along transform margins have also been proposed as a mechanism to release (albeit relatively small) microcontinents (Nemcok et al., 2016). Abera et al. (2016) proposed a mechanism in which an active spreading ridge becomes magma starved, resulting in cooling and strengthening of the lithosphere. Subsequent extension could then localize afterward in a nearby continental margin, provided it is weak, due to the fact that the force required to initiate continental rifting is an order of magnitude less than breaking-up oceanic lithosphere (Abera et al., 2016).

Most research into microcontinent and continental fragment formation focuses on microcontinents formed in divergent tectonic settings and the formation of associated passive continental margins. However, some microcontinents and continental fragments may have formed in convergent tectonic settings in association with subduction. We have identified several examples where small microcontinents and continental fragments are part of a tectonic system that includes subduction. Examples include the Corsica-Sardinia block in the central Mediterranean (Advokaat et al., 2014; Faccenna et al., 2001), the Louisiade Plateau off northeastern Australia (Gaina et al., 1999; Taylor & Falvey, 1977), and the Reed and Macclesfield Banks in the South China Sea (Cullen et al., 2010; Pichot et al., 2014; Figure 1a). These microcontinents and continental fragments are formed in a complex tectonic setting where trench rotation or oblique convergence likely played an important role in their formation. For simplicity we group microcontinents and continental fragments associated with subduction systems from now on and refer to them as continental fragments.

Most of the in situ preserved continental fragments that are associated with subduction systems have formed in regions with a long and complex tectonic history. It has been shown that for passive margins, inherited structures, including but not limited to, old sutures and failed rifts, can localize the extension required for continental rifting and breakup (Brune et al., 2017; Corti, 2008; Heron et al., 2019). Inherited structures in active margins, together with subduction-related tectonic forces, may likewise be the main ingredients for the fragmentation of continental lithosphere and formation of continental fragments in a subduction setting, but the mechanisms controlling this process are still unclear. Recently, Koptev et al. (2019) postulated that the impingement of a mantle plume on a subducting plate that carries a continental block can lead to microcontinent formation on the downgoing plate. However, we consider this scenario rather unique in the geological history. Here we aim to investigate continental fragment formation on the overriding plate focusing on inherited heterogeneities in the continental upper plate and tectonic forces involved in subduction processes.

### 1.2. Corsica-Sardinia: A Continental Fragment in the Mediterranean Sea

Of the subduction-associated continental fragments mentioned above, the Corsica-Sardinia block in the Mediterranean (Figure 1b) is, from a geological point of view, undoubtedly the best-studied example. We have therefore chosen this region to look for potential clues on continental fragment formation mechanisms. The contemporary geological setting of the Mediterranean region is the result of a long tectonic history of oceanic basin opening and closure, from the Late Paleozoic until present (Figure 1b; Dewey & Şengör, 1979; von Raumer et al., 2003; Vissers et al., 2013). Closure of the Tethys due to Africa-Eurasia convergence

dominated the Cenozoic evolution of the Mediterranean and resulted in the opening of several back-arc basins from Oligocene to Pliocene times (Advokaat et al., 2014; Faccenna et al., 2001; van Hinsbergen et al., 2014).

The various amalgamated terranes (Figure 1b) that constitute the present-day geological setting of the central Mediterranean region are likely bounded by lithospheric-scale inherited structures. Such examples can be found in the margins and the crustal structure of the Liguro-Provençal basin (Lacombe & Jolivet, 2005). The southernmost onshore areas of the Provençal margin contain thrusts that placed crystalline basement onto Permian and Mesozoic formations (Arthaud & Séguret, 1981 after Lacombe & Jolivet, 2005). Crustal-scale thrust faults have been interpreted on seismic reflection data from both the Gulf of Lion and the Northern Liguro-Provençal basin (De Voogd et al., 1991; Rollet et al., 2002).

At 30 Ma, south-eastward retreat of the Calabrian slab initiated rifting of the Liguro-Provençal back-arc basin (Advokaat et al., 2014; Gattacceca et al., 2007; Seranne, 1999), while at the same time the Adriatic microplate was colliding with the southern Eurasian margin (Turco et al., 2012; van Hinsbergen et al., 2014). Breakup of the Liguro-Provençal basin occurred at 21 Ma (Faccenna et al., 1997) and was followed by a 5-Myr-long ocean spreading phase during which the Corsica-Sardinia block experienced 45–50° of counterclockwise rotation (Advokaat et al., *2014;* Gattacceca et al., *2007*). Extension ceased in the Liguro-Provençal basin at 16 Ma, before jumping east of the Corsica-Sardinia block at 10 Ma when formation of the Tyrrhenian basin started due to the continued Calabrian slab retreat (Faccenna et al., 2001). At present, Corsica-Sardinia is surrounded by oceanic crust to the west and southeast, by a postulated transfer zone to the southwest, while connected with Italy through thinned continental crust in the northeast (Figure 1b).

From the Corsica-Sardinia example we infer that inherited tectonic structures may play an important role in subduction-associated formation of continental fragments, as they facilitate localization of deformation and continental rifting. Additionally, Wallace et al. (2005, 2009) noted a correlation between the arrival of a buoyant indenter at the trench, observed trench rotation, and associated back-arc extension. Subduction below such a buoyant indenter will cease, while subduction of the laterally present oceanic lithosphere continues, exerting a torque on the trench resulting in trench rotation and potentially back-arc extension. This suggests a potential link between Calabrian slab rotation and the collision of the Adriatic microplate with Eurasia.

Partly based on observations made on the evolution of the Corsica-Sardinia block, we aim to investigate the role of an inherited lithospheric weakness and rotational tectonic forces in continental breakup and subsequent formation of a continental fragment on the overriding plate in a subduction system. To achieve this aim, we run two-dimensional (2-D) and 3-D experiments simulating an oceanic plate subducting under a continental plate with an imposed weak zone to simulate an inherited tectonic heterogeneity.

## 2. Methodology

### 2.1. Governing Equations and Experimental Setup

The numerical experiments are set up in a 2-D and 3-D Cartesian geometry assuming incompressible flow. We solve for the conservation of mass (equation (1)), momentum (equation (2)), energy (equation (3)), and composition (equation (4)) in a nondimensional manner, using the Boussinesq approximation (symbols defined in Table 1):

$$\nabla \cdot \mathrm{u} = 0 \tag{1}$$

$$-\nabla p + \nabla \cdot \left(\eta\left(\nabla u + \nabla^T u\right)\right) + \left(R_T\, T + R_C\, C\right) e_z = 0 \tag{2}$$

$$\frac{\partial T}{\partial t} + u \cdot \nabla T = \nabla^2 T \tag{3}$$

$$\frac{\partial C}{\partial t} + u \cdot \nabla C = 0 \tag{4}$$

The compositional ($R_C$) and thermal ($R_T$) Rayleigh numbers in equation (2) are defined as

**Table 1**
*Symbols, Units, and Values of Experimental Parameters*

| Parameter | Symbols | Value | Unit |
|---|---|---|---|
| Composition | C | 0 (mantle)/1 (cont. crust) | - |
| Gravitational acceleration | g | 9.8 | $m\ s^{-2}$ |
| Vertical unit vector | $e_z$ | - | - |
| Time | t | - | S |
| Velocity | u | - | $m\ s^{-1}$ |
| Reference mantle density | $\rho_0$ | $3.30 \times 10^3$ | $kg\ m^{-3}$ |
| Density contrast | $\Delta\rho_c$ | $6.00 \times 10^2$ | $kg\ m^{-3}$ |
| Deviatoric pressure | p | - | Pa |
| Lithostatic pressure | $p_0$ | - | Pa |
| Temperature | T | - | °C |
| Reference mantle temperature | $T_m$ | 1350 | °C |
| Absolute temperature | $T_{abs}$ | - | K |
| Reference viscosity | $\eta_0$ | $1.00 \times 10^{20}$ | Pa s |
| Effective viscosity | $\eta$ | - | Pa s |
| Maximum viscosity | $\eta_{max}$ | $1.00 \times 10^{23}$ | Pa s |
| Thermal diffusivity | $\kappa$ | $1.00 \times 10^{-6}$ | $m^2/s$ |
| Thermal expansion coefficient | $\alpha_T$ | $3.50 \times 10^{-5}$ | $K^{-1}$ |
| Compositional Rayleigh number | $R_C$ | $1.70 \times 10^7$ | - |
| Thermal Rayleigh number | $R_T$ | $4.39 \times 10^6$ | - |
| Rheological preexponent | A | $2.4763 \times 10^8$ (diff. c.), $6.52 \times 10^6$ (disl. c.) | $Pa^n\ s^{-1}$ |
| Activation energy | E | 360 | $kJ\ mol^{-1}$ |
| Rheologial power law exponent | N | 1 (diff. c.), 3.5 (disl. c.) | - |
| Gas constant | R | 8.3 | $J\ K^{-1}\ mol^{-1}$ |
| Strain rate | $\dot{\varepsilon}_{ij}$ | - | $s^{-1}$ |
| Second invariant of the strain rate | $\dot{\varepsilon}_{II}$ | - | $s^{-1}$ |
| Friction coefficient | $\mu$ | 0–0.1 | - |
| Stress | $\sigma$ | - | Pa |
| Yield stress | $\tau_y$ | - | MPa |
| Surface yield stress | $\tau_0$ | 40–200 | MPa |
| Maximum yield stress | $\tau_{max}$ | 200–400 | MPa |
| Model geometry | | | |
| Box height | h | 660 | km |
| Box length | l | 3300 | km |
| Box width (3-D only) | w | 3960 | km |
| Mesh resolution (2-D) | - | $5 \times 8$–$12 \times 8$ | km |
| Mesh resolution (3-D) | - | $7.5 \times 10 \times 8$–$16 \times 18 \times 8$ | km |
| Continental crust thickness | $H_c$ | 40 | km |

$$R_C = \frac{\Delta\rho_c g h^3}{k\eta_0} \tag{5}$$

$$R_T = \frac{\alpha_T \rho_0 g \Delta T h^3}{k\eta_0} \tag{6}$$

With $\Delta T$ the temperature difference between the top and the bottom of the experimental domain and $\Delta\rho_c = 600\ kg/m^3$ the density difference between the positively buoyant felsic continental crust and the mantle. This density difference assumes a density $\rho_0$ of 2,700 $kg/m^3$ for continental crust, which represents typical values for felsic continental crust, and 3,300 $kg/m^3$ for the mantle (Bittner & Schmeling, *1995;* Turcotte & Schubert, *2002*). The governing equations are solved using the finite element code Citcom (Moresi & Gumis, 1996; Zhong et al., 2000) with an iterative conjugate gradient solver. Our mesh is fixed, but has a higher resolution in the trench region and in regions in which the viscosity contrast is high. Elements of the mesh are quadrilateral in shape and their size varies between $5 \times 8$ and $12 \times 8$ km in the 2-D experiments and between $7.5 \times 10 \times 8$ and $17 \times 20 \times 8$ km in all directions in the 3-D experiments.

In the 2-D and 3-D setups, the bottom of the experimental domain corresponds to the 660-km upper-lower mantle discontinuity. The 2-D experiments have an aspect ratio of 1:5 ($660 \times 3{,}300$ km) while the 3-D experiments have an aspect ratio of 1:5:6 ($660 \times 3{,}300 \times 3{,}960$ km; Figure 2). On the side boundaries as well as the

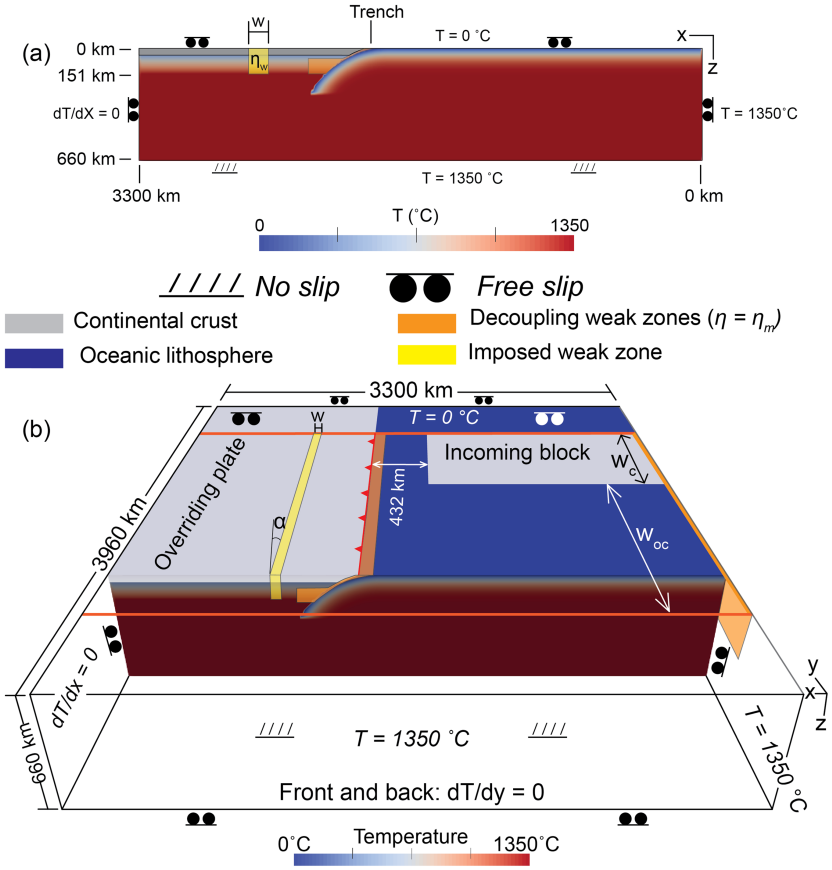


**Figure 2.** Initial experimental setup showing the initial geometry and thermal structure and the mechanical and thermal boundary conditions for (a) 2-D oceanic subduction experiments. The experimental domain is 660 km deep and has a 1:5 aspect ratio. (b) The 3-D experiments with an incoming continental block. For 3-D oceanic subduction experiments, we utilize the exact same setup, but without a continental block on the subducting plate. The experimental domain has an aspect ratio of 1:5:6 and is 660 km deep.

top boundary we impose a free-slip boundary condition while the bottom boundary is no slip (Figure 2), simulating the viscosity contrast between the upper and lower mantle. The temperature at the top boundary is set to 0 °C whereas at the bottom and right-hand side boundaries a temperature of 1,350 °C is imposed, with the latter simulating an oceanic spreading ridge that allows a free right-hand boundary. All other boundaries have insulating boundary conditions (Figure 2). In order to avoid domain induced boundary effects in 3-D, toroidal flow patterns around the subducting slab must be possible (Chen et al., 2016; Funiciello et al., 2003). We achieve this by imposing two 20-km-wide transform faults at $y = 660$ km and at $y = 3{,}300$ km that act as lateral boundaries to the subducting and overriding plate (orange borders in Figure 2b). These 20-km-wide boundaries have a maximum viscosity of $10^{20}$ Pa s.

Composition is defined by a compositional tracer function $C$, where continental crust has the composition of $C = 1$ and mantle material has the composition of $C = 0$. Oceanic crust is not modeled as the buoyancy effect of oceanic crust in subduction dynamics is negligible at the modeled scale (Cloos, *1993*) and we use an imposed weak zone at the trench to decouple the downgoing and overriding plates. The compositional tracers are advected via a particle tracing technique (Wang et al., 2015) in which the tracers are moved with the velocity field allowing discrimination between buoyant continental crust and mantle and lithospheric materials (Ballmer et al., 2007; Di Giuseppe et al., 2008). All experiments have the continental overriding plate fixed to the left-hand boundary of the model domain, simulating the presence of a large(r) continental mass (Figure 2). Following the compilation by Christensen and Mooney (1995), the thickness of continental crust is set to 40 km. We assume a linear temperature gradient for continental crust, from 0 °C at the surface to

1,350 °C at 150-km depth. The initial thermal structure of the downgoing oceanic lithosphere is given by the solution of the half-space cooling model for a 50-Myr-old oceanic lithosphere (Turcotte & Schubert, 2002). In order to initiate dynamic subduction without imposing any external forces, the initial setup contains an oceanic slab already partially subducted to 260-km depth with an initial bending radius of 500 km. A 20-km-wide zone with a maximum viscosity of $10^{20}$ Pa s is imposed at the right domain boundary to 198-km depth, simulating an oceanic spreading ridge, allowing the downgoing plate to move freely during subsequent experimental evolution (Figure 2b).

In order to decouple the subducting and overriding plates and allow subduction to occur, we impose a subduction weak zone with a maximum viscosity of $10^{20}$ Pa s and width of 20 km which extends down to a depth of 50 km. This weak subduction interface has a fixed shape. Below this interface we impose a 200-km-wide weak mantle wedge that extends to 150-km depth. This weak mantle wedge simulates the area of weakened mantle above the slab, resulting from slab dehydration and mantle melting processes and has a maximum viscosity of $10^{20}$ Pa s. Deformation of the weak mantle wedge is allowed to accommodate changes in slab dip during the experiment (Magni et al., 2012). The initial position of the trench is imposed at $x = 1{,}850$ km (Figure 2), but the trench is allowed to move freely along the $x$ axis during the evolution of subduction.

### 2.2. Imposed Weak Zone and Initial Experiment Configuration

In order to investigate the relationship between the parameters of an inherited continental weak zone and the extension in the overriding plate, we first run 2-D experiments of oceanic subduction with an imposed lithospheric scale weak zone in the continental overriding plate (Figure 2) followed by 3-D experiments of pure oceanic subduction. This weak zone is imposed at approximately 500 km from the trench in both 2D and in 3D (Figure 2). Variation of the distance between the trench and the imposed weak zone between 250 and 750 km did not lead to different results. We vary the weak zone width between 60 and 260 km and its viscosity between $0.5 \times 10^{22}$ and $1.5 \times 10^{22}$ Pa s while the thickness is kept constant at 150 km. As we use a crustal viscosity of $10^{23}$ Pa s, this implies that we impose, at the 0 °C surface, a viscosity contrast of between 1.5 and 0.5 orders of magnitude.

Many contemporary microcontinents and continental fragments found close to subduction systems have formed due to extensional and, possibly, rotational tectonic processes. In order to induce such rotation in our 3-D experiments we introduce a 990-km-wide continental block into the lower plate (Figure 2b). The collision of this block induces a torque on the trench, resulting in differential trench retreat and thus trench rotation (Magni et al., 2014; Magni et al., 2017). We vary the ratio of continental to oceanic material in the downgoing plate (as defined by their along-trench widths) to investigate potential links between this ratio and upper plate extension. This ratio ($R_{c/oc}$) is quantified by dividing the width of the continental indenter on the downgoing plate ($W_c$) by the width of the oceanic material on the downgoing plate ($W_{oc}$).

Due to the nature of the experimental setup the, initially straight, imposed weak zone deforms. In order to measure rotations we find the point in the imposed weak zone that has experienced no translation or rotation and utilize this as our rotation pole for measuring rotations. However, it should be noted that these experiments are fundamentally 3D and as such quantifying rotations is difficult as every part of the detaching continental fragments experiences different amounts of rotation. To take into account this complexity we measure two angles: the angle between a line running from the widest part of the newly formed back-arc basin and the original weak zone orientation at the rotation pole (Figure 5a, dashed yellow line and angle), we call this angle the “primary rotation angle.” Secondly, we measure the angle between the rotation pole and the southernmost end of the detaching continental fragment (Figure 5a, dashed orange line and angle), we call this angle the “secondary rotation angle.” When these two angles have similar values, it means that the southern edge of the continental fragment experienced an amount of rotation similar to the central part and, thus, the continental fragment has rotated as one-piece with little deformation. On the other hand, when the secondary rotation angle is much lower than the primary one, it means that the southern edge did not move as much as the central part, indicting a significant curvature of the continental fragment. Therefore, the highest the difference between the primary and secondary angle is, the higher the curvature of the continental fragment is.

The initial distance between the incoming continental block and the overriding plate is 462 km (Figure 2b); thus, the slab will reach the 660-km discontinuity before collision between the incoming continental block and the overriding plate occurs. This allows the investigated processes to occur without the complex effects of the slab interacting with the 660-km discontinuity influencing the results (Funiciello et al., *2003*). Finally, the potential relationship between the angle of the weak zone (α) with respect to the initial strike of the trench and upper plate extension is also investigated (Figure 2b).

### 2.3. Rheology

The materials in our models can deform by viscous creep or brittle yielding. Viscous behavior is governed by both diffusion and dislocation creep (Hirth & Kohlstedt, 2004; Karato & Wu, 1993; Korenaga & Karato, 2008). Each mechanism has its effective viscosity, η (symbols in Table 1):

$$\eta = A\,\dot{\varepsilon}_{II}^{\frac{1-n}{n}} \exp\left(\frac{E}{nRT_{abs}}\right) \tag{8}$$

where $\dot{\varepsilon}_{II}$ is the second invariant of the strain rate, which is defined by

$$\dot{\varepsilon}_{II} = \sqrt{\frac{1}{2}\dot{\varepsilon}_{ij}^{'}2} \tag{9}$$

With $\dot{\varepsilon}_{ij}^{'} = \frac{\partial v_i}{\partial x_j} + \frac{\partial v_j}{\partial x_i}$

The value of the rheological preexponent $A$ for diffusion creep is chosen in such a way that at the mantle reference temperature (1,350 °C) the effective viscosity is the reference viscosity ($10^{20}$ Pa s). For dislocation creep, the reference mantle viscosity is reached for a strain rate of $1.52 \times 10^{-14}$ $s^{-1}$, which is comparable to the strain rates in a convective upper mantle (Bercovici & Ricard, 2016). We use a value of $n = 1$ for diffusion creep and a value of $n = 3.5$ for dislocation creep (Karato & Wu, 1993). Published values of the activation energy ($E$) vary from 250 to 530 kJ $mol^{-1}$ (Karato & Wu, 1993). We use an average of $E = 360$ kJ $mol^{-1}$ for both diffusion and dislocation creep. Furthermore, we assume dry materials and do not consider (de-) hydration or melt processes.

A viscosity for yielding behavior is calculated using

$$\eta_y = \frac{\tau_y}{\dot{\varepsilon}_{II}} \tag{10}$$

$$\tau_y = \min(\tau_0 + \mu\, p_0, \tau_{\max}) \tag{11}$$

where $\tau_y$ is the yield stress and $\tau_{max}$ is the maximum yield stress. $\tau_0$+$\mu$ $p_0$ is Byerlee's law (Byerlee, 1978), where $\tau_0$ is the yield stress (cohesion) at the surface, $\mu$ is the friction coefficient, and $p_0$ is the lithostatic pressure. The code calculates the viscosity for all the mechanisms described above and the effective viscosity at any point is determined by taking the minimum value of the calculated viscosities. A maximum viscosity value of $10^{23}$ Pa s is imposed to limit lithospheric strength to realistic values. Rheology for the mantle and the crust is assumed to be the same.

### 2.4. Experimental Variables

We conducted 45 experiments classified into three distinct sets based on their initial geometry: 2-D oceanic subduction experiments, 3-D oceanic subduction experiments, and 3-D experiments with an incoming continental block. We run reference experiments with a homogeneous overriding plate for all three geometries. All subsequent experiments contain an imposed weak zone. To investigate the effect of weak zone configuration on the evolution of upper plate extension, we conduct a parametric study where we vary both the width $w$ (from 66 to 264 km), and the viscosity $\eta_w$ (from 0.5 to $1.5 \times 10^{22}$ Pa s) of the imposed weak zone in all three experimental setups. Using the configuration deemed most effective in terms of generated back-arc extension, we then run a set of experiments where the ratio of continental to oceanic material in the downgoing plate is varied. Finally, we run four additional experiments where we vary the angle of the imposed weak zone by ±15°. In these experiments, a counterclockwise angle is defined as negative and a clockwise angle is defined as positive (Figure 2b).

## 3. Results

### 3.1. Reference Experiments

Our 2-D reference experiment considers an oceanic plate subducting below a continental overriding plate without an imposed weak zone (Figure 2a; see also Animation MS01 in the supporting information). After 2 Myr of experimental time, the subducting slab reaches the bottom of the experimental box and starts folding several times (Animation MS01). Trench retreat in this experiment is limited, with an average trench retreat velocity of 0.5 cm/year.

In order to see the difference between 2-D and 3-D setups, we add a third dimension to our 2-D models, creating a 3-D oceanic subduction experiment. The setup is otherwise the same, representing an oceanic plate subducting below a continental overriding plate without an imposed weak zone (Figure 2b). After an experimental period of 4 Myr, the subducting slab reaches the bottom and after a period of draping, it folds several times (see Animation MS02). We observe an average trench retreat velocity of 0.4 cm/year. Deformation is mostly focused above the weak mantle wedge (Animation MS02). Additionally, there was no appreciable difference in the results when we ran a 2-D experiment with the mesh resolution of our 3-D setup.

By imposing a weak zone with an initial width of 66 km and an initial viscosity of $5 \times 10^{21}$ Pa s, we test the influence of a preexisting weakness on oceanic subduction in 3D (Figure FS01 and Animation MS03). Except for the introduction of the weak zone, the setup is the same as the 3-D oceanic experiment described above. The evolution of the experiment is similar to the 3-D oceanic experiment with no imposed weak zone (see Animation MS03). We observe an average trench retreat velocity of 0.3 cm/year and an average extension rate of 0.2 cm/year for the imposed weak zone. Thus, in these 3-D models with a purely oceanic subducting plate the overriding plate experiences very little deformation.

In our 3-D setup, trench rotation is induced by introducing a 990-km-wide continental block on the downgoing plate (Figure 2b). The rest of the downgoing plate consists of oceanic material, which subducts below a continental overriding plate that has no imposed weak zone. After 4 Myr, the subducting slab reaches the bottom of the experimental domain and folds several times. Collision between the incoming continental block and the overriding plate occurs after 9 Myr. After 35 Myr, slab breakoff initiates below the incoming continental block, but the adjacent oceanic lithosphere continues to subduct (see Animation MS04). Here trench retreat has an average velocity of 0.6 cm/year. Extension is again mainly focused above the weak mantle wedge (Animation MS04).

### 3.2. The Role of Continental Heterogeneities in Continental Breakup

The introduction of a weak zone in the overriding continental lithosphere of 2-D and 3-D oceanic subduction experiments yielded no significant upper plate extension. When introducing such a weak zone in a 3-D setup with an incoming continental block we do observe significant upper plate extension (Figure 3). The weak zone is imposed at 528 km from the trench in the overriding plate (Figures 2 and 3a and Animation MS05) and has an initial width of w = 66 km and a viscosity of $\eta_w = 0.5 \times 10^{22}$ Pa s. We track the evolving width of the extending zone through time by sampling a profile across the widest part of the final back-arc basin. While our experiments do not produce any volcanic arc, any extensional basin that forms in the upper plate is referred to as a "back-arc basin." In order for a direct comparison between different subsequent weak zone configurations, we nondimensionalize the width of the extended zone ($w$) by the initial weak zone width. North, south, east, and west are defined with respect to the top, bottom, right-, and left-hand side of the modeling domain to aid in describing the results (Figure 3a).

Collision between the incoming continental block and the overriding plate initiates at the northern end of the experimental domain after 9 Myr of model time. At this time, some early extensional structures are visible at the base of the overriding continental crust close to the trench (cross section in Figure 3a). The onset of collision results in deceleration of subduction below the incoming continental block. Slab tearing initiates at depth below the subducted continental lithosphere initiates at ~22 Myr after collision initiates (Animation MS05). The slab tear starts below the northern side of the continental block, then propagates toward the center of the model. Laterally toward the south, below the downgoing oceanic lithosphere, the slab does not detach and continues to subduct. Extension then localizes in the overriding plate above the continuous oceanic subduction, as indicated by the steeper slope of the curve that describes the evolution of the extended

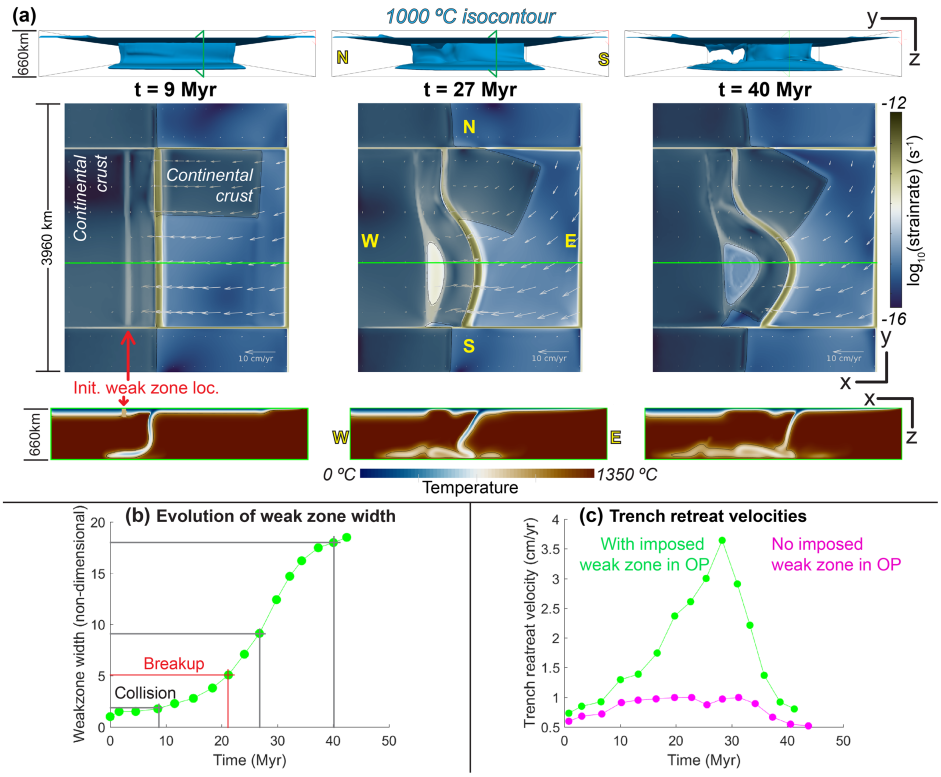


**Figure 3.** (a) Snapshots of the evolution of a representative 3-D experiment with an incoming continental block on the subducting plate and an imposed weak zone in the upper plate. (top panel) The 1,000 °C isocontour of the subducting slab. (middle panel) Top views depicting the $\log_{10}$(strain rate) at 8-km depth. Shaded areas indicate the presence of continental crust. The green line corresponds to the cross section displaying the temperature field in the bottom panel. Cardinal directions are defined to aid description and discussion of the experiments. The high strain rate lines north and south of the experimental domain indicate lateral domain boundaries, which are zones with weak viscosity decoupling the modeling domain from the sides to avoid boundary effects. (b) Evolution of the width of the upper plate extended zone through experimental time along the green line in the top view panels in (a). The grey lines correspond to the times of the displayed snapshots in (a). (c) Comparison of trench retreat velocities of experiments with an initial imposed weak zone in the overriding plate (a) and no initial imposed weak zone in the overriding plate (3-D reference experiment with incoming continental block; Animation MS03 in the supporting information). The measurements are made along the green line in the top view panels in (a).

zone through time (Figure 3b). We define breakup of the overriding plate as the moment when the percentage of continental material in the crust at 8-km depth is lower than 70%. When breakup of the overriding plate occurs, oceanic spreading starts in the back-arc basin. In nature, continental breakup is usually followed by seafloor spreading which may be preceded by subcontinental mantle exhumation. As we do not model mantle melt production, no oceanic crust forms at back-arc basins in our experiments. However, for simplicity and because in nature eventually oceanic lithosphere is always formed, we consider that after continental breakup a back-arc basin floored by oceanic lithosphere is formed.

In this case, continental breakup occurs around 21 Myr (Figure 3b), 12 Myr after the initiation of collision, and before slab break-off occurs. At this time, the rate of upper plate extension accelerates, as visible in Figure 3b. Formation of a back-arc basin is well underway after 27 Myr of experimental time (Figure 3a, middle panels), corresponding to around 1,500 km of subduction of oceanic lithosphere, which is the total amount of initially defined lithosphere. Subsequently subducted oceanic lithosphere is newer and thus younger and hotter. It thus experiences less slab pull, and a decrease in trench retreat velocity occurs around 30 Myr (Figure 3b). After 40 Myr, the rate of upper plate extension has slowed down significantly. The extended zone is now roughly 18 times wider than the original weak zone (Figure 3b) and a continental block has partly detached from the initial overriding plate due to continental breakup and back-arc

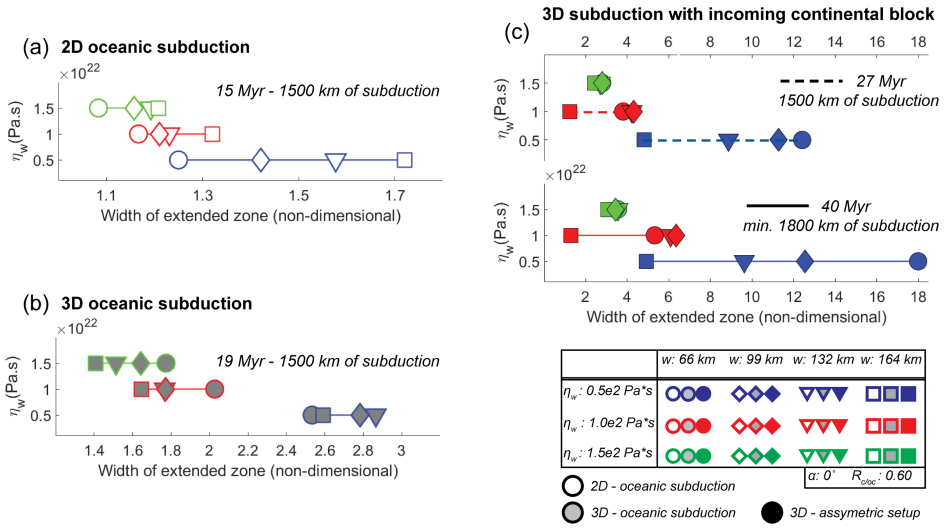


**Figure 4.** Comparison of the final, nondimensional, width of the imposed weak zone versus the initial weak zone viscosity for (a) 15 Myr and 1,500 km of subduction in the 2-D oceanic subduction setup, (b) 19 Myr and 1,500 km of subduction in the 3-D oceanic setup, and (c) after 27 Myr and 1,500 km of subduction (dotted lines) and 40 Myr and a minimum of 1,800 km of subduction (solid lines) for the 3-D setup with an incoming continental block. Colors and symbols used in the graphs are shown at the bottom right of the figure.

spreading. A roughly triangular shape defines the back-arc basin geometry (Figure 3a). Where trench retreat velocity is highest, we observe an extension in the overriding plate of 650 km, corresponding to an extension rate of 1.6 cm/year.

When we compare these results with the 3-D reference experiment with an incoming continental block, we observe that the presence of a weak zone plays an important role in facilitating continental breakup. Although their initial evolution is similar, once the weak zone activates and localizes deformation, extension starts and trench retreat and upper plate extension rates accelerate. We also observe that the weak zone on the overriding plate facilitates and speeds up continental extension (Figure 3c).

### 3.3. The Role of the Weak Zone Configuration

The experiment described above (Figure 3) shows that the presence of an initially imposed weak zone facilitates extension and breakup of the upper plate. We investigate the influence of weak zone configuration by varying its width (w) from 66 to 264 km, and its viscosity ($\eta_w$) from 0.5 to1.5 $\times$ $10^{22}$ Pa s. After we implement these new parameters, we run all previously presented experiments in 2D, in 3-D oceanic subduction, and in 3D with an incoming continental block on the lower plate (Figures 2 and 4). Our expectations are that weak zones with a lower viscosity will yield wider back-arc basins as they allow for more efficient extension localization.

We compare the results of different 2-D experiments after roughly 1,500 km of subduction was completed (Figure 4a). Both narrow and wide weak zones experience some extension (up to 110–170%), but the weak zone with the lowest viscosity ($\eta_w = 0.5 \times 10^{22}$ Pa s) enables the highest amount of upper plate extension (125–170%). In 2-D models, wider weak zones facilitate more extension; thus, it follows that wider back-arc basins will form if the initial weak zone is wider and weaker. However, Figure 4a shows that initially narrower weak zones with lower viscosities extend more than wider weak zones with slightly higher viscosity. This implies that, in our 2-D experiments, viscosity is the dominant factor controlling the amount of extension facilitated by weak regions on the upper continental plate. Therefore, although widest initially imposed weak zone results in the most extension in 2D, the viscosity appears to be more dominant.

Three-dimensional experiments with oceanic subduction, visualized after 1,500 km of subduction, show a different pattern compared to the 2-D cases (Figure 4b). Firstly, the amount of stretching of the extended zone increases significantly (140–280% depending on the configuration) for all tested width and viscosity configurations. Secondly, the trend of the experiments with the lowest viscosity weak zone ($\eta_w = 0.5 \times$

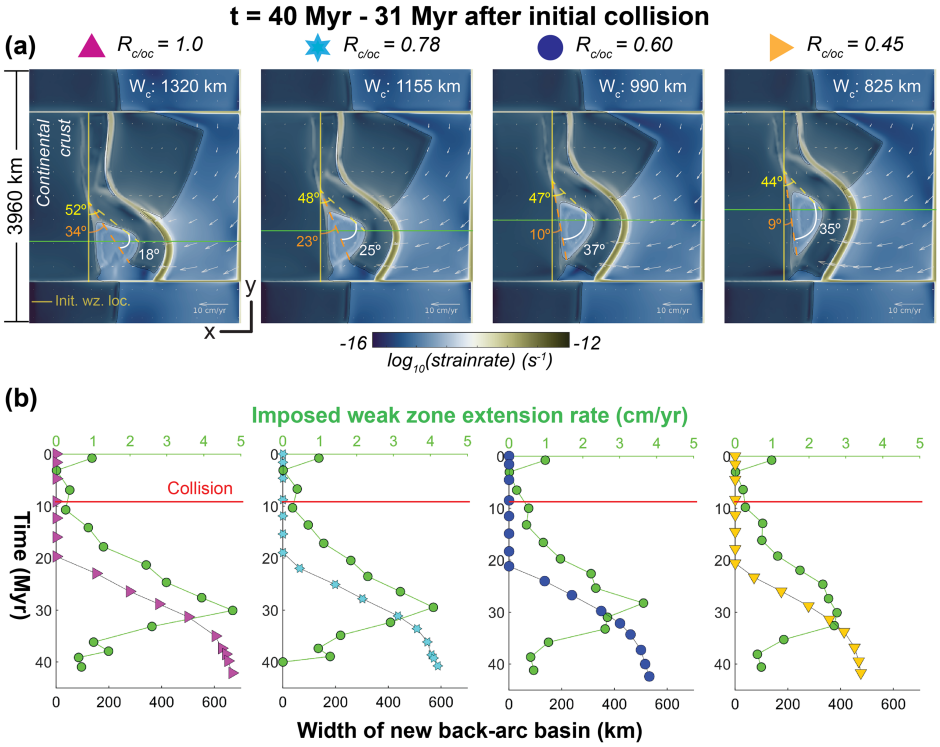


**Figure 5.** (a) Top view sections at 8-km depth for experiments with varying $R_{c/oc}$ ratios of along-strike continental to oceanic widths on the downgoing plate. Colors show $\log_{10}$(strain rate) at 8-km depth. Shaded areas indicate the presence of continental crust. We track the evolution of the upper plate extended zone as well as the width of the rifted region along the green section. All initially imposed weak zones have a configuration of w = 66 km and $\eta_w = 0.5 \times 10^{22}$ Pa s. (b) Plots of trench retreat velocity (in green with values on top axis) and width of new back-arc basin (bottom axis) versus experimental time (*y* axis) for the different experiments displayed in (a).

$10^{22}$ Pa s) differs significantly. The widest imposed weak zone (w = 264 km) experiences less extension than the two narrower imposed weak zones (w = 99 and 132 km) with the same viscosity (Figure 4b).

Experiments with the same weak zone parameters, but also containing a continental block on the lower plate, yield the highest amount of upper plate extension after 1,500 km of subduction (Figure 4c). The two narrowest weak zones (w = 66 and 99 km) with the lowest viscosity ($\eta_w = 0.5 \times 10^{22}$ Pa s) have extended approximately 1,000–1,200% with respect to their original width. As in the 3-D experiment with a purely oceanic lower plate, the weak zones with the lowest viscosity ($\eta_w = 0.5 \times 10^{22}$ Pa s) stretch around 3 times more than those with a higher viscosity (Figure 4c). Stretching of the weakest and narrowest weak zone increases dramatically after 1,500 km of subduction (Figure 4c). Toward the end of the experiments, after 40 Myr and subduction of a minimum of 1,800 km of oceanic material, the back-arc basin has experienced approximately 1,800% extension with respect to its initial width (Figure 4c). Thus, we conclude that, with this setup, the narrowest and weakest weak zone allows the highest amount of extension, which is opposite to the results obtained in 2D. Furthermore, for a given viscosity, the width of the weak zone seems to be the most important factor that controls back-arc basin extension in the 3-D experiments we conducted.

### 3.4. The Role of the Continental/Oceanic Area Distribution on the Subducting Plate

Results from Magni et al. (2017) suggest that there is a potential link between the ratio of continental to oceanic material in the downgoing plate and kinematics of upper plate extension. Following this line of investigation, we performed an additional set of experiments, in which we vary the ratio $R_{c/oc}$ on the downgoing plate (Figure 2). We tested ratios $R_{c/oc}$ of 1.0, 0.78, 0.6, and 0.45 (Figure 5a). In these experiments, we impose a 66-km-wide weak zone (w) with a viscosity of ($\eta_w$) $0.5 \times 10^{22}$ Pa s in the overriding plate. The width of the

upper plate extended zone through time is tracked along a profile that crosses the widest part of the final back-arc basin. As different ratios result in different final geometries, the location of this section varies for each experiment.

Figure 5a shows top views of the four experiments with different continent/ocean ratio at 40 Myr, which is 31 Myr after the initiation of collision of the incoming continental block. The results display a trend: the highest $R_{c/oc}$ ratio (1.0) results in the widest back-arc basin, the rotation angles (primary rotation: 52°; secondary rotation: 34°) and lateral detachment of the rifted continental crust from the overriding plate at the southern boundary of the modeling domain (Figure 5 and Animation MS06). When the ratio decreases ($R_{c/oc}$ = 0.78), the rifted continental lithosphere still separates laterally from the overriding plate, but less than in the previous experiment while the rotation angles are lower (primary rotation: 48°; secondary rotation: 23°; Figure 5 and Animation MS07). With a further decrease of the $R_{c/oc}$ ratio (0.6), the rotation decreases to 47° (primary rotation) and 10° (secondary rotation), and no lateral detachment of the rifted continental fragment from the southern side of the overriding plate is observed, a trend which is also observed for lower values of $R_{c/oc}$ (0.45; Figure 5a and Animations MS05 and MS08, respectively). Moreover, the difference between the primary and secondary rotation angles increases, indicating a larger curvature of the continental fragment. All experiments yield back-arc basins with breakup as defined above (less than 70% continental material in the crust at 8-km depth).

In all four experiments, continental breakup initiates in the back-arc domain at roughly 20 Myr of experimental time, approximately 11 Myr after the initiation of continental collision. We measure the rift evolution by tracking the width of the newly forming oceanic domain along a profile that crosses the widest part of the final back-arc basin (the green lines in Figure 5a). The trend of decreasing back-arc basin width with decreasing $R_{c/oc}$ ratios observed in the top views is also present in the plots of the rift evolution (Figure 5b). The highest ratio of continental to oceanic material produces the widest back-arc basin and thus has the fastest back-arc extension. For each successive experiment where the ratio of continental to oceanic material decreases, the final rifted width of the back-arc basin decreases. The evolution of this extension through time is similar for the different experiments with the main difference being the final rifted width and the extension rate (Figure 5b).

### 3.5. The Role the Imposed Continental Weak Zone Angle

In previous experiments we imposed the weak zone parallel to the trench to limit model complexity. However, as this geometry is seldom found in nature, we perform an additional set of experiments to test the influence of the initial angle of the weak zone with respect to the trench. Taking the experiments with $R_{c/oc}$ ratios of 0.6 and 1.0, an imposed weak zone width (w) of 66 km and a viscosity ($\eta_w$) of $0.5 \times 10^{22}$ Pa s, we vary the angle of the weak zone with respect to the trench with 15° in both clockwise (positive) and counterclockwise (negative) directions. Top views depicting the $\log_{10}$ (second invariant of the strain rate) with continental crust contours, after 40 Myr of experimental time, are displayed in Figure 6a. Rotation angles are measured in the same manner as in section 3.4.

Different geometries are observed for different initial weak zone orientations. For $\alpha = -15°$ counterclockwise angle on the experiment with $R_{c/oc} = 0.6$, we observe lateral detachment of the continental crust from the southern lateral domain boundary and a 29° primary (yellow) and 21° secondary (orange) angle (Figure 6a (top right panel) and Animation MS09). This is different from the experiment with the same setup ($w = 66$ km, $\eta_w = 0.5 \times 10^{22}$ Pa s, $R_{c/oc} = 0.6$), but with a different weak zone angle $\alpha$ (0°) in which there is no lateral detachment of continental crust from the rest of the continental overriding plate (Figure 6a (top middle panel) and Animation MS05). The geometry of the newly formed back-arc basin has a wedge shape, whereas the basin in the 0° experiment is triangular. When we impose a weak zone with an angle $\alpha = +15°$ clockwise in an otherwise similar setup, the detached continental block is around 2 times wider when compared to the experiment with a $\alpha = 0°$ weak zone, but back-arc basin width is much narrower and more elongated (Figure 6a (top right panel) and Animation MS10). The rotation angles are also lower, with a 27° primary angle (yellow) and 8° secondary angle (orange). Compared to the $\alpha = 0°$ experiment, the shape of the back-arc basin is narrower and more elongated.

The experiment with $w = 66$ km, $\eta_w = 0.5 \times 10^{22}$ Pa s, and $R_{c/oc} = 1.0$ showed significant lateral detachment of continental crust from the southern lateral domain boundary, as well as a wide back-arc basin

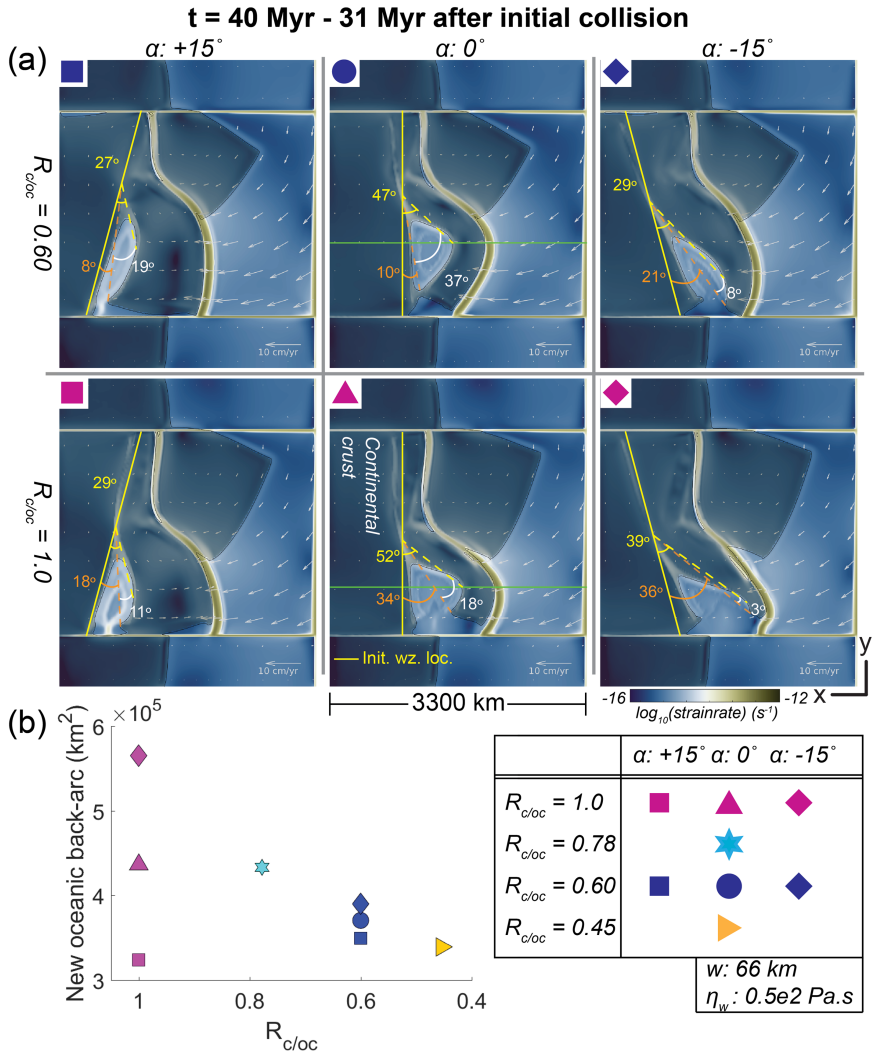


**Figure 6.** (a) Comparison of the influence of the initial weak zone angle α. Sections depict top views of $\log_{10}$(strain rate) at 8-km depth. All imposed weak zones have an initial configuration of w = 66 km and $\eta_w = 0.5 \times 10^{22}$ Pa s. (b) Plot comparing the total area of newly created oceanic back-arc lithosphere for various experiments with different $R_{c/oc}$ ratio's and imposed weak zone angle α after 40 Myr of experimental time.

(Figure 6a, middle bottom panel). A counterclockwise angle α of −15° in this setup (w = 66 km, $\eta_w = 0.5 \times 10^{22}$ Pa s, $R_{c/oc} = 1.0$) results in a relatively narrow sliver of continental material that detaches laterally from the southern side of the continental overriding plate behind a large *v*-shaped back-arc basin (Figure 6a and Animation MS11). Rotation angles have very similar values 39° (primary rotation) and 36° (secondary rotation), indicating a large rotation of the entire block of the continental fragment. Imposing an angle of α = +15° clockwise on the weak zone yields similar results to those obtained for the $R_{c/oc} = 0.6$, α = +15° experiment. The geometry of the back-arc basin in this experiment ($R_{c/oc} = 1.0$, α = +15°) is more *v*-shaped and somewhat wider when compared to the one describe in the previous paragraph ($R_{c/oc} = 0.6$, α = −15°; Figure 6a (bottom right panel) and Animation MS12). Rotation angles are also similar to the $R_{c/oc} = 0.6$, α = +15° experiment with a 29° primary rotation and 18° secondary rotation angle.

In order to quantify the effect of the initial weak zone angle, we calculate the area of the new back-arc basin. Using the position of the trench to delineate the overriding plate, the back-arc basin area is calculated by summing the area of all cells in the overriding plate where continental material is <70%. Experiments

where the weak zone is imposed under a negative angle ($\alpha = -15°$ counterclockwise) angle yield a higher area (29% and 5% more for $R_{c/oc} = 1.0$ and $R_{c/oc} = 0.6$, respectively) of newly formed oceanic back-arc lithosphere when compared to the experiment with no angle on the imposed weak zone ($\alpha = 0°$; Figure 6b). Conversely, experiments where the weak zone is imposed under a positive angle ($\alpha = +15°$ clockwise) yield a lower area (26% and 6% less for $R_{c/oc} = 1.0$ and $R_{c/oc} = 0.6$, respectively) of newly formed oceanic back-arc lithosphere when compared to the experiment with no angle on the imposed weak zone ($\alpha = 0°$; Figure 6b).

## 4. Discussion

### 4.1. Conditions Enabling the Formation of Continental Fragments in Subduction Settings

We find that extension in the overriding plate does not always result in continental breakup. In order to induce extension and trigger breakup of the overriding plate in our relatively unconfined setup, the presence of a preexisting weak zone is required. While experiments without such an imposed weak zone do experience limited trench retreat (Animation MS04), extensional stress in the overriding plate does not localize sufficiently considering our current rheology, and breakup does not occur (Animations MS02 and MS04). In the 2-D cases, this is consistent with previous 2-D numerical models that showed that extension is not achieved in strong overriding plates (Garel et al., 2014) and, in some cases, a weak back-arc lithosphere is needed to create a back-arc basin (Wolf & Huismans, 2019). For the 3-D cases, this differs from previous models, in which back-arc basins can form without a preexisting weak zone in the overriding plate (e.g., Magni et al., 2014). However, these back-arc basins formed in a very confined setup where two separate continental blocks on the downgoing plate collide with a continental overriding plate. Subsequent back-arc basin formation is then due to the continued subduction of oceanic material between the two continental blocks and associated trench retreat.

Deformation of the lithosphere, whether it is brittle or ductile, can result in permanent damage of the rocks and thus in inheritance. Brittle failure usually occurs in (semi)discrete planes when the surrounding stress exceeds the yield stress of the material (Byerlee*, 1978*). Due to strain(-rate) weakening processes, the resulting structure can be weaker than the surrounding material and will thus be preferentially activated during subsequent application of stress. Localization of ductile deformation is usually associated with the switch to grain size sensitive deformation mechanisms (Drury*, 2005*). However, in polycrystalline mixtures the presence of more than a single phase inhibits grain growth and healing of damaged material due to grain boundary pinning (Manohar et al., *1998*). This results in slow grain growth and long healing times, providing damage memory and tectonic inheritance (Bercovici & Ricard*, 2014, 2016*). Inherited structures can thus be the result of numerous tectonic processes and therefore have different geometries, extent, and rheological properties. They include, but are not limited to, old failed rifts (El Harfi et al., 2006; Ziegler et al., 2001), old orogenic sutures, and subduction zones (Morgan et al., 1994; Schiffer et al., 2015). These previously deformed regions can contain faults, (ductile) shear zones and deformed mantle material, all of which can locally influence the strength of the lithosphere (Mazzotti & Gueydan, 2018). Subsequent deformation can localize along these inherited, weaker structures (Balázs et al., 2017; Bercovici & Ricard, 2014; Heron et al., 2016), facilitating further rift development within the tectonic system. Due to the inherent complexities of nature, quantifying the strength of inherited structures is difficult. However, numerical and rock deformation experiments indicate that inherited rheological weaknesses can be 1–2 orders of magnitude weaker than the surrounding lithosphere (Mazzotti & Gueydan, 2018).

Our variation of weak zone configurations implies that the viscosity contrast at the surface between the imposed weak zone and its surroundings must be of a certain magnitude, before sufficient localization of extension and breakup occurs. We find that in our setup this viscosity contrast must be at least 1 order of magnitude, implying that, in nature, lower magnitude viscosity variations might be negligible for the larger-scale evolution of the subduction system. Indeed, in our experiments, the most efficient back-arc rifting and separation of a continental block from its parent continent occurs when the initial imposed weak zone has a viscosity that is 1.5 times lower at the surface than the surrounding crust (Figures 4 and 5). Results from 3-D experiments also indicate that narrow weak zones within the overriding continental plate facilitate relatively more extension than wider weak zones (Figure 4). This is most likely because higher stresses are localizing in a smaller unit area, resulting in higher strain rates. The final shape of the continental fragment and the back-arc basin is controlled by the orientation of the initially imposed weak zone in the

overriding plate relative to the trench (Figure 6). While we did not test variations in the convergence direction relative to the trench, such variations could potentially impose additional differential stress on the upper plate. This can result in further variations in the evolution and final geometry of the continental fragment and back-arc basin.

The initial geometry of the subducting plate can be important for the dynamics of subduction and its influence on overriding plate extension. By introducing a continental block on the downgoing plate, we induce lateral variation in the upper plate stress that causes trench rotation and a more pronounced, local, extensional regime in the overall convergent setting (Figure 3). Trench rotation by an indenter has been previously proposed based on observations of contemporary convergent plate boundaries (Wallace et al., *2009*). A torque that acts on the trench results from the opposing forces created by the subducting continental part of the subducting plate and the slab pull force of the laterally ongoing oceanic subduction (Wallace et al., *2005*). Together with upper plate heterogeneities, lateral along trench stress gradients in the upper plate caused by slab rotation are the second necessary requirement for separation of continental crustal material from active continental margins and formation of continental fragments. Previous 3-D experiments with a similar rotational setup (e.g., Magni et al., 2017) obtained back-arc basin formation and very narrow continental fragments without introducing a weak zone in the overriding plate. However, in these models, the rifting starts very close to the trench and yields fragments of around 150 km wide, whereas our experiments produce fragments with a minimum width of 200 km yielding more substantial continental fragments. Additionally, analogue modeling of a divergent tectonic setting has also found that rotational opening kinematics and preexisting weak zones are required for continental fragment formation in such a setting (Molnar et al., 2018).

Our results also indicate that relatively high ratios of along-strike width of continental to oceanic material (high $R_{c/oc}$) result in wider back-arc basins, (single-sided) lateral detachment of the rifted continental lithosphere from its parent continent along the southern lateral domain boundary, and larger rotation angles (primary and secondary; Figure 5). Such a high $R_{c/oc}$ ratio implies a relatively narrow subducting oceanic slab after the initiation of collision between the incoming continental block and the overriding plate (Figures 2 and 5). This observation fits with previously proposed hypotheses that narrow subducting plates have a lower viscous resistance in the mantle and that narrow slabs as well as slab edges experience more trench retreat and rotation (Schellart et al., 2007; Wallace et al., 2009). Such increased rates imply a higher differential stress in the overriding plate resulting in more efficient back-arc basin formation. Additionally, this effect is also seen in the measured rotation angles. When we define a "residual rotation angle" as the difference between the primary and secondary rotation angles, results indicate that a higher $R_{c/oc}$ ratios (and weak zone angles) result in a lower residual angle of the continental fragment. Comparing Figures 5 and 6, this residual angle can be considered as a proxy for the bulk rotation of the continental fragment; that is, a high residual angle implies a curved continental fragment, while a low residual angle implies a relatively straight continental fragment that is laterally detached from its parent continent.

### 4.2. Model Limitations

As all modeling studies, our models required several simplifications of complex natural features and properties in order to be able to run the experiments. The rotation of the oceanic slab is favored by the presence of transform faults that we impose as weak regions adjacent to the subducting and overriding plate. This is a simplified model representation of transform faults in nature that accommodates the migration of the trench (i.e., STEP faults; Govers & Wortel, 2005). Moreover, this setup allows for toroidal mantle flow around the subducting slab, which is crucial to avoid domain induced boundary effects (Chen et al., *2016;* Funiciello et al., *2003*). A free surface, instead of free slip, boundary condition might affect the stresses at the surface. This is relevant for the evolution of topography in subduction settings (Quinquis et al., 2011), but we do not expect the overall dynamics to change significantly for our scale of interest. We neglected an oceanic crust, but as we include yielding, the strength of the oceanic plate at Earth's surface is sufficiently low to allow the downgoing plate to decouple from the surface free-slip boundary and subduct (Quinquis et al., *2011*).

Our setup imposes a weak mantle wedge between the subducting and overriding plate to facilitate decoupling between the two plates and to simulate the weak mantle wedge present in nature. By imposing, rather

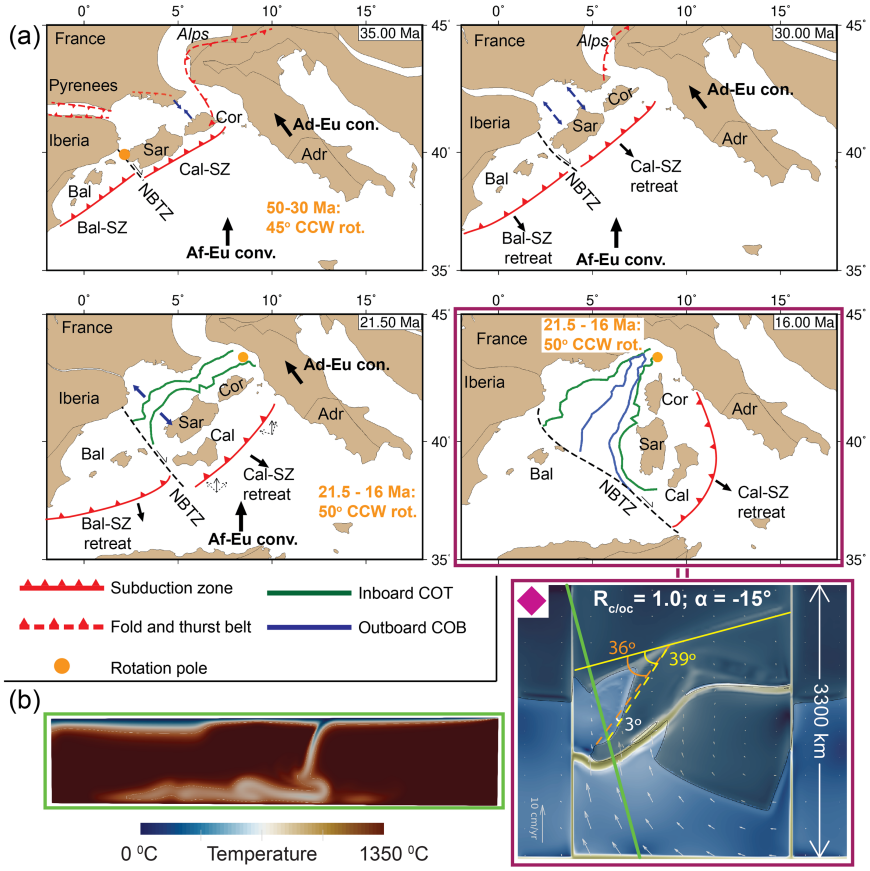


**Figure 7.** (a) Tectonic reconstruction snapshots of the central Mediterranean showing the evolution from 35 Ma (prerifting), via 30 Ma (initiation of trench retreat and rifting), and 21.5 Ma (breakup) to 16 Ma (cessation of spreading in the Liguro-Provençal basin). Reconstruction after Advokaat et al. (2014) and van Hinsbergen et al. (2014). The transitional and oceanic crust boundaries are from Rollet et al. (2002). Adr = Adriatic microplate, Bal = Balearic islands, Cal = Calabria; other abbreviations as in Figure 1. (b) Top view section at 8-km depth and cross section along the yellow line of the $R_{c/oc} = 1.0$; $\alpha = -15°$ experiment after 40 Myr of experimental time (Figure 6a). Note the geometric similarities with the central Mediterranean at 16 Ma (a).

than dynamically calculating this weak mantle wedge, we potentially influence the effects of the toroidal mantle flow on the base of the overriding plate lithosphere, something that has been suggested to play an important role in upper plate back-arc extension (Chen et al., *2016*). However, other authors argue for a more dominant role of shallow crustal forces related to the collision of a positively buoyant indenter at the trench in the nucleation and evolution of back-arc rifting (Wallace et al., 2009).

Although the composition and structure of the continental crust can vary widely, we have used an initial homogeneous crust. We use an average density of $\rho_c = 2{,}700$ kg m$^3$, which is a commonly used value for the upper crust (Bittner & Schmeling*, 1995;* Turcotte & Schubert*, 2002*). Changes to the crustal density result in changes to the buoyancy of the continental material, which controls the occurrence and timing of slab break-off (Magni et al., 2017; van Hunen & Allen, 2011). For our study it is relevant that slab break-off occurs, but the exact timing and depth is of lesser importance. In general, a denser continental crust would delay the time of slab break-off, but would not change the model evolution (van Hunen & Allen*, 2011*).

Potential geometrical variations, such as variable lithospheric thicknesses of an inherited weak zone, are not taken into account in our setup. However, as we are mainly interested in the first-order processes controlling activation of our imposed weak zone and its subsequent evolution in a subduction setting, we feel that these limitations do not significantly influence the dynamics of the system.

### 4.3. Model Comparison With the Central Mediterranean Sea

Our results have first-order geometric and kinematic similarities with the evolution and present-day architecture of the Corsica-Sardinia block in the central Mediterranean. The model with $R_{c/oc} = 1.0$ and $\alpha = -15°$ is probably the closest to this natural example (Figures 6 and 7), although our experiments aimed to investigate basic ingredients for the formation of continental fragments in subduction systems, not this particular setting.

It has been postulated that the initial African slab that subducted below Eurasia was initially very wide, stretching from, at least, the western side of the Balearic islands to southern part of the Alps (Figure 7a; Advokaat et al., *2014 ;* van Hinsbergen et al., *2014*). However, upon the initiation of trench retreat, the slab segmented into two distinct slabs: the Calabrian and Balearic (Figure 7a), formed along the then forming North Balearic Transfer Zone. This North Balearic Transfer Zone is a postulated lithospheric STEP fault whose existence is inferred in many reconstructions (Rosenbaum et al., 2002; van Hinsbergen et al., 2014). This proposed segmentation evolved in a much narrower Calabrian slab, which allowed for more trench retreat and slab rotation, which it experienced during its subsequent evolution (Advokaat et al., *2014;* Gattacceca et al., *2007*). This rotation was likely caused by the collision of an incoming continental block (Adriatic microplate) with the overriding plate (Eurasia). The Ligurian margin from which the Corsica-Sardinia detached, also experienced a long tectonic history and its structure is rather heterogeneous, as it contains Pyrenean, basement involved thrust structures (Lacombe & Jolivet, 2005), as well as various geological boundaries (Figure 1b). While there are no evidences that these structures affected the entire lithosphere, we infer that prior to breakup (Advokaat et al., *2014;* van Hinsbergen et al., *2014*), the Ligurian-Corsican region had a composite continental crust (or lithosphere); therefore, we postulated that the presence of a preexisting weak zone was very likely. Furthermore, the geometry of the back-arc basin in our $R_{c/oc} = 1.0$, $\alpha = +15°$ experiment and that of the Liguro-Provençal basin are similar. Both in nature and in our models, separated continental blocks rotated around a nearby pole and experienced rotational basin opening that resulted in a *v*-shaped back-arc basin (Figure 7).

In the case of the central Mediterranean, the locus of extension relocated from the Liguro-Provençal basin to the Tyrrhenian basin around 10 Ma (Faccenna et al., 2001). The mechanisms that control this plate boundary relocation are still debated. Using results obtained from analogue modeling, Faccenna et al. (2001) postulated that, when the subducting slab reaches the 660-km transition zone, the combination of a reduced subduction velocity and the weight of the slab itself results in bending of the slab and curving of the trench. Consequently, trenchward relocation of extensional stress at the surface occurred, and caused the extension to relocate to the Tyrrhenian basin. Other authors suggest that the collision of the Calabrian trench with the African continent and Adriatic microplate caused lateral cessation of subduction and slab tearing along the margins. This potentially caused acceleration of the trench retreat velocity, strong toroidal mantle flow around the slab, and changes in the stresses in the back-arc (Faccenna et al., 2005, 2007; Magni et al., 2014). Our experiment only captured the first step in continental fragment formation, but failed to reproduce the plate boundary relocation. Further experiments investigating more ad hoc geometries, as well as the mechanisms controlling relocation of extension, may provide additional insight into the interplay between subduction mechanisms and formation and complete isolation of a microcontinent or continental fragment.

## 5. Conclusions

We used 2-D and 3-D numerical experiments to investigate the conditions required for localizing extension and to breakup a continental overriding plate that leads to the separation of a continental block from the active plate margin. Our results indicate that formation of a continental fragment or microcontinent from the overriding plate requires a preexisting, inherited weak zone with a viscosity that is, at minimum, 1 order of magnitude lower than the surrounding lithosphere at the surface. Furthermore, the presence of along-trench stress gradients in the upper plate due to slab rotation is a second requirement to attain sufficiently high stress values able to localize and initiate upper plate extension (Figures 3 and 5). This localization is most efficient in narrower (66 km wide) weak zones where stress is higher over a smaller unit area. Single-sided detachment of the rifted block from its parent continent occurs for systems with relatively

narrow subducting oceanic plates, as these narrow slabs result in the highest differential stress in the upper plate (Figure 5). Our results shed some light on the processes that controlled the separation of the Corsica-Sardinia block from Eurasia by highlighting the roles of tectonic inheritance and the Adriatic indenter in the formation of the Liguro-Provençal basin.

**Acknowledgments**
We thank the Editor, Associate Editor, an anonymous reviewer, and Phil Herron for their excellent and extensive suggestions that substantially improved our manuscript. All authors acknowledge support from the Research Council of Norway through its Centers of Excellence funding scheme, project 223272. They also acknowledge funding from the Horizon 2020 Marie Sklodowska Curie Initial Training Network grant 674899—SUBITOP. Maps in Figure 1 were made using Generic Mapping Tools (GMT; Wessel et al., 2013). In order to avoid distortion of data we utilized perceptually uniform colour schemes (Crameri, 2018a; Crameri, 2018b). All input and output files used in this manuscript are available under doi: *10.5281/zenodo.3588255*. The version of the CitCom code used in this manuscript can be found under doi: *10.5281/zenodo.3588268*.

## References

Abera, R., van Wijk, J., & Axen, G. (2016). Formation of continental fragments: The Tamayo Bank, Gulf of California, Mexico. *Geology*, *44*(8), 595–598. https://doi.org/10.1130/G38123.1

Advokaat, E. L., Van Hinsbergen, D. J. J., Maffione, M., Langereis, C. G., Vissers, R. L. M., Cherchi, A., et al. (2014). Eocene rotation of Sardinia, and the paleogeography of the western Mediterranean region. *Earth and Planetary Science Letters*, *401*, 183–195. https://doi.org/10.1016/j.epsl.2014.06.012

Arthaud, F., & Séguret, M. (1981). Les structures pyrénéennes du Languedoc et du Golfe du Lion (Sud de la France). *Bulletin de La Société Géologique de France*, *7*(1), 51–63. https://doi.org/10.2113/gssgfbull.s7-xxiii.1.51

Balázs, A., Burov, E., Matenco, L., Vogt, K., Francois, T., & Cloetingh, S. (2017). Symmetry during the syn- and post-rift evolution of extensional back-arc basins: The role of inherited orogenic structures. *Earth and Planetary Science Letters*, *462*, 86–98. https://doi.org/10.1016/j.epsl.2017.01.015

Ballmer, M. D., van Hunen, J., Ito, G., Tackley, P. J., & Bianco, T. A. (2007). Non-hotspot volcano chains originating from small-scale sublithospheric convection. *Geophysical Research Letters*, *34*, 1–5. https://doi.org/10.1029/2007GL031636

Bercovici, D., & Ricard, Y. (2014). Plate tectonics, damage and inheritance. *Nature*, *508*(7497), 513–516. https://doi.org/10.1038/nature13072

Bercovici, D., & Ricard, Y. (2016). Grain-damage hysteresis and plate tectonic states. *Physics of the Earth and Planetary Interiors*, *253*, 31–47. https://doi.org/10.1016/j.pepi.2016.01.005

Bittner, D., & Schmeling, H. (1995). Numerical modelling of melting processes and induced diapirism in the lower crust. *Geophysical Journal International*, *123*(1), 59–70. https://doi.org/10.1111/j.1365-246X.1995.tb06661.x

Bouysse, P. (2014). *Geological Map of the World at 1: 35 000 000 (3rd ed.)*. 3rd ed. Paris: CCGM.

Brune, S., Heine, C., Clift, P. D., & Pérez-Gussinyé, M. (2017). Rifted margin architecture and crustal rheology: Reviewing Iberia-Newfoundland, Central South Atlantic, and South China Sea. *Marine and Petroleum Geology*, *79*, 257–281. https://doi.org/10.1016/j.marpetgeo.2016.10.018

Byerlee, J. (1978). Friction of rocks. *Pure and Applied Geophysics*, *116*, 615–626. https://doi.org/10.1007/bf00876528

Chen, Z., Schellart, W. P., Stark, V., & Duarte, J. C. (2016). Does subduction-induced mantle flow drive backarc extension? *Earth and Planetary Science Letters*, *441*, 200–210. https://doi.org/10.1016/J.EPSL.2016.02.027

Christensen, N. I., & Mooney, W. D. (1995). Seismic velocity structure and composition of the continental crust: A global view. *Journal of Geophysical Research*, *100*(B6), 9761–9788. https://doi.org/10.1029/95JB00259

Cloos, M. (1993). Lithospheric buoyancy and collisional orogenesis: Subduction of oceanic plateaus , continental margins , island arcs, spreading ridges, and seamounts. *Geological Society of America Bulletin*, *105*, 715–737. https://doi.org/10.1130/0016-7606(1993)105<0715:lbacos>2.3.co;2

Corti, G. (2008). Control of rift obliquity on the evolution and segmentation of the main Ethiopian rift. *Nature Geoscience*, *1*(4), 258–262. https://doi.org/10.1038/ngeo160

Crameri, F. (2018a). Geodynamic diagnostics, scientific visualisation and StagLab 3.0. *Geoscientific Model Development*, *11*(6), 2541–2562. https://doi.org/10.5194/gmd-11-2541-2018

Crameri, F. (2018b). Scientific colour-maps. *Zenodo*. https://doi.org/10.5281/zenodo.1243862

Cullen, A., Reemst, P., Henstra, G., Gozzard, S., & Ray, A. (2010). Rifting of the South China Sea: New perspectives. *Petroleum Geoscience*, *16*(3), 273–282. https://doi.org/10.1144/1354-079309-908

De Voogd, B., Nicolich, R., Olivet, J. L., Fanucci, F., Burrus, J., Mauffret, A., et al. (1991). *First deep seismic reflection transect from the Gulf of Lions to Sardinia (Ecors-Crop profiles in Western Mediterranean)* (pp. 265–274). Deep Seismic Reflections: Continental Lithosphere. https://doi.org/10.1029/gd022p0265

Dewey, J. F., & Şengör, A. M. (1979). Aegean and surrounding regions: Complex multiplate and continuum tectonics in a convergent zone. *Geological Society of America Bulletin*, *90*(1), 84–92. https://doi.org/10.1130/0016-7606(1979)90<84:aasrcm>2.0.co;2

Di Giuseppe, E., Van Hunen, J., Funiciello, F., Faccenna, C., & Giardini, D. (2008). Slab stiffness control of trench motion: Insights from numerical models. *Geochemistry, Geophysics, Geosystems*, *9*(2), 1–19. https://doi.org/10.1029/2007GC001776

Drury, M. R. (2005). Dynamic recrystallization and strain softening of olivine aggregates in the laboratory and the lithosphere. *Geological Society Special Publication*, *243*(2), 143–158. https://doi.org/10.1144/GSL.SP.2005.243.01.11

El Harfi, A., Guiraud, M., & Lang, J. (2006). Deep-rooted "thick skinned" model for the High Atlas Mountains (Morocco). Implications for the structural inheritance of the southern Tethys passive margin. *Journal of Structural Geology*, *28*(11), 1958–1976. https://doi.org/10.1016/j.jsg.2006.08.011

Faccenna, C., Civetta, L., Antonio, M. D., Funiciello, F., Margheriti, L., & Piromallo, C. (2005). Constraints on mantle circulation around the deforming Calabrian slab. *Geophysical Research Letters*, *32*. https://doi.org/10.1029/2004GL021874

Faccenna, C., Funiciello, F., Civetta, L., Antonio, D., Moroni, M., & Piromallo, C. (2007). Slab disruption, mantle circulation, and the opening of the Tyrrhenian basins. *Special Papers-Geological Society of America*, *418*, 153. https://doi.org/10.1130/2007.2418(08)

accenna, C., Funiciello, F., Giardini, D., & Lucente, P. (2001). Episodic back-arc extension during restricted mantle convection in the central Mediterranean. *Earth and Planetary Science Letters*, *187*(1–2), 105–116. https://doi.org/10.1016/S0012-821X(01)00280-1

Faccenna, C., Mattei, M., Funiciello, R., & Jolivet, L. (1997). Styles of back-arc extension in the central Mediterranean. *Terra Nova*, *9*(3), 126–130. https://doi.org/10.1046/j.1365-3121.1997.d01-12.x

Funiciello, F., Faccenna, C., Giardini, D., & Regenauer-Lieb, K. (2003). Dynamics of retreating slabs: 2. Insights from three-dimensional laboratory experiments. *Journal of Geophysical Research*, *108*(B4), 1–16. https://doi.org/10.1029/2001JB000896

Gaina, C., Gernigon, L., & Ball, P. (2009). Palaeocene-Recent plate boundaries in the NE Atlantic and the formation of the Jan Mayen microcontinent. *Journal of the Geological Society*, *166*(4), 601–616. https://doi.org/10.1144/0016-76492008-112

Gaina, C., Müller, R. D., Brown, B., & Ishihara, T. (2003). Microcontinent formation around Australia. *Geological Society of Australia Special Publication 22*, *372*(2001), 399–410. https://doi.org/10.1130/0-8137-2372-8.405

Gaina, C., Müller, R. D., Royer, J., & Symonds, P. (1999). Evolution of the Louisiade triple junction. *Journal of Geophysical Research*, *104*(B6), 12927. https://doi.org/10.1029/1999JB900038

Gaina, C., Torsvik, T. H., van Hinsbergen, D. J. J., Medvedev, S., Werner, S. C., & Labails, C. (2013). The African plate: A history of oceanic crust accretion and subduction since the Jurassic. *Tectonophysics*, *604*, 4–25. https://doi.org/10.1016/j.tecto.2013.05.037

Ganerød, M., Torsvik, T. H., van Hinsbergen, D. J. J., Gaina, C., Corfu, F., Werner, S., et al. (2011). Palaeoposition of the Seychelles microcontinent in relation to the Deccan Traps and the Plume Generation Zone in Late Cretaceous-Early Palaeogene time. *Geological Society, London, Special Publications*, *357*(1), 229–252. https://doi.org/10.1144/SP357.12

Garel, F., Goes, S., Davies, D. R., Davies, J. H., Kramer, S. C., & Wilson, C. R. (2014). Interaction of subducted slabs with the mantle transition-zone: A regime diagram from 2-D thermo-mechanical models with a mobile trench and an overriding plate. *Geochemistry, Geophysics, Geosystems*, *15*(5), 1739–1765. https://doi.org/10.1002/2014gc005257

Gattacceca, J., Deino, A., Rizzo, R., Jones, D. S., Henry, B., Beaudoin, B., & Vadeboin, F. (2007). Miocene rotation of Sardinia: New paleomagnetic and geochronological constraints and geodynamic implications. *Earth and Planetary Science Letters*, *258*(3–4), 359–377. https://doi.org/10.1016/j.epsl.2007.02.003

Govers, R., & Wortel, M. J. R. (2005). Lithosphere tearing at STEP faults: Response to edges of subduction zones. *Earth and Planetary Science Letters*, *236*(1), 505–523. https://doi.org/https://doi.org/10.1016/j.epsl.2005.03.022

Heron, P. J., Peace, A. L., McCaffrey, K. J. W., Welford, J. K., Wilson, R., van Hunen, J., & Pysklywec, R. N. (2019). Segmentation of rifts through structural inheritance: Creation of the Davis Strait. *Tectonics*, *38*(7), 2411–2430. https://doi.org/10.1029/2019TC005578

Heron, P. J., Pysklywec, R. N., & Stephenson, R. (2016). Lasting mantle scars lead to perennial plate tectonics. *Nature Communications*, *7*(May), 11834. https://doi.org/10.1038/ncomms11834

Hirth, G., & Kohlstedt, D. L. (2004). Rheology of the upper mantle and the mantle wedge: A view from the experimentalists. *Inside the Subduction Factory*, *138*, 83–106. https://doi.org/doi:10.1029/138GM06

Karato, S., & Wu, P. (1993). Rheology of the upper mantle: A synthesis. *Science*, *260*(5109), 771–778. https://doi.org/10.1126/science.260.5109.771

Koptev, A., Beniest, A., Gerya, T., Ehlers, T. A., Jolivet, L., & Leroy, S. (2019). Plume-induced breakup of a subducting plate: Microcontinent formation without cessation of the subduction process. *Geophysical Research Letters*. https://doi.org/10.1029/2018GL081295

Korenaga, J., & Karato, S.-I. (2008). A new analysis of experimental data on olivine rheology. *Journal of Geophysical Research*, *113*(B2). https://doi.org/10.1029/2007JB005100

Lacombe, O., & Jolivet, L. (2005). Structural and kinematic relationships between Corsica and the Pyrenees-Provence domain at the time of the Pyrenean orogeny. *Tectonics*, *24*(1), 1–20. https://doi.org/10.1029/2004TC001673

Magni, V., Allen, M. B., van Hunen, J., & Bouilhol, P. (2017). Continental underplating after slab break-off. *Earth and Planetary Science Letters*, *474*, 59–67. https://doi.org/10.1016/j.epsl.2017.06.017

Magni, V., Van Hunen, J., Funiciello, F., & Faccenna, C. (2012). Numerical models of slab migration in continental collision zones. *Solid Earth*, *3*(2), 293–306. https://doi.org/10.5194/se-3-293-2012

Magni, V., Faccenna, C., van Hunen, J., & Funiciello, F. (2014). How collision triggers backarc extension: Insight into mediterranean style of extension from 3-D numerical models. *Geology*, *42*(6), 511–514. https://doi.org/10.1130/G35446.1

Manohar, P. A., Ferry, M., & Chandra, T. (1998). Five decades of the Zener equation. *ISIJ International*, *38*(9), 913–924. https://doi.org/10.2355/isijinternational.38.913

Mazzotti, S., & Gueydan, F. (2018). Control of tectonic inheritance on continental intraplate strain rate and seismicity. *Tectonophysics*, *746*, 602–610. https://doi.org/https://doi.org/10.1016/j.tecto.2017.12.014

Molnar, N. E., Cruden, A. R., & Betts, P. G. (2018). Unzipping continents and the birth of microcontinents. *Geology*, 1–4. https://doi.org/10.1130/g40021.1

Moresi, L., & Gumis, M. (1996). Constraints on the lateral strength of slabs from three-dimensional dynamic flow models. *Earth and Planetary Science Letters*, *38*(95), 15–28. https://doi.org/10.1016/0012-821x(95)00221-w

Morgan, J. V., Hadwin, M., Warner, M. R., Barton, P. J., & Morgan, R. P. L. (1994). The polarity of deep seismic reflections from the lithospheric mantle: Evidence for a relict subduction zone. *Tectonophysics*, *232*(1), 319–328. https://doi.org/10.1016/0040-1951(94)90093-0

Müller, R. D., Gaina, C., Roest, W. R., & Hansen, D. L. (2001). A recipe for microcontinent formation. *Geology*, *29*(3), 203–206. https://doi.org/10.1130/0091-7613

Nemcok, M., Sinha, S. T., Dore, A. G., Lundin, E. R., Mascle, J., & Rybar, S. (2016). Mechanisms of microcontinent release associated with wrenching-involved continental break-up: A review. *Geological Society, London, Special Publications*, *431*, 323–359. https://doi.org/10.1144/SP431.14

Peron-Pinvidic, G., & Manatschal, G. (2010). From microcontinents to extensional allochthons: Witnesses of how continents rift and break apart? *Petroleum Geoscience*, *16*(3), 189–197. https://doi.org/10.1144/1354-079309-903

Peron-Pinvidic, G., Gernigon, L., Gaina, C., & Ball, P. (2012a). Insights from the Jan Mayen system in the Norwegian-Greenland Sea: I—Mapping of a microcontinent. *Geophysical Journal International*, *191*(2), 413–435. https://doi.org/10.1111/j.1365-246X.2012.05623.x

Peron-Pinvidic, G., Gernigon, L., Gaina, C., & Ball, P. (2012b). Insights from the Jan Mayen system in the Norwegian-Greenland Sea: II—Architecture of a microcontinent. *Geophysical Journal International*, *191*(2), 413–435. https://doi.org/10.1111/j.1365-246X.2012.05623.x

Pichot, T., Delescluse, M., Chamot-Rooke, N., Pubellier, M., Qiu, Y., Meresse, F., et al. (2014). Deep crustal structure of the conjugate margins of the SW South China Sea from wide-angle refraction seismic data. *Marine and Petroleum Geology*, *58*(PB), 627–643. https://doi.org/10.1016/j.marpetgeo.2013.10.008

Quinquis, M. E. T., Buiter, S. J. H., & Ellis, S. (2011). The role of boundary conditions in numerical models of subduction zone dynamics. *Tectonophysics*, *497*(1–4), 57–70. https://doi.org/10.1016/j.tecto.2010.11.001

Rollet, N., Déverchère, J., Beslier, M. O., Guennoc, P., Réhault, J. P., Sosson, M., & Truffert, C. (2002). Back arc extension, tectonic inheritance, and volcanism in the Ligurian Sea, Western Mediterranean. *Tectonics*, *21*(3). https://doi.org/10.1029/2001TC900027

Rosenbaum, G., Lister, G. S., & Duboz, C. (2002). Reconstruction of the tectonic evolution of the western Mediterranean since the Oligocene. *Journal of the Virtual Explorer*, *8*(January). https://doi.org/10.3809/jvirtex.2002.00053

Schellart, W. P., Freeman, J., Stegman, D. R., Moresi, L., & May, D. (2007). Evolution and diversity of subduction zones controlled by slab width. *Nature*, *446*(7133), 308–311. https://doi.org/10.1038/nature05615

Schiffer, C., Stephenson, R. A., Petersen, K. D., Nielsen, S. B., Jacobsen, B. H., Balling, N., & Macdonald, D. I. M. (2015). A sub-crustal piercing point for North Atlantic reconstructions and tectonic implications. *Geology*, *43*(12), 1087–1090. https://doi.org/10.1130/g37245.1

Scrutton, R. A. (1976). Microcontinents and their significance. *Geodynamics: Progress and Prospects*, *5*, 177–189. https://doi.org/10.1029/sp005p0177

Seranne, M. (1999). The Gulf of Lion continental margin (NW Mediterranean) revisited by IBS: An overview. *Geological Society, London, Special Publications*, *156*(1), 15–36. https://doi.org/10.1144/gsl.sp.1999.156.01.03

Taylor, L., & Falvey, D. (1977). Queensland Plateau and Coral Sea Basin: Stratigraphy, structure and tectonics. *The APPEA Journal*, *17*(1), 13. https://doi.org/10.1071/aj76002

Tetreault, J. L., & Buiter, S. J. H. (2014). Future accreted terranes: A compilation of island arcs, oceanic plateaus, submarine ridges, seamounts, and continental fragments. *Solid Earth*, *5*(2), 1243–1275. https://doi.org/10.5194/se-5-1243-2014

Torsvik, T. H., Amundsen, H., Hartz, E. H., Corfu, F., Kusznir, N., Gaina, C., et al. (2013). A Precambrian microcontinent in the Indian Ocean. *Nature Geoscience*, *6*(3), 223–227. https://doi.org/10.1038/ngeo1736

Turco, E., Macchiavelli, C., Mazzoli, S., Schettino, A., & Pierantoni, P. P. (2012). Kinematic evolution of Alpine Corsica in the framework of Mediterranean mountain belts. *Tectonophysics*, *579*, 193–206. https://doi.org/10.1016/j.tecto.2012.05.010

Turcotte, D., & Schubert, G. (2002). *Geodynamics*. *Geodynamics* (Second ed.). New York: John Wiley and Sons. Retrieved from citeulike-article-id:236644

van Hinsbergen, D. J. J., Vissers, R. L. M., & Spakman, W. (2014). Origin and consequences of western Mediterranean subduction, rollback, and slab segmentation. *Tectonics*, *33*(4), 393–419. https://doi.org/10.1002/2013TC003349

van Hunen, J., & Allen, M. B. (2011). Continental collision and slab break-off: A comparison of 3-D numerical models with observations. *Earth and Planetary Science Letters*, *302*(1), 27–37. https://doi.org/https://doi.org/10.1016/j.epsl.2010.11.035

Vissers, R. L. M., van Hinsbergen, D. J. J., Meijer, P. T., & Piccardo, G. B. (2013). Kinematics of Jurassic ultra-slow spreading in the Piemonte Ligurian ocean. *Earth and Planetary Science Letters*, *380*, 138–150. https://doi.org/10.1016/j.epsl.2013.08.033

von Raumer, J. F., Stampfli, G. M., & Bussy, F. (2003). Gondwana-derived microcontinents: The constituents of the Variscan and Alpine collisional orogens. *Tectonophysics*, *365*(1–4), 7–22. https://doi.org/10.1016/S0040-1951(03)00015-5

Wallace, L. M., Ellis, S., & Mann, P. (2009). Collisional model for rapid fore-arc block rotations, arc curvature, and episodic back-arc rifting in subduction settings. *Geochemistry, Geophysics, Geosystems*, *10*(5). https://doi.org/10.1029/2008GC002220

Wallace, L. M., McCaffrey, R., Beavan, J., & Ellis, S. (2005). Rapid microplate rotations and backarc rifting at the transition between collision and subduction. *Geology*, *33*(11), 857–860. https://doi.org/10.1130/G21834.1

Wang, H., Agrusta, R., & Hunen, J. (2015). Advantages of a conservative velocity interpolation (CVI) scheme for particle-in-cell methods with application in geodynamic modeling. *Geochemistry, Geophysics, Geosystems*, *16*(6). https://doi.org/10.1002/2015gc005824

Wessel, P., Smith, W. H. F. F., Scharroo, R., Luis, J., & Wobbe, F. (2013). Generic Mapping Tools: Improved version released. *Eos, Transactions American Geophysical Union*, *94*(45), 409–410. https://doi.org/10.1002/2013EO450001

Wolf, S. G., & Huismans, R. S. (2019). Mountain building or backarc extension in ocean-continent subduction systems-a function of backarc lithospheric strength and absolute plate velocities. *Journal of Geophysical Research: Solid Earth*, *124*, 7461–7482. https://doi.org/10.1029/2018jb017171

Zhong, S., Zuber, M. T., & Moresi, L. (2000). Role of temperature-dependent viscosity and surface plates in spherical shell models of mantle convection. *Journal of Geophysical Research*, *105*, 11,063–11,082. https://doi.org/10.1029/2000jb900003

Ziegler, P. A., Cloetingh, S., Guiraud, R., & Stampfli, G. M. (2001). Peri-Tethyan platforms: Constraints on dynamics of rifting and basin inversion. *Mémoire Du Museum National d'Histoire Naturelle*, *186*, 9–49.

A

# Supplementary to Manuscript 1

*Tectonics*

Supporting Information for

# Microcontinents and continental fragments associated with subduction systems

J.M. van den Broek[1*] and C. Gaina[1]

The Centre for Earth Evolution and Dynamics (CEED), Department of Geosciences, University of Oslo, Oslo, Norway

## Contents of this file



## Introduction

This supplementary information contains seven additional figures and a table summarizing our observations on the various microcontinents and continental fragments described in the companion paper. We present a figure comparing the extracted geophysical profiles for each region.

Furthermore, we also present additional tectonic reconstruction for the time at which lateral translation of the microcontinent ceases and extension is relocated away from the initial divergence center. In other words, the time at which the microcontinent 'forms'. Details on the reconstructions are presented in the main paper, section 2.

In addition to the UU-P07 seismic tomographic model, we also provide the exact same sections extracted from the tomographic MITP08 [*Li et al.*, 2008], DETOX-P3 [*Hosseini et al.*, 2019] and TX2019slab [*Lu et al.*, 2019] models. All sections where plotted using the SubMachine web application [*Hosseini et al.*, 2018].

We provide a figure showing the extent and thickness of the continental crust used to calculate the total area and volume of non-cratonic continental crust on Earth. We use the global continental COB from *Straume et al.* [2019] which is based on *Torsvik and Cocks* [2016]. For the cratonic outlines we use polygons from *Bouysse* [2014]. The same figure also shows the distribution of microcontinents associated with (classic) passive margin formation. The microcontinents used are from *Gaina and Whittaker* [2020]. For crustal thickness we used the CRUST1.0 global crustal thickness model from *Laske et al.*, [2012].

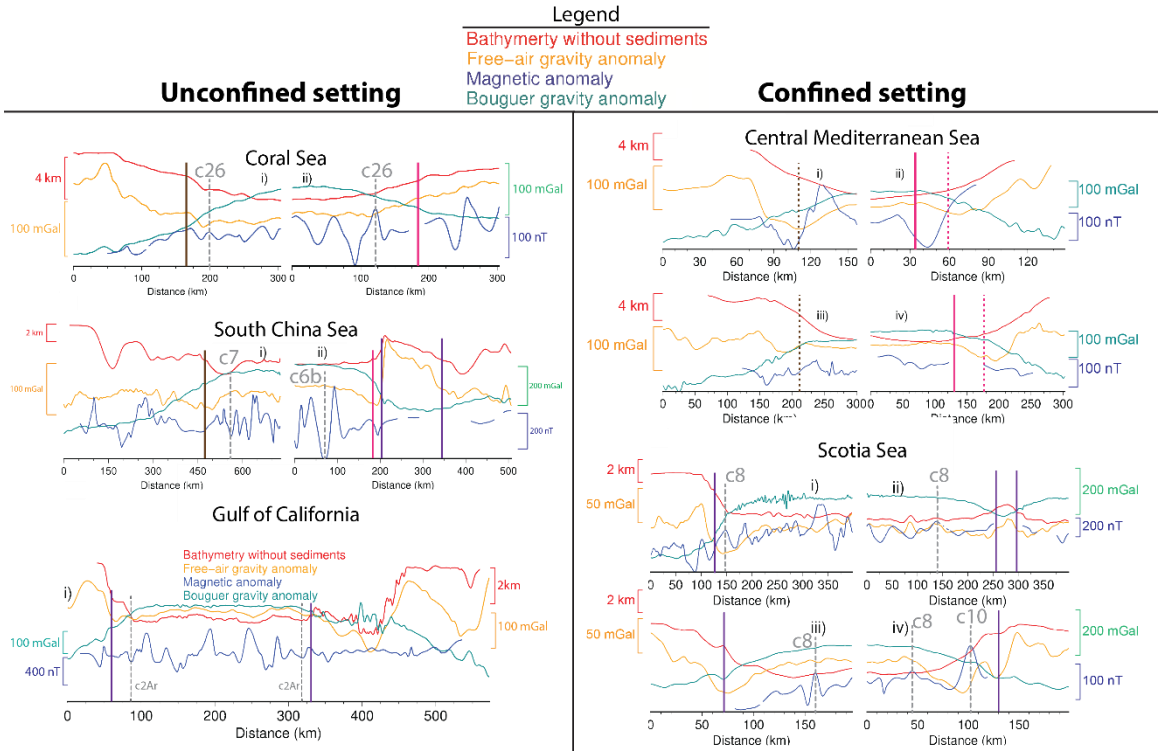


**Figure S1.**

Comparison of the geophysical architecture of all investigated margins. We grouped them into confined and unconfined settings. For details regarding this grouping, the reader is referred to the main article.

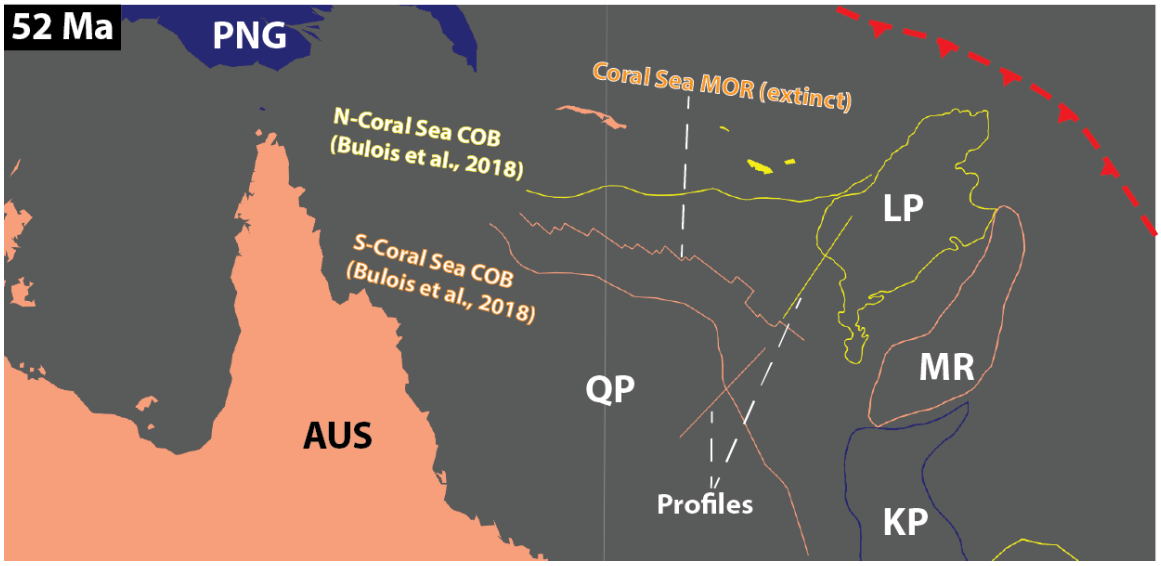


**Figure S2.**

Tectonic reconstruction of the Coral Sea Region at 52 Ma. Spreading in the Coral Sea ceased at this time, with subduction relocating northeast, isolating the Louisiade plateau. Reconstruction is relative to a fixed Australian plate. The separate tectonic blocks are shown as outlines or filled polygons of different colors.

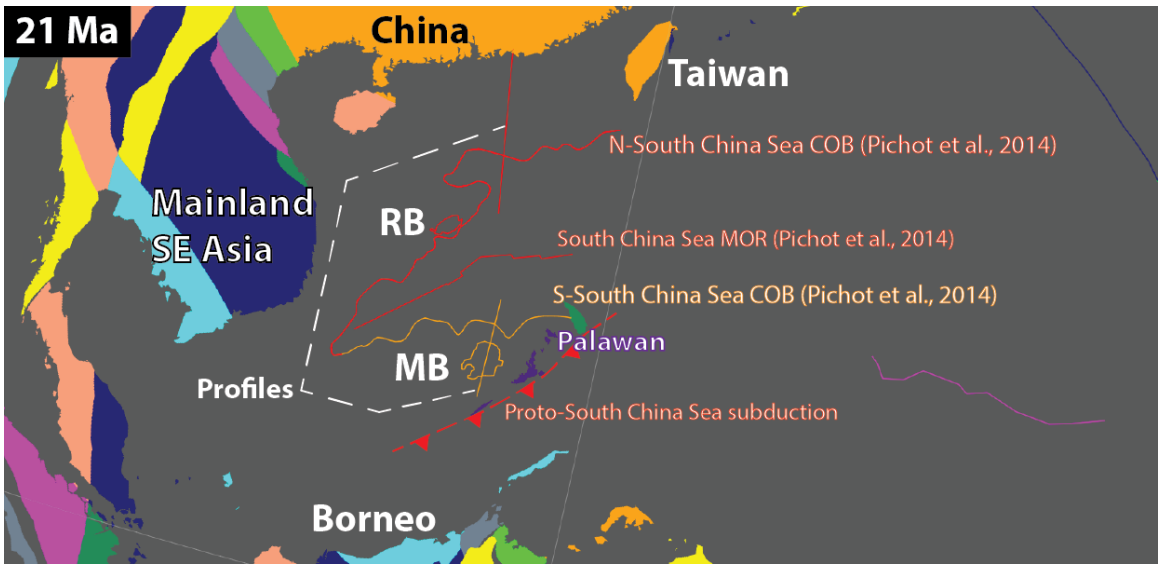


**Figure S3.**

Tectonic reconstruction of the South China Sea Region at 21 Ma. Collision of Palawan and Mindoro with the trench of the Proto-South China Sea resulted in a cessation of spreading in the South China Sea, isolating the Macclesfield bank. China is fixed in its present day position (fixed plate). The separate tectonic blocks are shown as outlines or filled polygons of different colors.

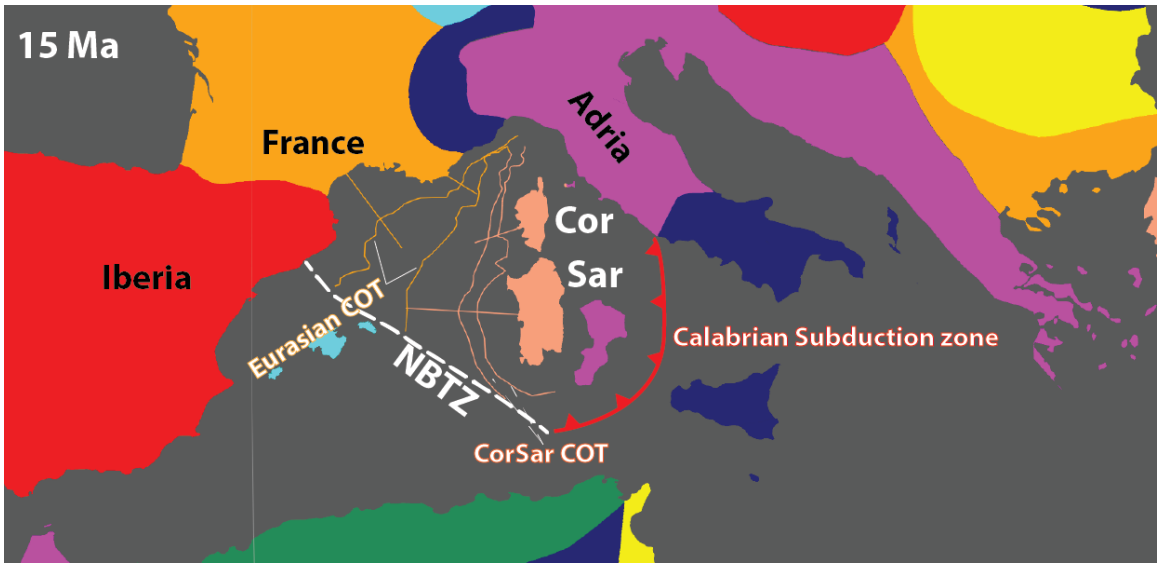


**Figure S4.**

Tectonic reconstruction of the central Mediterranean at 15 Ma. At this time extension ceased in the Liguro-Provençal basin and relocated east to form the Tyrrhenian basin as the Calabrian slab retreated south-eastwards. Reconstruction is relative to a fixed Eurasian plate. The separate tectonic blocks are shown as outlines or filled polygons of different colors.

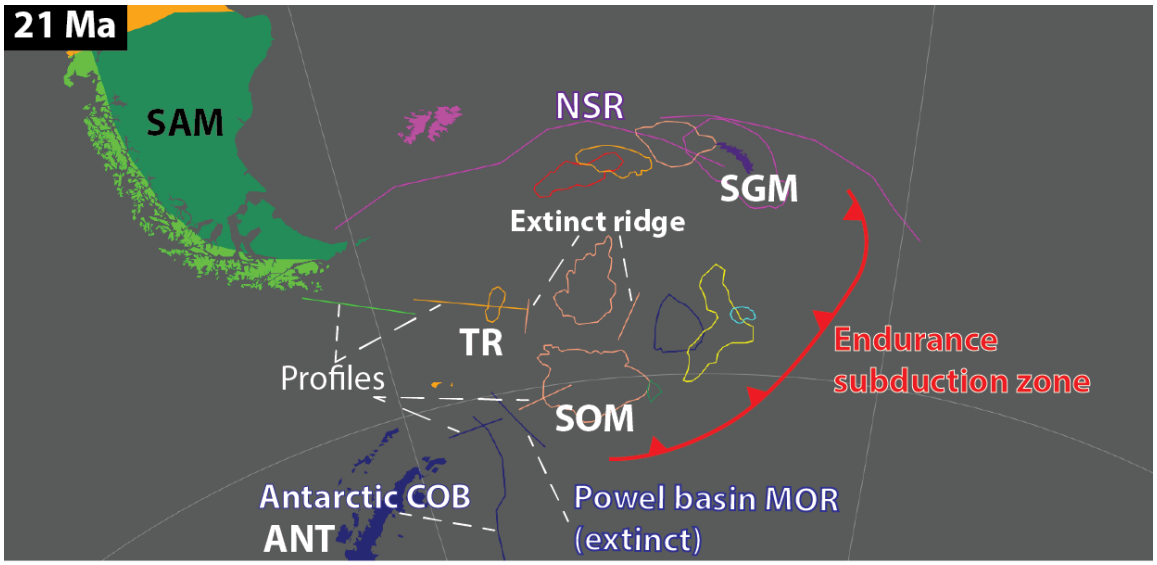


**Figure S5.**

Tectonic reconstruction of the Scotia Sea Region at 21 Ma. Spreading in the Powell Basin, between the South Orkney Microcontinent and Antarctica ceased at this time. This isolated the South Orkney Microcontinent. Spreading between the Terror rise and South America already initiated before this time, forming the Terror Rise Microcontinent. Regional movement are relative to a fixed Antarctic plate. The separate tectonic blocks are shown as outlines or filled polygons of different colors.

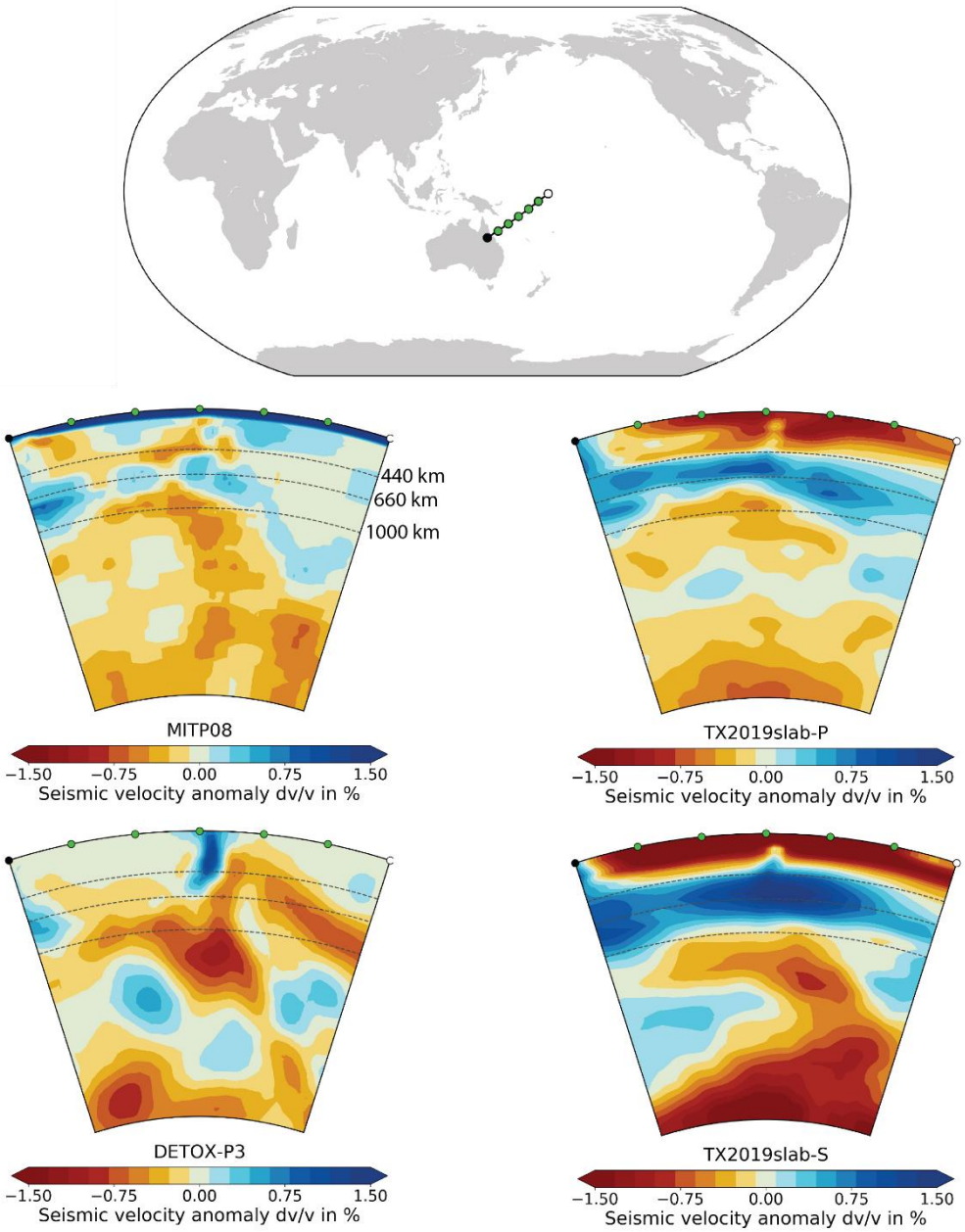


**Figure S6.**
Additional seismic tomographic models for the Coral Sea region.

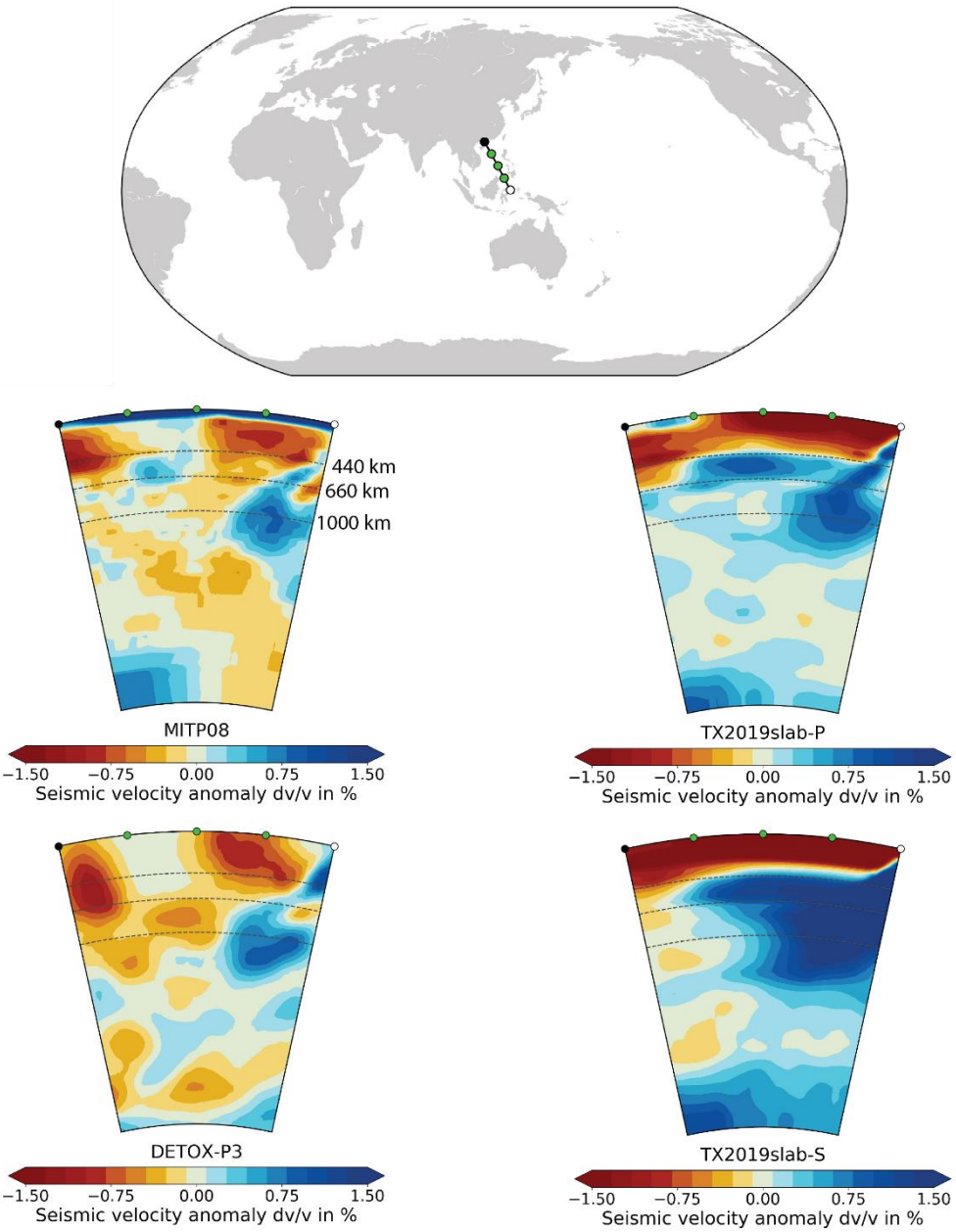


**Figure S7.**

Additional seismic tomographic models for the South China Sea region.

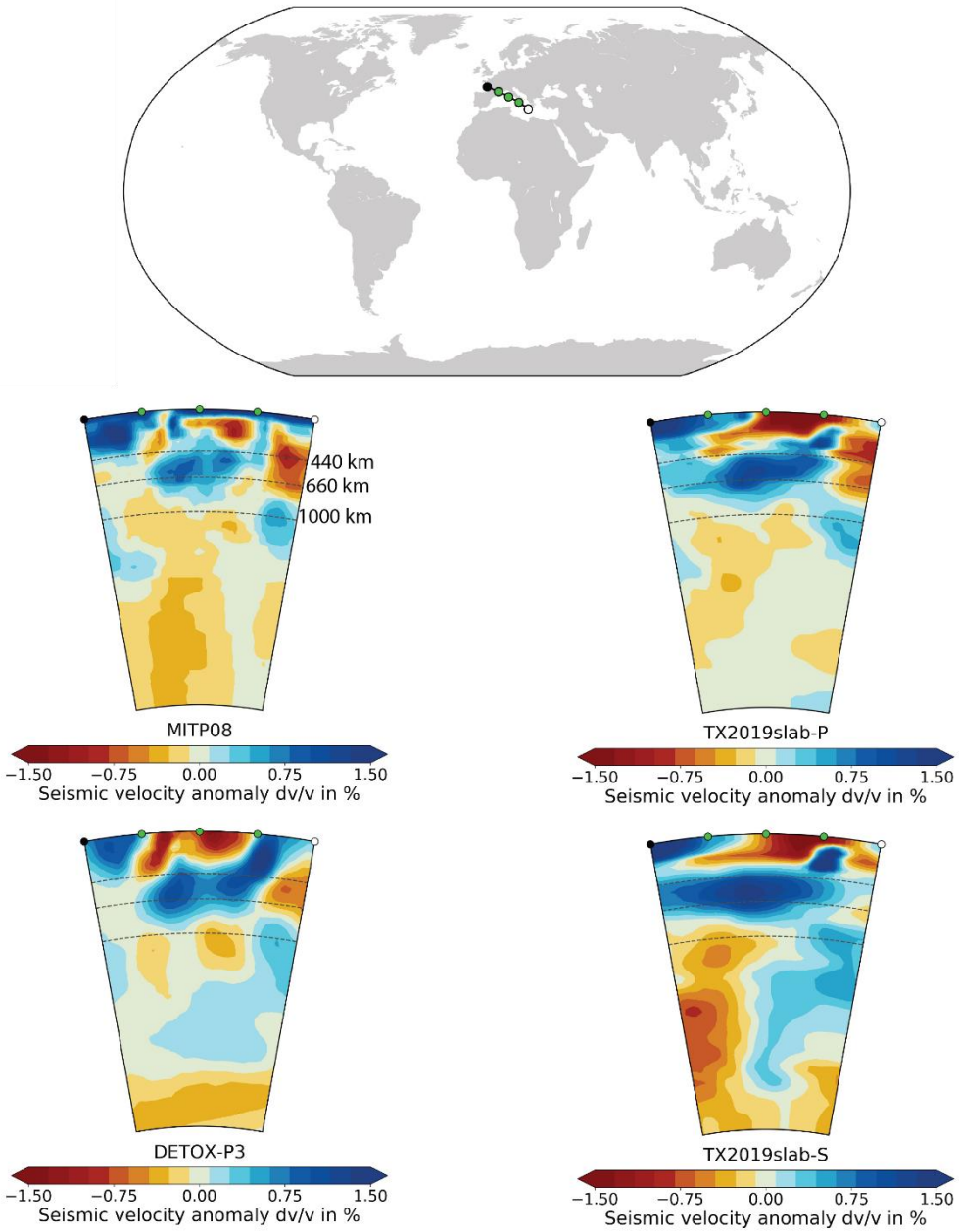


**Figure S8.**
Additional seismic tomographic models for the Central Mediterranean region.

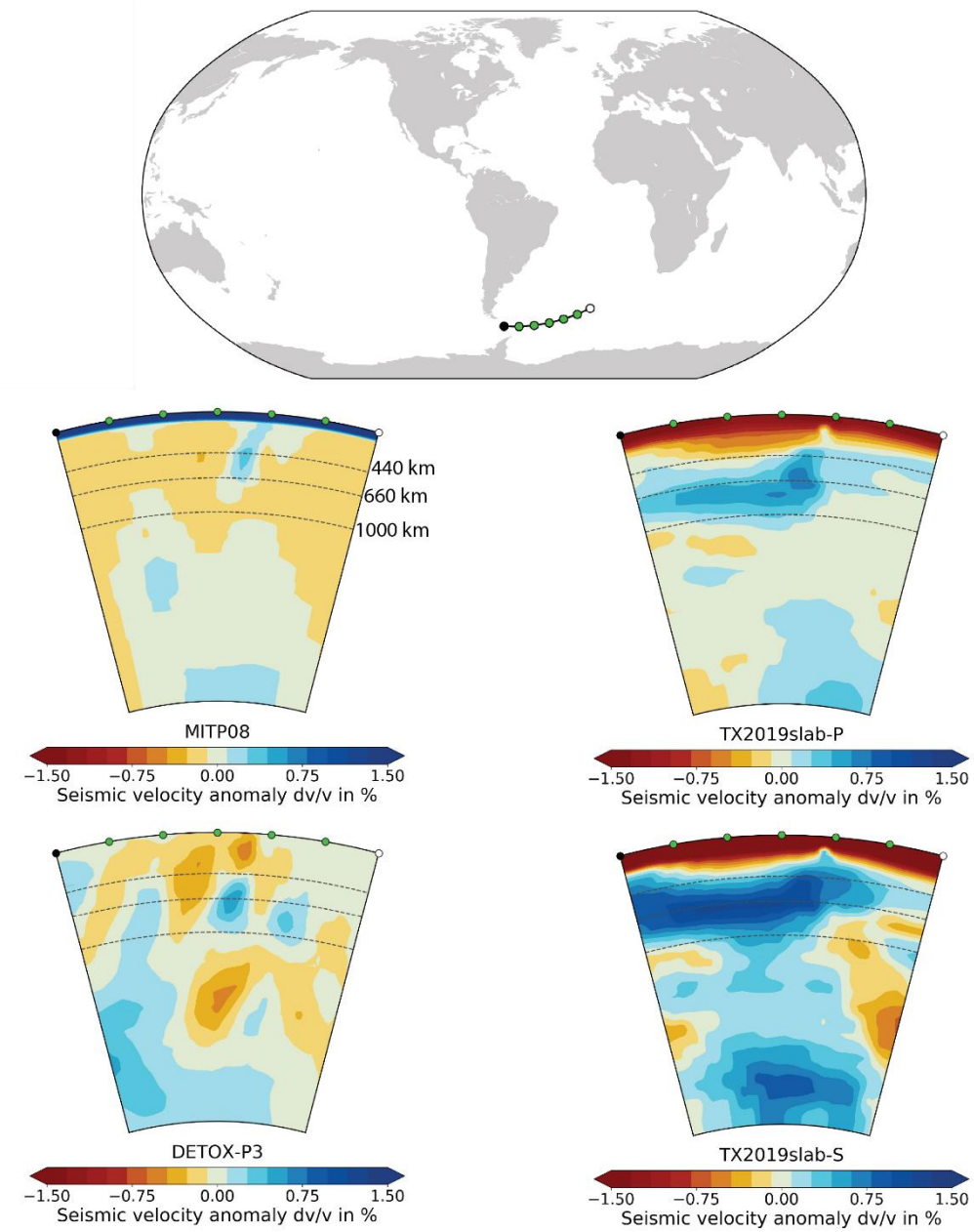


**Figure S9**

Additional seismic tomographic models for the Scotia Sea region.

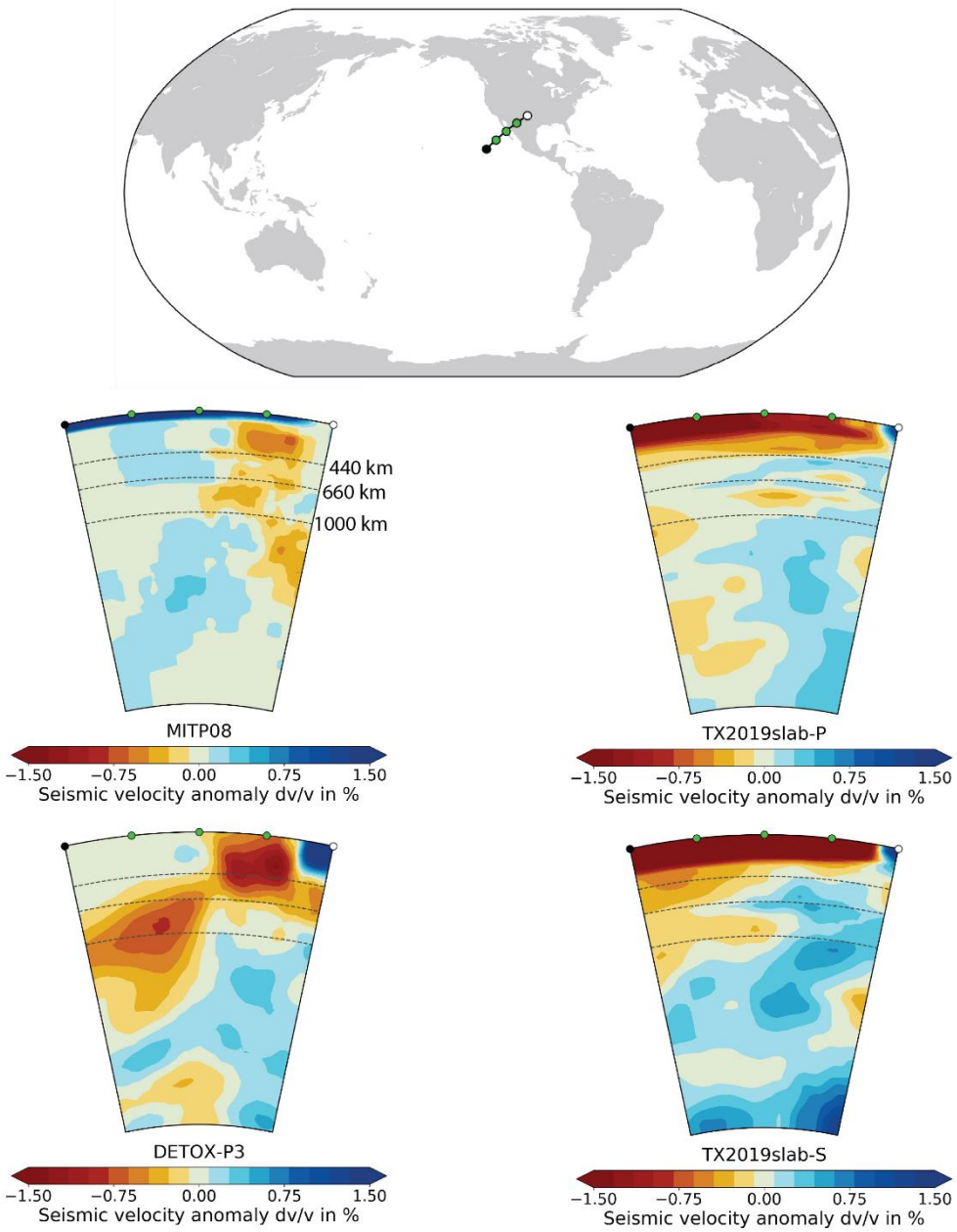


**Figure S10.**

Additional seismic tomographic models for the Gulf of California region.

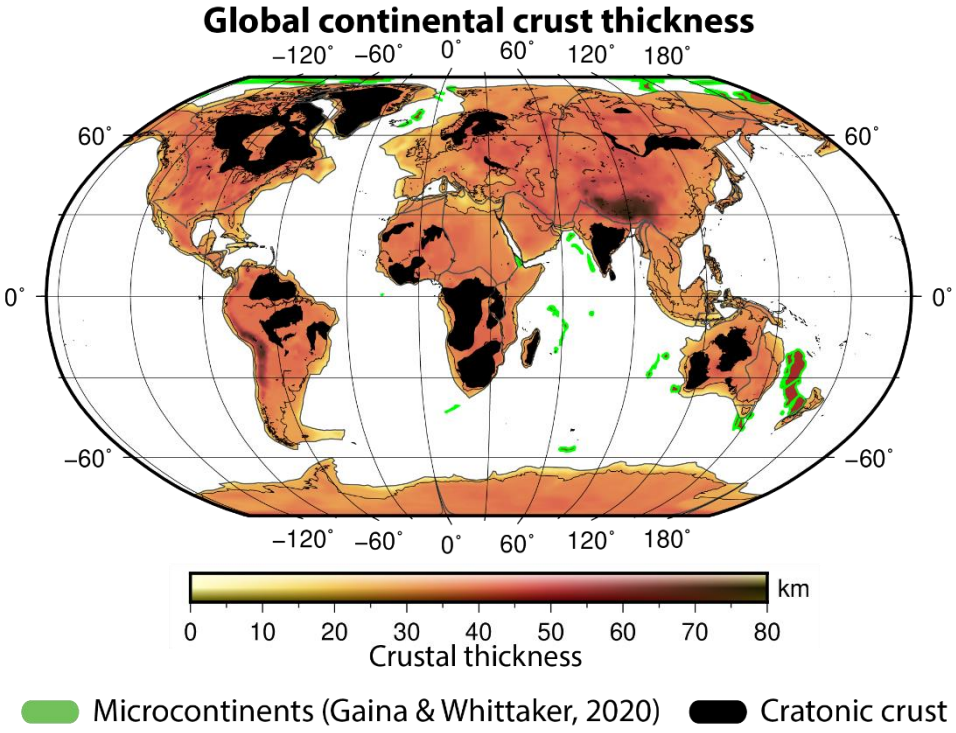


**Figure S11.**

Map showing the extent and thickness of the continental crust used for the calculation of global continental crustal area and volume. Black areas delineate cratonic continental crust which was neglected in the calculations. Green lines delineate microcontinents associated with passive margin formation, polygons from [*Gaina and Whittaker*, 2020].

**Caption to Table T1.**

Table displaying various quantitative and qualitative observations of all subduction associated microcontinents in this paper. MC-CF: Microcontinent/ Continental fragment

**References**


Bouysse. (2014). *Geological Map of the World at 1: 35 000 000* (3rd ed.). 3rd ed. Paris: CCGM.

Gaina, and Whittaker. (2020). Microcontinents. In Gupta (Ed.), *Encyclopaedia of Solid Earth Geophysics*. Springer International Publishing.

Hosseini, Matthews, Sigloch, Shephard, Domeier, and Tsekhmistrenko. (2018). SubMachine: Web-Based Tools for Exploring Seismic Tomography and Other Models of Earth's Deep Interior. *Geochemistry, Geophysics, Geosystems*, *19*(5), 1464–1483. https://doi.org/10.1029/2018GC007431

Hosseini, Sigloch, Tsekhmistrenko, Zaheri, Nissen-Meyer, and Igel. (2019). Global mantle structure from multifrequency tomography using P, PP and P-diffracted waves. *Geophysical Journal International*, *220*(1), 96–141. https://doi.org/10.1093/gji/ggz394

Laske, Masters, Ma, and Pasyanos. (2012). *CRUST1. 0: An updated global model of the Earth's crust, EGU General Assembly, 14*.

Li, van der Hilst, Engdahl, and Burdick. (2008). A new global model for P wave speed variations in Earth's mantle. *Geochemistry, Geophysics, Geosystems*, *9*(5). https://doi.org/10.1029/2007GC001806

Lu, Grand, Lai, and Garnero. (2019). TX2019slab: A New P and S Tomography Model Incorporating Subducting Slabs. *Journal of Geophysical Research: Solid Earth*, 1–19. https://doi.org/10.1029/2019JB017448

Straume, Gaina, Medvedev, Hochmuth, Gohl, Whittaker, … Hopper. (2019). GlobSed: Updated total sediment thickness in the world's oceans. *Geochemistry, Geophysics, Geosystems*, *20*(4), 1756–1772. https://doi.org/10.1029/2018GC008115

Torsvik, and Cocks. (2016). Tectonic units of the Earth. In *Earth history and palaeogeography* (pp. 38–76). Cambridge, UK: Cambridge University Press.

B

# Supplementary to Manuscript 3

*Journal of Geophysical Research: Solid Earth*

Supporting Information for

# The formation of continental fragments in subduction settings: the importance of structural inheritance and subduction system dynamics

J.M. van den Broek[1], V. Magni[1], C. Gaina[1], S. J. H. Buiter[1,2]

[1] The Centre for Earth Evolution and Dynamics (CEED), Department of Geosciences, University of Oslo, Oslo, Norway. [2] Team for Solid Earth Geology, Geological Survey of Norway, Trondheim, Norway

## Contents of this file



## Additional Supporting Information (Files uploaded separately)

1. Animations of all experiments

## 1. Introduction

This supplementary information contains the captions to the animations of all experiments described in the paper as well as an explanation of the viewing angles of the animations. It also contains a summary figure of a 3D oceanic subduction experiment with an imposed weak zone in the overriding plate (Fig. S1). The animations are uploaded to a data repository and the doi to this repository is in the acknowledgements of the manuscript.

Post-processing was done using MatLab and the animations (.avi files) are created using a bash shell script (2D experiment) and Paraview visualization software (3D experiments).

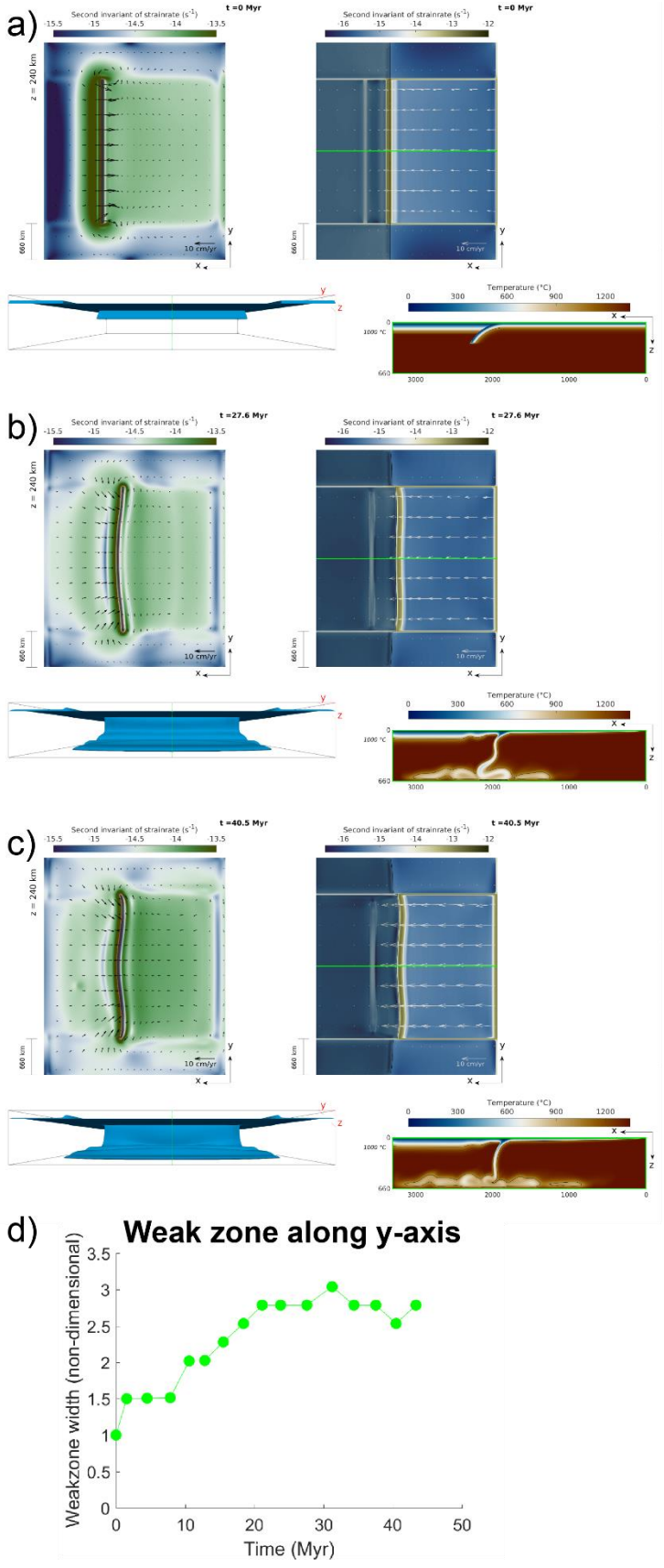


**Figure S1 (next page):** Overview figure of a 3D oceanic subduction experiment with an imposed weak zone in the overriding plate. Left top views show a horizontal mantle slice at 240 km, right top views depict $\log_{10}$(strain rate), bottom right: cross sections taken along the green line depict the temperature field. Bottom left shows the 1000 °C isocontour of the subuducting slab. We show three different model times a) 0 Myr, b) 27.6 Myr and c) 40 Myr. d) Bottom graph shows evolution of non-dimensionalized width of the weak zone with model time. Note that although some limited activation of the imposed weak zone occurs, no real back-arc basin formation takes placeforms and the width of the imposed weak zone width increases to max. 3 times its original width.

## 2. Animation explanation

The animation of the 2D reference experiment contains two panels, the top panel displays the evolution of the temperature field through time and the lower panel shows the evolution of the viscosity field through time. For all 3D experiments, we show 4 perspectives: a horizontal slice of the mantle at 240 km depth (top left in Fig. S1), a top view of a horizontal section at 8 km depth with a shaded contour for continental crust (top right in Fig. S1), a vertical cross section displaying the temperature field along the green line indicated in the horizontal section (bottom right in Fig. S1), and a frontal view displaying the 1000 °C isocontour of the slab (bottom left of Fig. S1).

All experiments where the $R_{c/oc}$ ratio (animations MS04-07) or the weak zone angle α (animations MS09-12) is varied, contain a single imposed weak zone in the overriding plate with w = 66 km and $\eta_w$=0.5e22 Pa*s.

All experiments where the $R_{c/oc}$ ratio of continental to oceanic material on the downgoing plate (animations MS04-07) or the weak zone angle α (animations MS09-12) is varied, contain a single imposed weak zone in the overriding plate with w = 66 km and $\eta_w$=0.5e22 Pa*s.

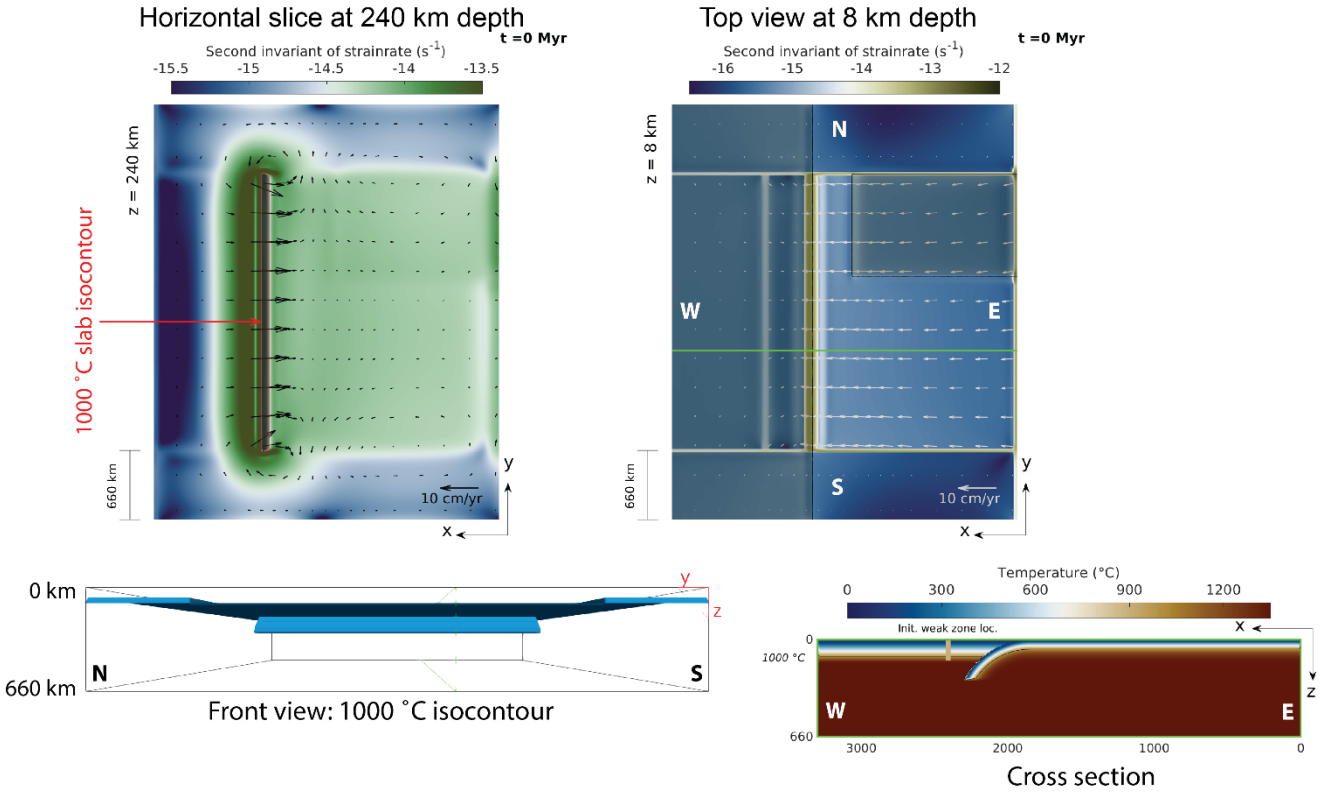


**Figure S2:** Details of the different viewing angles used in the supplementary animations.
The top left panel shows a horizontal mantle slice at 240 km. The top right panel shows a top view of the experiment displaying the $\log_{10}$(second invariant of the strain rate). Continental crust is contoured and shaded. Bottom right is a cross section (E-W) along the green line (top right panel) displaying the temperature. Bottom left panel displays a front view (from the W) of a 1000 °C isocontour of the slab.

## 3. Captions of animations in data repository (see acknowledgements for DOI):

**Animation MS01:**

2D reference experiment of oceanic subduction with no imposed weak zone in the overriding plate.

**Animation MS02**:

3D reference experiment of oceanic subduction with no imposed weak zone in the overriding plate.

**Animation MS03:**

3D oceanic subduction experiment with an imposed weak zone in the overriding plate.
$\alpha$ = 0°; w = 66 km; $\eta_w$=0.5e22 Pa*s.

**Animation MS04:**

3D reference experiment of subduction with a continental block on the downgoing plate. $R_{c/oc}$= 0°; w = 66 km; $\eta_w$ = .6; $\alpha$=0°.

**Animation MS05:**

3D experiment with a continental block on the downgoing plate.
$R_{c/oc}$ = 0.6; $\alpha$ = 0°; w = 66 km; $\eta_w$ = 0.5e22 Pa*s.

**Animation MS06:**

3D experiment with a continental block on the downgoing plate.
$R_{c/oc}$ = 0.78; $\alpha$ = 0°; w = 66 km; $\eta_w$ = 0.5e22 Pa*s.

**Animation MS07:**

3D experiment with a continental block on the downgoing plate.
$R_{c/oc}$ = 0.60; $\alpha$ = 0°; w = 66 km; $\eta_w$ = 0.5e22 Pa*s.

**Animation MS08:**

3D experiment with a continental block on the downgoing plate.
$R_{c/oc}$ = 0.45; $\alpha$ = 0°; w = 66 km; $\eta_w$ = 0.5e22 Pa*s.

**Animation MS09:**

3D experiment with a continental block on the downgoing plate.
$R_{c/oc}$ = 0.60; $\alpha$ = +15°; w = 66 km; $\eta_w$ = 0.5e22 Pa*s.

**Animation MS10:**

3D experiment with a continental block on the downgoing plate.
$R_{c/oc}$ = 0.60; $\alpha$ = -15°; w = 66 km; $\eta_w$ = 0.5e22 Pa*s.

**Animation MS11:**

3D experiment with a continental block on the downgoing plate.
$R_{c/oc}$ = 1.0; $\alpha$ = +15°; w = 66 km; $\eta_w$ = 0.5e22 Pa*s.

**Animation MS12:**

3D experiment with a continental block on the downgoing plate.
$R_{c/oc}$ = 1.0; $\alpha$ = -15°; w = 66 km; $\eta_w$ = 0.5e22 Pa*s.